Group 2 Innate Lymphoid Cells in Ovarian Health and Disease

Sara Asif

Thesis submitted to the University of Ottawa in partial fulfillment of
the requirements for the Ph.D. in Microbiology and Immunology

Department of Biochemistry, Microbiology, and Immunology
Faculty of Medicine
University of Ottawa

Abstract

Group 2 innate lymphoid cells (ILC2s) are a subset of tissue-resident lymphocytes that function as first responders to physiological tissue inflammation, and during malignant transformation, can direct tumor immunity in its early stages. How ILC2s contribute to ovarian health and whether they can be harnessed to improve anti-tumor therapy has not yet been elucidated. Herein, we identified the novel presence of ILC2s in the mouse ovary, and found that they represent a dynamic population that is regulated by hormonal signalling and epithelial-derived cytokines. Our data provides a phenotypic and functional characterization of ILC2s in the ovary during normal reproductive cycling, ovulation, and in a mouse model of polycystic ovarian syndrome.

Having identified ILC2s in the healthy cycling mouse ovary, we next sought to extend our studies to ovarian cancer, where the role of ILC2s is undefined. Herein, we report that IL-33 treatment increases ILC2 abundance, activation, and effector function in mouse ovarian tumors. IL-33-activated ILC2s upregulate surface expression of PD-1, providing a rationale to consider anti-PD-1 (αPD-1) immunotherapy in combination. Indeed, we found that IL-33+αPD-1 treatment significantly improves survival in mice bearing ovarian tumors compared to either monotherapy. IL-33 treatment enriches ILC2s in the tumor microenvironment where they exhibit enhanced cytotoxic capabilities and expression of effector molecules IL-5 and IL-13. Survival analyses revealed that IL-5, but not IL-13 is dispensable for the therapeutic efficacy of IL-33+αPD-1 treatment. Beyond ILC2s, T cells, B cells, and NK cells all contribute to the therapeutic effect of IL-33+αPD-1 unveiling a model in which this combination treatment exerts its effects through multiple immune pathways. Together these data position ILC2s as key mediators of ovarian homeostasis and disease.

Table of Contents

List of Figures

List of Tables

Abbreviations

APCs — antigen presenting cells

Areg – amphiregulin

αPD-1– anti-PD-1

CAFs — cancer associated fibroblasts

CAMs — cancer-associated macrophages

cNK — conventional NK

CTLA-4 — cytotoxic T-lymphocyte associated protein 4

DC — dendritic cell

EMT — epithelial-to-mesenchymal transition

EOMES — eomesodermin

FACS — fluorescence-associated cell sorting

FBS — fetal bovine serum

FDA — Food and Drug Administration

FSH — follicle stimulating hormone

GATA3 — GATA binding protein 3

GITR — glucocorticoid-induced tumor necrosis factor

HBSS — Hank's balanced salt solution

hCG — human chorionic gonadotropin

HGSC — High grade serous carcinoma

ICOS — T-cell co-stimulator

ICOS-L — ICOS ligand

IFN-g — interferon-gamma

Ih2 — innate helper type 2

ILC1 — group 1 innate lymphoid cell

ILC2 — group 2 innate lymphoid cell

ILC3 — group 3 innate lymphoid cell

iILC2s — inflammatory ILC2s

LH — luteinizing hormone

NFkB — nuclear factor kappa-light-chain-enhancer of activated B cells

NH — natural helper

nILC2s — natural ILC2s

NK — Natural Killer

ORR — objective response rate

OS — overall survival

OSE — ovarian surface epithelium

PD-1 — programmed cell death protein 1

PFS — progression-free survival

PMSG — pregnant mares' serum gonadotropin

RORa — retinoic acid-related orphan receptor alpha

ST2 — suppressor of tumorigenicity 2

T-bet — T-box expressed in T cells

TGF-b — transforming growth factor-beta

Th2 — T helper 2

trNK— tissue-resident natural killer cells

TME — tumor microenvironment

TNF — tumor necrosis factor

TNFR — tumor necrosis receptor

TP53 — tumor suppressor p53 protein

Treg — regulatory T cells

Significant Contributions

Dr. John Abou-Hamad committed endless hours to assist in mouse surgeries for this thesis. Dr. David Cook and Dr. Sarah Nersessian performed all bioinformatic analyses presented in this thesis. Dr. Yoanna Poutou generated all oncolytic viruses used in this thesis.

Acknowledgements

Foremost, I would like to express my deepest gratitude to my thesis supervisors, Dr. Ardolino and Dr. Vanderhyden, whose mentorship and guidance have shaped me into the scientist I am today. Thank you for believing in my abilities and granting me the academic freedom to pursue my scientific inquiries. I am profoundly grateful for your support, which has helped me succeed both academically and professionally, and the opportunities that have opened as a result. I also extend my gratitude to my thesis advisory committee for their guidance and support throughout my research.

It has been a pleasure to train at the Cancer Research Program over the past few years. I would like to thank John Abou-Hamad, Jonathan Hodgins, Marie Marotel, Reem Kurdieh, Olivia Makinson, Dalia Ibrahim, and Paul Al Haddad for their friendship and unwavering support – I am truly indebted to all of you. To the Ardolino and Vanderhyden lab as a whole, thank you for being a part of my journey; I will carry many happy memories from my time here.

My sincere and affectionate gratitude goes to my family for their unconditional support and encouragement throughout this journey. To my parents, whose prayers sustained my morale, I owe you a special thanks.

Finally, all praise belongs to The Almighty God, without whose blessings this thesis would not have been possible.

Chapter 1

General Introduction

1. Introduction

1.1. The mammalian ovary and ovulation

The ovary is an interminably active organ that undergoes continuous cycles of tissue remodeling and wound repair throughout the female reproductive lifespan. The growth and maturation of the ovarian follicle, its rupture during ovulation, and subsequent differentiation into the corpus luteum, all necessitate tightly regulated inflammatory processes that support ovarian function. However, over time, these repetitive cycles create signs of "wear and tear", leading to conditions of chronic inflammation. With age, the repetitive cycles of monthly ovulation alongside sustained inflammation, introduces a fibrotic niche in the ovary, possibly making it more susceptible to developing cancer (*1, 2*). In this regard, the ovary is unique in its need to constantly balance tissue inflammation – promoting it for tissue repair while tightly controlling it to prevent immunopathology.

The ovary undergoes profound morphological changes through the progression of the reproductive cycle, known in mice as the estrus cycle. This cycle spans four to five days and consists of four stages: proestrus, estrus, metestrus, and diestrus. The transition from each stage is governed by hypothalamus-pituitary-ovarian reproductive axis. During sexual maturity, the hypothalamus releases gonadotropin-releasing hormone, which, in turn, signals the anterior pituitary gland to secrete follicle-stimulating hormone (FSH) and luteinizing hormone (LH). These gonadotropins target the ovaries, specifically, the ovarian follicle. The ovarian follicle represents the functional unit of the ovary and is comprised of the oocyte (egg) surrounded by concentric layers of granulosa and theca cells (*3*).

In response to FSH signalling, granulosa and theca cells of the ovarian follicle undergo steroidogenesis to produce estrogen and progesterone and drive folliculogenesis (*3*). Early folliculogenesis begins with the activation of primordial follicles, a period marked by rapid granulosa cell proliferation and increased vasculature. During proestrus, the preovulatory surge of LH marks the beginning of ovulation, and the transition to estrus where a mature oocyte is released by the ovarian follicle, enters the opening of the oviduct (ostium), and moves along to the lower ampulla region where fertilization can take place. The success of the ovulatory event is contingent on a highly coordinated series of structural changes in the follicle, starting with the degradation of the extracellular matrix (ECM), breakdown of the basal lamina that separates the granulosa and theca cells, increase in intrafollicular pressure, and the eventual loss of the ovarian surface epithelium (OSE) in the apical region of the ovulatory follicle (*4*). After ovulation, the female mouse enters estrus, where the remaining granulosa and theca cells of the ovarian follicle differentiate to form the corpus luteum in the ovary. The corpus luteum functions as an endocrine gland, producing progesterone and low amounts of estrogen, eventually undergoing degradation if fertilization does not occur (*4, 5*)

Nearly 50 years ago, Epsey proposed that ovulation is fundamentally an inflammatory process (*6, 7*). Epsey posited that ovulation and inflammation share many parallels, but central to his proposal was the downstream effect of the LH hormone which primarily functions through prostaglandins to promote follicular rupture during ovulation. Since this initial proposal, numerous studies over the past few decades have has broadened the scope of LH-induced mediators in ovulation to include epidermal growth factor-like genes (*Areg*) and interleukin genes (*Il6*, and *Il1b*), which are

common to both inflammation and ovulation (*8*). Therefore, because ovulation and inflammation share key features, the immune system plays an indispensable role in the ovary during ovulation. The ovarian vasculature also supplies circulating leukocytes to the ovary, some of which will extravasate into the ovarian stroma to become resident immune cells (*7*). Thus, the intersection of the immune system and the female reproductive system not only facilitates ovulation, but also contributes overall ovarian health, with its dysregulation linked to ovarian pathologies (*9*).

1.2. Group 2 innate lymphoid cells (ILC2s)

Discovery and identification of ILCs

Innate lymphoid cells (ILCs) are tissue-resident lymphocytes that are found weaved in the fabric of connective tissue underling barrier organs. ILCs mirror T helper (Th) cell subsets, but unlike their adaptive counterparts, ILCs fail to undergo somatic recombination, and instead express germ line encoded receptors that regulate their activation. As cells of the innate immune system, ILCs are one of the first responders to tissue inflammation, providing rapid, non-antigen specific responses to a wide array of pathogenic and non-pathogenic perturbations.

Over a decade ago, three independent research groups identified a unique cell population involved in type 2 immunity, laying the groundwork for the discovery of ILC2s. Moro and colleagues noted the presence of a novel cell population present in fat-associated lymphoid clusters, which they termed natural helper (NH) cells (*10*). In parallel, Neil and colleagues observed that IL-25 or IL-33 administration in IL-13 reporter mice led to the aggregation of IL-13-secreting cells, and termed these cell nuocytes (*11*). Building on these observations, Price and colleagues identified lineage-negative cells that also produced IL-13 and named them Innate helper type 2 (Ih2) cells (*12*). In

2013, a universal classification of ILC nomenclature was proposed based on shared phenotypic, transcriptional, and functional characteristics (*13*). Three major ILC subsets were recognized: ILC1 (including NK cells), ILC2, and ILC3 (including lymphoid tissue inducer (LTi) cells) (*14*). Collectively, NH cells, nuocytes, and Ih2 cells depend on the transcription factors GATA binding protein 3 (GATA3) and retinoic acid-related orphan receptor alpha (RORα) for their development and survival, and in response to IL-25 and IL-33 stimulation, functionally produce IL-5 and IL-13. Based on these shared characteristics, these populations were collectively classified as ILC2s.

Group 1 ILCs, which include NK cells, mount type 1 pro-inflammatory immune responses against viruses and intracellular bacteria by producing interferon-gamma (IFN-γ) and tumor necrosis factor (TNF). ILC1 and NK cell effector functions are transcriptionally regulated by T-box expressed in T cells (T-bet), the latter of which is further distinguished by the expression of Eomesdermin (EOMES). Group 2 ILCs secrete T_H-2-like cytokines such as IL-4, IL-5, IL-6, IL-9, and IL-13 in response to parasitic helminth infection and are defined by the expression of GATA3 and RORα. Lastly, group 3 ILCs, which mirror T_H-17 cells, are defined by the expression of RORγt and secrete IL-22 in response to extracellular bacterial and fungal infections. ILC3s have been found to predominantly populate mucosal membranes, such as the gastrointestinal tract where they have a role in intestinal immunity (*13, 14*).

ILC2 development

ILC2 emerge from common lymphoid progenitors (CLPs) in the bone marrow. CLP progenitors require IL-7 signalling which leads to increased STAT5 transcription factor activity, followed by Nfil3 and Id2 expression. CLP cells differentiate into common helper innate lymphoid cell

precursors (CHILP) which further differentiate into ILC2 progenitors before terminally differentiating into ILC2s, via GATA3 transcription factor activity (*15*).

ILC2 trafficking

ILC2s arise from fetal progenitors and colonize distal tissues in the perinatal phase. In the neonate, ILC2s seed the lung, reaching peak levels three-fold higher than that of the adult mouse lung on day 10, and by day 13 the population contract to that of the adult lung (*16*). This rapid expansion of ILC2s appears to be mediated by lung epithelial-derived IL-33 attributed to the first-time exposure to air. Furthermore, neonatal ILC2s were more proliferative and produced higher levels of IL-5 and IL-13 compared to adult lung ILC2s (*16*).

Lineage-tracing experiments indicate that ILC2s are distributed in tissues during the prenatal period where they form established pools until adulthood. (*17*). These established ILC2 pools in tissues are largely tissue-resident, long-lived, can self-renew, and undergo minimal replenishment (*17-19*). In settings of allergic lung inflammation or chronic parasitic infection, some of the local ILC2 pools are responsible for replenishment, and in some later stages of infection, hematogenous trafficking of ILC2s to the lungs occur (*18, 20*). During hematogenous trafficking, IL-33 dictates ILC2 egress from the bone marrow as progenitors (*21*).

Studies using parabiotic mice revealed that lung ILC2s did not appreciably change in parabiotic partners suggesting that, at steady state, lung ILC2s are largely self-maintained and progenitors from the bone marrow constitute very little to their population. Intestinal ILC2s revealed ~10% exchange rate between parabiotic partners, indicating that these cells replenished at a low rate

under steady state conditions. However, when IL-25 was injected in the CD45.1^{+} mouse of a parabiotic pair, KLRG1^{hi} inflammatory ILC2s (iILC2s) were observed in both CD45.1^{+} and its partner, CD45.2^{+} mice, suggesting that under inflammatory conditions iILC2s are circulating cells. It was later identified that the small intestine lamina propria (siLP) housed "pre-iLC2s" that were induced under inflammatory or infectious conditions to enter circulation and traffic to other tissues. On the other hand, IL-33 treatment induced in situ proliferation of natural ILC2s (nILC2s) in the lungs as evidenced by Ki67 expression, but this nILC2 exchange between parabiotic mice did not occur, indicating that nILC2s are not circulating cells (*22*). Thus, under steady-state conditions, ILC2s are tissue-resident cells; however, during tissue inflammation or infection, a transient iILC2 population emerges from the small intestine with the capacity to migrate to the lung, convert to nILC2s, or return to the gut.

ILC2 phenotype and function

ILC2s reside in multiple organs in the body but are notably abundant within the lining of the lungs where they have been implicated in the pathogenesis of several respiratory disorders such as allergic lung asthma and rhinitis (*23*). Phenotypically, ILC2s lack expression of somatically rearranged antigen receptors. Instead ILC2s respond to pathogenic and non-pathogenic insults by integrating pleiotropic signals from epithelial, immune, endocrine, and neurogenic compartments. Additionally, ILC2s express several co-stimulatory molecules such as (ICOS) and ICOS-L (*24, 25*), tumor necrosis receptor (TNFR) and glucocorticoid-induced tumor necrosis factor receptor (GITR). Similar to their adaptive counterparts, ILC2s also express the inhibitory receptors PD-1 and CTLA-4, which function as negative checkpoints for ILC2 activity.

A cardinal feature of ILC2s is their ability to respond to epithelial-derived cytokines, IL-25 and IL-33, and produce copious amounts of effector cytokines. Activated ILC2s produce type 2 cytokines, mainly IL-5 and IL-13. IL-5 primarily functions to induce eosinophilia, where activated eosinophils secrete several cytotoxic molecules stored in their secondary granules, such as major basic protein (MBP), eosinophil peroxidase (EPO), cationic protein (ECP) and eosinophil-derived neurotoxin (EDN). IL-13 enhances smooth muscle contractility and goblet cell hyperplasia, which concertedly aids in the expulsion of helminths – known as the "weep and sweep" method. ILC2-derived IL-13 has been shown to be essential for the migration of activated dendritic cells (DCs) to the draining lymph node where they prime naïve T cells to differentiate into T helper 2 (Th2) cells (*26*).

Tissue-specific features of ILC2s

ILC2s exhibit tissue-specific heterogeneity and functional plasticity (*27*) – attributes that make these cells relevant in a wide variety of disease contexts. ILC2s from various mouse tissues including the lung, gut, fat, and skin exhibit striking phenotypic differences. Gut ILC2s abundantly expressed *Il17rb*, the gene encoding for IL-25R, while expression of *Il1rl1* encoding for the IL-33R, was enriched among fat and lung ILC2s. By contrast, skin ILC2s expressed low levels of *Il17rb* and *Il1rl1*, but high levels of *Il18r1*, the receptor for IL-18. Expression of IL-18R on skin ILC2s was required for their activation and effector function, as loss of IL-18 signalling led to reduced numbers of IL-5^+ and IL-13^+ ILC2s in the skin tissue, and ameliorated skin inflammation in a mouse model of atopic dermatitis-like inflammation (*27*). Expression of IL-25R on gut ILC2s is critical for their homeostasis that is maintained by tuft cells, which are a constitutive source of IL-25. During helminth infection, tuft-cell derived IL-25 activates ILC2s to secrete IL-13,

promoting goblet cell hyperplasia and worm expulsion (*28*). In the lung, ILC2s robustly respond to IL-33 derived from the epithelial lining of the cells.

In all, ILC2s exist as a heterogenous group of immune cells that exhibit unique tissue-specific properties, which ultimately influences their roles in inflammation and disease.

1.3. IL-33-ST2 signalling

ILC2s robustly respond to the epithelial-derived cytokine interleukin 33 (IL-33). IL-33, also known as IL-1f11, belongs to the IL-1 superfamily of cytokines and functions as a pro-inflammatory cytokine that promotes type 2 immunity, prominently through ILC2 and T helper 2 (Th2) responses (*29*). IL-33 is encoded by the *IL33* gene located on human chromosome 9 (9p24.1) and was originally identified in canine vasospastic cerebral arteries following subarachnoid hemorrhage (*30*), and subsequently in human tissues (*31*). Later, IL-33 was identified as a member of the IL-1 superfamily of cytokines and as ligand to suppressor of tumorgenicity 2 (ST2, also known as IL1RL1) due to its structural and functional homology to IL-1 and IL-18 (*32*). IL-33 is normally sequestered in the nuclei of many cell types (i.e., fibroblasts, epithelial cells, and smooth muscle cells) but is released upon tissue perturbation or cellular activation through ATP signalling (*33*).

IL-33 is a dual function protein that acts intracellularly as a nuclear factor regulating transcription, and extracellularly as a potent cytokine. IL-33 is released in its full-length form into the extracellular space, where it is subsequently cleaved by extracellular proteases (derived from neutrophils, mast cells, etc.), to produce a truncated “mature” IL-33, which is 30-fold more potent for the activation of ILC2s than the full-length IL-33 (*34*). IL-33 binds to its receptor, a

heterodimer comprised of ST2 and its coreceptor, IL-1 receptor accessory protein (IL-1RAcP). The ST2 receptor belongs to the toll-like receptor/interleukin-1 receptor (TIR) superfamily and can be found in three isoforms: predominantly the full-length transmembrane isoform (ST2L), a soluble form (sST2), which lacks the transmembrane domain and binds to IL-33 as a decoy receptor, or as a lesser-known variant isoform (ST2V) (*32, 35, 36*).

IL-33's structure possesses β-trefoil fold which binds to ST2 to induce a conformation change in the receptor, followed by recruitment and dimerization with IL-1RAcP (*37*). Together, ST2, IL-1RAcP, and MyD88 form the scaffold for IRAK1,4 and TRAF6 to activate downstream nuclear factor kappa-light-chain-enhancer of activated B cells (NF-kB) and MAPK signalling pathways. Phosphorylation of GATA3 by p38, promotes its binding to the *Il5* and *Il13* promoter regions of ILC2s to induce the phosphorylation of Th2 cytokines (*29, 38*). Thus, as a short-lived, locally active cytokine, IL-33 provides acute but robust responses, effectively functioning as an "alarmin" to alert the immune system in response to tissue perturbations under both pathogenic and non-pathogenic conditions.

1.4. IL-33-ST2 axis in female reproduction

A recent body of literature supports a role for IL-33 in ovulation and ovarian physiology. In the murine ovary, IL-33 protein expression was among the highest compared to other tissues, including the lung, and this expression remained stable from prepubescent to aged mice (*39*). Furthermore, IL-33 gene expression was significantly upregulated transiently during human chorionic gonadotropin (hCG)-induced superovulation (*39*). In the murine ovary, IL-33 expression was identified in the endothelial cells of veins surrounding the follicle, whereas IL-33^{+} oocytes

were surrounded by IL-33R^{+} granulosa cells in human ovaries (*39, 40*). Thus, IL-33 presents a unique and significant pattern of expression in the mouse ovary.

Functionally, IL-33 has emerged as a pivotal cytokine in several processes in the ovary. Neutralization of IL-33 in female mice induced to superovulate led to a reduction in oocyte number but did not prevent ovulation (*40*). This implicates an IL-33-ST2 axis in the ovary, where a possible oocyte-granulosa cell cross-talk facilitates the process of ovulation. Ovarian atresia, or follicle loss, is a process that regulates the pool of developing follicles, but this process results in cellular waste that must be disposed of to prevent ovarian toxicity. Ovarian atresia is impaired in IL-33-deficient (*Il33*$^{-/-}$) mice, resulting in the accumulation of ovarian tissue and catabolic waste, and ultimately, increased ovarian aging and functional decline (*41*). Later it was found that IL-33 activates granulosa cells in the early stages of atresia through NFkB signalling and that IL33$^{-/-}$ female mice present with shrunken ovarian reservoirs and significantly shortened reproductive lifespan (*42*).

In the uterus, IL-33 responsive ILC2s contribute to pregnancy and fetal growth outcomes. Uterine ILC2s, co-localized with IL-33 in the myometrium, expand during pregnancy (*43*). ILC2s promote fetal growth, and in their absence, lead to uteri-placental abnormalities, poor vascular remodelling, fetal growth restriction in fetuses, and dampened type 2 gene signature. Uterine ILC2s also have an important role in late gestation and labour onset. In late gestation, IL-33 secreted from uterine interstitial fibroblasts resulted in ILC2 expansion, activation, and eosinophil recruitment shortly before labour onset, promoting parturition (i.e. the act of giving birth) via uterus-intrinsic pathways. In *Il33*$^{-/-}$ mice, this labour onset is delayed, thus highlighting the role of uterine ILC2s which depend on IL-33 activation for labor onset (*44*).

ILC2s have been found in a study exploring a single-cell atlas of the aging ovary. In this study, no differences in ILC2 proportions were reported in young (3 months) versus old (9 months) mice, and no further transcriptional characterization of these cells was described (*45*). Previous work in our lab also identified an ILC2-like population in the mouse ovary but found that this population increased 2-fold in young versus aged mice (*46*).

Collectively, these data underpin the significance of IL-33 in regulating several reproductive processes. Emerging evidence of uterine ILC2s in studies of endometriosis, fetal growth, spontaneous abortion, and pregnancy have established the IL-33-ILC2 axis in the uterus. However, the abundance and function of IL-33-responsive ILC2s have not, to our knowledge, been investigated in the ovary.

1.5. IL-33-ILC2 axis in tumor immunology

ILC2s function as a double-edged sword in cancer; they can coordinate with other immune cells within the tumor to mediate anti-tumoral responses or maintain a tumor-permissive microenvironment. For instance, in the widely used B16-F10 melanoma model of metastasis, ILC2s have been implicated in both tumor progression and clearance. IL-33-activated ILC2s were shown to promote lung metastasis via eosinophil-induced suppression of NK cells. ILC2-derived IL-5 recruited eosinophils to dampen IFN-γ production by NK cells and ultimately promote metastatic lesions in the lung (*47*). On the other hand, in a separate study, IL-33 was shown to delay tumor burden and promote survival in B16-F10 tumor-bearing mice. Depletion of eosinophils impaired recruitment and activation of cytotoxic lymphocytes and abolished the anti-

tumor function of IL-33 in this model (*48*). An ILC2-eosinophil axis was uncovered in the same B16-F10 melanoma model, where ILC2-derived granulocyte macrophage colony stimulating factor (GM-CSF) was found to be necessary to augment eosinophil recruitment and anti-tumor immunity (*49*).

ILC2s were also found to infiltrate mouse orthotopic pancreatic tumors, where IL-33 activated ILC2s primed $CD8^+$ T cells to unleash tissue-specific anti-tumor immunity. IL-33-activated ILC2s secreted CCL5, a chemokine that promoted $CD103^+$ DC recruitment to the tumor bed, and, in turn, priming of tumor antigen-specific $CD8^+$ T cells. Mechanistically, IL-33 activation of ILC2s was found to be indispensable for this therapeutic effect, thus uncovering an ILC2-DC-$CD8^+$ T cell axis in pancreatic cancer. In murine lung tumors, ILC2s were found to be more abundant in metastatic lesions compared primary tumors. In the absence of ILC2s, these tumors showed heightened ability to metastasize, thus exemplifying a role of ILC2s in immunosurveillance to limit tumor growth and spread (*50*). Conversely, ILC2s were also shown to contribute to an immunosuppressive tumor microenvironment by interacting with myeloid-derived suppressor cells (MDSCs) to promote tumorigenesis in bladder and colorectal tumors (*51, 52*).

There is now emerging evidence indicating that ILC2s can independently mediate anti-tumor cytotoxicity via granzyme secretion. This finding was unexpected, as helper ILCs were not previously thought to possess cytotoxic capabilities. In a flagship study on tumor-infiltrating ILC2s, single-cell RNA sequencing (scRNA-seq) revealed that a unique pro-inflammatory Th1 ILC subpopulation emerges during the development and growth of tumors. This Th1-related population downregulated *Gata3* while concomitantly upregulating Th1-related markers such as

IFN-induced genes including *Ifit1*, *Ifit3*, *Ifitm1*, *Gzmb*, and *Gzmc* (*53*). These data suggested that during tumor growth ILC2s take cues from the local microenvironment and phenotypically shift to express non-conventional markers such as granzymes that can directly mediate anti-tumor cytotoxicity. Human ILC2s were also shown to produce the cytotoxic molecule Granzyme B (GZMB) when stimulated by alarmins (*54*). Mechanistically human ILC2s released GZMB and perforin to trigger caspase-3-mediated apoptosis in tumor cells. Furthermore, the expression of DNAM-1 (CD226) enhanced GZMB production by human ILC2s. Interaction of DNAM-1 with its ligands CD112 and CD155 on acute myeloid leukemia cells inactivates the negative regulator FOXO1 in ILC2s and subsequent release of GZMB. These papers were fundamental to the discovery of cytolytic ILC2s, which opens the door to uncovering more about how these cells can be harnessed for the treatment of cancer.

The role of ILC2s in ovarian cancer has not yet been investigated, despite emerging evidence that IL-33-ST2 signalling modulates the ovarian tumor microenvironment. Human studies show that mRNA expression levels of IL-33 and ST2 were significantly upregulated in ovarian cancer tissues and metastatic tumor lesions compared to healthy ovarian tissue. Additionally, IL-33 and ST2 expression has been associated with poor overall survival in patients with epithelial ovarian cancer (*55, 56*). IL-33 has been implicated in the migration and invasion of human ovarian cancer cells, which is facilitated by cancer associated fibroblasts (CAFs) and cancer-associated macrophages (CAMs). IL-33-containing exosomes released from CAFs were shown to induce an M2 like phenotype which induced epithelial-to-mesenchymal transition (EMT) by transforming growth factor-beta (TGF-β) signalling in ovarian cancer cells (*56*).

However, in mouse studies, treatment with IL-33 delays ovarian cancer tumor progression and enhances peritoneal $CD4^+$ T cell and B cell activation as well as eosinophil recruitment (*57*). Similarly, the overexpression of IL-33 significantly extended the survival of mice in a murine model of peritoneal carcinomatosis (*58*). Although ILC2s have not been implicated in these studies, the context-specific roles of IL-33-ST2 signalling in ovarian cancer may provide clues on ILC2 function. The literature supporting the antitumoral role of IL-33-ILC2s axis is divisive, thus emphasizing the need to establish the role of IL-33-responive ILC2s in the ovarian tumor microenvironment.

1.6. PD-1 checkpoint blockade

In 2018 the Nobel Prize in Physiology or Medicine was jointly awarded to James P. Allison and Tasuku Honjo for their pioneering work in the discovery of the checkpoint proteins cytotoxic T-lymphocyte-associated protein 4 (CTLA-4) and programmed cell death protein-1 (PD-1), respectively. The discovery transformed the field of immunotherapy, leading to the approval of the first anti-PD-1 (αPD-1) therapy, pembrolizumab, for the treatment of melanoma (*59*).

Although both CTLA-4 and PD-1 engagement leads to T cell inhibition, the mechanism by which they maintain peripheral tolerance are fundamentally distinct. PD-1 is a member of the B7/CD28 family and is expressed on several cell types of the innate and adaptive immune system such as T cells, B cells, and ILCs. PD-1 binds to its ligands, programmed death-ligand 1 (PD-L1) and PD-L2 which are expressed on antigen presenting cells (APCs) or tumor cells. The canonical PD-1/PD-L1 pathway triggers an intracellular signalling cascade resulting in immune cell inhibition and exhaustion (*60*). T cell exhaustion via PD-1/PD-L1 interaction was identified in studies of

chronic viral infection in mice where PD-1/PD-L1 axis functioned as a negative feedback loop to ensure immune homeostasis (*61*). The PD-1/PD-L1 pathway is now recognized as a key axis for suppression of anti-tumor immunity. CTLA-4 also inhibits T-cell function through intracellular signalling regulation. CTLA-4 competes with the co-stimulatory molecule, CD28, for binding to shared ligands, CD80 (also known as B7.1) and CD86 (also known as B7.2). Monoclonal antibodies that block PD-1/PD-L1 and CTLA-4 interactions have revolutionized the field of immunotherapy of many solid tumors due to their ability to restore T cell function.

In recent years, the expression and function of PD-1 on ILC2s in tumor settings have been described. PD-1 is expressed on ILC2 progenitors and acts as a cell-intrinsic negative regulator of ILC2 function both in mice and humans (*62, 63*). In the healthy lung, PD-1^+ ILC2s account for 20-40% of total ILC2s, and under influenza infection this population increases substantially (*62*). Although human ILC2s do not express PD-1 at steady state, its expression is greatly induced upon allergic inflammation or IL-33 stimulation, which induces KLRG1 expression on ILC2s (*63, 64*). ILC2s in orthotopic mouse pancreatic and melanoma tumors highly express PD-1, and αPD-1 immunotherapy led to the expansion and activation of tumor ILC2s in these models (*49, 65*). Thus, the recent identification of PD-1 expression on ILC2s reveals a novel target for PD-1 checkpoint blockade.

1.7. Ovarian cancer and current advances in immunotherapy

Ovarian carcinoma is the most lethal gynecological cancer, accounting for 2,000 deaths in Canada annually (Canadian Cancer Society, 2026). Epithelial ovarian cancer is the most common ovarian malignancy, with high grade serous carcinoma (HGSC) subtype representing 70% of all ovarian

carcinomas and being the most aggressive and lethal subtype (*66*). Clinically, HGSC often presents with bilaterial ovarian involvement at the time of diagnosis, with widespread peritoneal and omental carcinomatosis, and the presence of malignant ascites (*67*). A high frequency of HGSC patients harbor a tumor suppressor p53 protein (*TP53*) mutation. Moreover, people with deleterious germline mutations of BRCA1 or BRCA2 have a 30-70% risk of developing HGSC (*68*). Epithelial in origin, HGSC arises from the distal end of the fallopian tube (*69, 70*). Briefly, secretory epithelial cells in the fallopian tube fimbria acquire a *TP53* mutation and then undergo clonal expansion to form a neoplastic precursor lesion known as a "p53 signature". With a *TP53* null mutation, additional mutational "hits" drive these neoplastic lesions to acquire proliferative capacity and transformation into tubal intraepithelial carcinoma. Thus, HGSC involves a sequence of events where normal fallopian tube epithelium develops a p53 signature before transformation into a tubal intraepithelial carcinoma, and finally an invasive serous carcinoma (*71, 72*).

HGSC patients present with diverse symptoms such as nausea, bloating, and abdominal pain. Because of these non-specific symptoms and no efficacious early detection techniques, patients are often diagnosed at advanced stage of disease (*73*). Despite challenges with early detection, the majority of HGSC patients are sensitive to first-line therapy, with less than 10% being refractory to chemotherapy at this stage. Cytoreductive surgery followed by platinum-based chemotherapy remain the mainstay treatment for ovarian cancer. More recently, maintenance treatment with the anti-angiogenic drug bevacizumab and/or poly-ADP-ribose inhibitors (PARPis) has become a standard treatment strategy in the first- or second-line setting (*74, 75*). Anti-angiogenesis inhibitors such as bevacizumab function by blocking VEGF-mediated blood vessel formation that feed solid tumors, thereby restricting tumor growth. PARPi exploit homologous recombination DNA repair

deficiencies (BRCA1/2 mutations) present in almost half of ovarian cancer patients (*76*). Still, many patients suffer a recurrence within three years, with disease that has become refractory to treatment (*77*).

The advent of immunotherapy has revolutionized the field of cancer treatment; however, its clinical efficacy in ovarian cancer remains limited, effectively depriving patients of a valuable therapeutic option. Ovarian cancer responds poorly to immunotherapy as a monotreatment, including immune checkpoint inhibitors, with an overall response rate of less than 10% (*78*). Pembrolizumab is a monoclonal PD-1 antibody that has proven clinically efficacious for lung cancer, melanoma, and renal cancer, and is currently under active investigation for use in ovarian cancer. The phase II KEYNOTE-100 (NCT02674061) clinical trial evaluated pembrolizumab monotreatment in patients with advanced recurrent ovarian cancer. The study consisted of two cohorts: those who previously received 1-3 (cohort A) or 4-6 (cohort B) prior first- or second lines of treatment for ovarian cancer. Pembrolizomab monotherapy showed low antitumor activity in the overall study population (N=376) with an objective response rate (ORR) of 7.4% for cohort A and 9.9% for cohort B. Importantly, there was an apparent trend toward increased ORR in patients with higher tumor PD-L1 expression among both cohorts (*78*). Overall, results from the KEYNOTE-100 clinical trial showed that pembrolizumab monotherapy in recurrent ovarian cancer was associated with modest antitumoral activity, but overall therapeutic efficacy remains limited.

Recently, the FDA approved pembrolizumab for PD-L1-positive platinum-resistant ovarian cancer, marking the first immunotherapy approved for ovarian cancer. The FDA approval was

based on the findings from the phase III KEYNOTE-B96 study which showed, for the first time, an immune checkpoint regimen that demonstrated significant overall survival. The KEYNOTE-B96 trial was a randomized, double-blind, multi-centered phase II study conducted on 643 histologically confirmed cases of epithelial ovarian, fallopian tube, or primary peritoneal carcinoma that had previously received one or two lines of treatment, with at least one platinum-based chemotherapeutic regimen. In total 643 participants were enrolled and randomly assigned to pembrolizumab plus paclitaxel (*N*=322) or placebo plus paclitaxel (*N*=321). Pembrolizumab plus paclitaxel significantly improved progression-free survival and overall survival in participants, with or without bevacizumab, compared to placebo controls.

This FDA approval signifies a major breakthrough in ovarian cancer treatment, as previous studies have not demonstrated this level of clinical efficacy. However, although pembrolizumab treatment showed improvement in overall survival across all cohorts, approval is currently limited to platinum-resistant, PD-L1-positive tumors. Future work must therefore focus on expanding eligibility and improving access to pembrolizumab and other checkpoint inhibitors for ovarian cancer patients. At this stage of clinical testing, long-term side effects and the potential for treatment resistance remain unknown. This is particularly relevant in ovarian cancer, where treatment resistance and disease recurrence is a persistent challenge. Thus, results from phase IV studies will be essential for evaluating the long-term safety and effectiveness of this pembrolizumab regimen in ovarian cancer.

Immunotherapies, such as pembrolizumab, function to activate the host immune response, but mechanisms of immune evasion and immunosuppression contribute to poor responsiveness in

treatments for ovarian cancer (*79*). The resistance of ovarian cancer to immunotherapy can be attributed to several factors including inter- and intra-tumor heterogeneity, low abundance of tumor-infiltrating lymphocytes, and cellular and non-cellular immunosuppression in the tumor microenvironment (*79-81*). Still, ovarian cancer has been recognized as an immunogenic tumor. The accumulation of tumor-infiltrating lymphocytes has an established prognostic role in ovarian cancer; their presence correlates positively with patient progression-free survival (PFS) and overall survival (OS) (*82, 83*). However, other tumor-infiltrating immune cells such as Tregs, DCs, MDSCs, and macrophages have also been implicated in suppressing anti-tumor immunity in this setting (*84*). These findings highlight the complexity and need for an improved understanding of the tumor microenvironment to inform the development of new immunotherapeutic strategies for the treatment of ovarian cancer.

Based on clinical studies, the proposal of three tumor immune landscapes has been described that correlate with sensitivity to immune checkpoint blockade (ICI) (*85*). Firstly, the immune-inflamed phenotype, or "hot tumor", exhibits enrichment of $CD4^+$ and $CD8^+$ lymphocytes near tumor cells which are often PD-L1 positive. The second profile is the immune-excluded phenotype where immune cells are confined to the stromal periphery of the tumor, and despite activation upon PD-1/PD-L1 therapy, these immune cells do not infiltrate the tumor. Lastly, the immune desert phenotype, also known as "cold" tumors, are characterized by the paucity of tumor-infiltrating lymphocytes and unresponsiveness to PD-1/PD-L1 therapy (*85*). Ovarian tumors are often regarded as "cold tumors", predominantly due to the scarcity of tumor-associated antigens and an immunosuppressive tumor microenvironment. These tumors are composed of immunoregulatory immune cells, immunosuppressive factors and cytokines, which concertedly pose a critical barrier

for delivering effective immunotherapies. Recent efforts aim to convert “cold” ovarian tumors into “hot” ones using novel adjuvant therapies to enhance their responsiveness to standard line immunotherapies.

1.8. Rationale and Aim

ILC2s are emerging players in tissue inflammation and tumor immunology. However, to our knowledge, they have not been characterized in the mouse ovary and described in the context of ovulation or ovarian cancer. Thus, the aim of the current study was to uncover the role of ILC2s in the mammalian ovary under physiological conditions, and their dysregulation under pathologies such as PCOS and ovarian cancer. ***We hypothesize that mouse ILC2s are important regulators of inflammation that maintain ovarian homeostasis and mediate anti-tumor immunity in ovarian cancer***. The aims of the study are:

1) To characterize ILC2s in the mouse ovary and define their role in ovarian function.
2) To phenotypically and functionally profile ILC2s in mouse orthotopic tumors.
3) To uncover the mechanism underlying ILC2-mediated anti-tumor immunity.

The overarching goal of the study is to define the role of ILC2s in the mouse ovary during homeostasis and in response to immunotherapeutic strategies in ovarian cancer. These findings have the potential to inform clinical management and future translational efforts in ovarian cancer.

Chapter 2

Materials and Methods

2. Materials and Methods

2.1. Cell culture

2.1.1. Cell lines

Two mouse ovarian cancer cell lines were used in this study. Cells were cultured at 37°C in a humidified atmosphere incubator containing 5% CO_2. ID8*Trp53*$^{-/-}$*Brca1*$^{-/-}$ cells were maintained in DMEM medium supplemented with 4% FBS and 1X Insulin-Transferrin-Selenium (ITSS) (BioGems, catalog no.:00-102-100ML). STOSE cells were maintained in DMEM media with 5% FBS and 1x ITSS. Cells were regularly tested for mycoplasma using the Mycoplasma PCR detection kit (Abm, catalog no.: G238).

2.1.2. Lentiviral production and transduction

Expression plasmid pLenti-NL (Addgene, 113450) was amplified in DH5α bacterial cells and purified by Maxi-Prep (Invitrogen, catalog no.: K210006). 5-6x10^6 HEK293T cells were plated in 10 cm plates containing DMEM+10% FBS. The following day, HEK293T cells were transfected using standard Lipofectamine 3000 protocol (Invitrogen, catalog no.: L3000008) per manufacturer's protocol, and 8 μg of pCMV-dR8.2 (packaging plasmid for lentivirus, Addgene 8455), 2 μg of pCMV-VSV-G (envelope plasmid, Addgene 8454), and 10 μg of lentiviral construct to produce lentivirus. The following day, media was carefully removed from HEK293T cells and replaced with 5mL of warm ID8*Trp53*$^{-/-}$*Brca1*$^{-/-}$ media. At 48-72 hours post-transfection, culture supernatant containing lentivirus was collected and passed through a 0.2-0.44 μg filter using a sterile syringe to remove cell debris.

2.1.3. Generation of ID8*Trp53*$^{-/-}$*Brca1*$^{-/-}$ cell lines

To stably express nanoluciferase in ID8*Trp53*$^{-/-}$*Brca1*$^{-/-}$ cells, the expression plasmid pLenti-NL (Addgene, plasmid #113450) was used to make lentivirus. ID8*Trp53*$^{-/-}$*Brca1*$^{-/-}$ cells were infected with 1-2 mL of lentiviral containing supernatant supplemented with 8 μg/mL of polybrene. Spinfection was performed by centrifuging transduced cells for 2 hours at 2,000 rpm at 37°C. Cells were assayed for luciferase 4 days post-infection.

2.2. In vivo experiments

2.2.1. Mice

C57BL/6 mice (The Jackson Laboratory, strain #000664) or Rag1 KO mice (B6.129S7-*Rag1*^{tm1Mom}/J, The Jackson Laboratory, strain #002216) were used as recipient mice for the ID8*Trp53*$^{-/-}$*Brca1*$^{-/-}$ tumor model, and FVB/N (Charles River, strain #207) mice for STOSE tumor model. Female mice, 8-12 weeks old, received bilateral intrabursal injections of $0.3x10^6$ tumor cells for orthotopic tumor establishment. All mouse procedures were conducted under ethical guidelines approved by the University of Ottawa Animal Care and Veterinary Services in accordance with the Canadian Council on Animal Care guidelines (OHRIe-4377 and OHRIe-4414).

2.2.2. Superovulation

Superovulation was induced in immature C57Bl/6 mice (3-4 weeks old) using hormones for estrus cycle synchronizations. On day 1, between 1-2 PM, 5 IU/mouse of pregnant mares' serum gonadotropin (PMSG) (Prospec, catalog no.: HOR-272) was injected intraperitoneally (i.p.) to induce increased folliculogenesis. After 44-48 hours, between 11-12 PM, 5 IU/mouse of human

chorionic gonadotropin (hCG) (Sigma-Aldrich, catalog no.: C10630) was injected i.p to induce ovulation. PMSG and hCG were reconstituted at 50 IU stock concentration and stored at -20°C in 100 µL aliquots. At the time of injection 50 IU aliquots were thawed and diluted with 900 µL of sterile PBS for a working concentration of 50 IU/mL.

2.2.3. Oocyte retrieval and enumeration

Mice were injected with 5IU PMSG at 4pm on day 1 and exactly 48 hours later, injected with hCG at 4pm on day 3. Oocyte collection was performed 12-14 hours after hCG injections (around 6-7 AM on day 4). Mice were euthanized and the oviducts were dissected and placed in a 35 mm Petri dish with M2 media (Sigma-Aldrich, catalog no.: M7167) at room temperature. Oviducts were then transferred to a separate 35 mm Petri dish containing one drop of hyaluronidase solution (Sigma-Aldrich, catalog no.: H3506) (1mg/mL). Using top illumination of a dissecting microscope, the ampulla region of the oviduct was identified as it appears swollen and translucent with cumulus-oocyte complexes (COCs) visible inside. The COCs were released by tearing a hole in the ampulla with fine-tipped forceps, and incubated in the hyaluronidase solution for 3 minutes to allow the cumulus cells to separate from the oocytes. Then, using a p10 pipette with filter tips, oocytes were collected and transferred to a drop of M2 media to wash any residual cells and oocytes were visually enumerated.

2.2.4. Intrabursal injection

One hour prior to surgery, buprenorphine (0.1 mg/kg) was administered subcutaneously (s.c.) to mice for pain management. All surgical tools were autoclaved, and sterile technique was maintained throughout the procedure. Mice were initially anesthetized at 3% isoflurane then

maintained at 3% isoflurane/1% oxygen with a fitted nozzle for the duration of the surgery. Mice were administered 1 mL of saline s.c. and eye ointment (Optixcare Eye Lube; Aventix) to each eye for hydration. The dorsal side of the mouse was shaved from tail to midline, and the incision site was sterilized with antiseptic (SoluPrep; 2% chlorhexidine in 70% alcohol, 3M cat#7000136295). Once aseptically prepped, the mouse was laid dorsal side up and a small incision (2-3 cm) was made at the dorsomedial position and directly above the ovarian fat pad that envelops the ovary. Then, a small incision was made in the peritoneal wall lining (0.5 cm) at the location of the ovarian fat pad, which is visible beneath the surface of the translucent peritoneal wall. A sterile soaked saline gauze pad was placed in the midline adjacent to the incision. The ovarian fat pad was located and exteriorized by gently pulling it out and resting it on the gauze. The ovary was stabilized by clamping the fat pad with a bulldog clip. Under the dissecting microscope, the ovary was positioned in such a fashion to allow for the insertion of the needle into the oviduct bend leading to the ovarian bursa. Intrabursal injections were performed using a Hamilton syringe (50µL capacity, 4.0 point, 30-guage, 52O bevel, ¾" needle length, catalog no.:7803-07), and dispenser repeater (Hamilton, catalog no.:1482225). The cell suspension was prepared at a concentration of $0.75x10^5$ cells/µL. The repeater was pressed twice per ovary (1 click = 1µL) for a total of $0.15x10^6$ cells per ovary. After intrabursal injection, the fat pad was released from the bulldog clip and gently placed back into the peritoneal cavity. The peritoneal wall was closed with proline sutures (6/0 Surgipro, VP-718X, CV-11 (taper)), and the skin of the dorsal wall with surgical staples (VWR, catalog no.:CA-BD427631) and transdermal Bupivicane (2%, 0.1mL/animal BID; Chiron Compounding Pharmacy) was applied over the incision and staples as a topical analgesic. The mice were placed in an incubator box or heat pad for speedy recovery and monitored post-op for two days for pain or discomfort. The surgical staples were removed 7-10 days post-surgery.

2.2.5. Cytokine and antibody treatment

For tumor immune profiling experiments, treatment began on day 40 post tumor implantation. On day 40, mice were injected i.p. with 500ng of recombinant mouse (rm) IL-5 (BioLegend, catalog no.: 581506), rmIL-13 (BioLegend, catalog no.: 575906), rmIL-25 (Thermo Fisher Scientific, catalog no.: 210-17E-25UG), or rmIL-33 (BioLegend, catalog no.: 580508) daily for 5 days. In combination treatments with antibodies, mice received i.p. injections of αPD-1 (Leinco, clone: RMP1-30, catalog no.: C3442) or αCTLA-4 (Leinco, clone: 9D9, catalog no.: C2855) on days 41 and 43. Tissue collection was performed on day 45 for the ID8p53$^{-/-}$Brca1$^{-/-}$ model when tumor were expected to be established 75% into median survival.

For tumor survival experiments, mice began treatment 25% into expected median survival, which corresponds to day 14 in the ID8*Trp53*$^{-/-}$*Brca1*$^{-/-}$ model (median survival ~60d.). On day 14, mice began treatment with daily i.p. injections of 500ng rmIL-5, rmIL-13, rmIL-25, or rmIL-33 for seven days then every other day after for five days. Antibody treatment began on day 21 with daily i.p. injections of 250 μg of αPD-1 or αCTLA-4 for five days. The total treatment regimen for survival studies was 12 days.

In depletion experiments, CD4 and CD8 cells were depleted by i.p. injections of 250 μg of anti-CD4 (Leinco, clone: GK1.5, catalog no.: C1333) and anti-CD8b.2 (Leinco, clone: 53-5.8, catalog no.: C2832), NK cells with 250 μg of anti-NK1.1 (Leinco, clone: PK136, catalog no.: N123), B cells with 250 μg of anti-CD19 (Leinco, clone: 1D3, catalog no.: C2849), and IL-5 blockade with 250 μg of anti-IL-5 (BioXCell, clone: TRFK5, catalog no.: BE0198). Control mice were treated with rat IgG 1 isotype control (Leinco, clone GL113, catalog no.: I-1195). For survival studies,

depletion was initiated on days -1, and 0 of therapeutic treatment (i.e. IL-33+αPD-1), then maintained weekly for the duration of the experiment. Saphenous blood was collected for flow cytometry analysis to confirm depletion of immune cells (established at >85% depletion).

2.3. Oncolytic viruses

2.3.1. Oncolytic virus production

Vesicular stomatitis virus (VSV) with a mutation in the M protein (VSVΔ51) constructs were tested for oncolytic virus therapy. VSVΔ51-GFP and VSVΔ51-*Il33* were gifts from Dr. Ilkow (OHRI). Briefly, VSV viruses were propagated in Vero cells and cell supernatant was isolated 20-24 hours later for concentration of virus by high-speed centrifugation at 10,000 rpm for 2 hrs at 4°C.

2.3.2. Validation of IL-33 expression

ID8*Trp53*$^{-/-}$*Brca1*$^{-/-}$ cells were treated with VSVΔ51-GFP or VSVΔ51-*Il33* (MOI= 0.1 or 1) and ~24hrs later, cell supernatant and cell lysate was collected. IL-33 expression was tested using mouse IL-33 DuoSet ELISA (R&D Systems, catalog no.: DY3626) as per manufacturer's instructions.

2.3.3. Oncolytic virus treatment

Mice received intrabursal injections of ID8*Trp53*$^{-/-}$*Brca1*$^{-/-}$ cells to establish orthotopic ovarian tumors. Following tumor inoculation, on day 14 (25% of median survival) mice were treated with

$1x10^8$ PFU VSVΔ51-GFP or VSVΔ51-*Il33* i.p. every other day for a total of five days (days 14, 16, 18).

2.4. Tissue dissociation

2.4.1. Female reproductive tract and ovary dissociation

Ovaries, oviducts, and uteri were dissected and placed in a 35 mm Petri dish with cold PBS. Each tissue was transferred to an Eppendorf tube with an enzymatic mix containing HBSS media supplemented with 0.25 mg/mL Liberase TL (Sigma, catalog no.: 5401020001) and 30 μg/mL DNase I (Sigma, catalog no.: 10104159001). Tissue was mechanically minced with a blade or dissection scissors and incubated at 37°C for 1h in a shaking incubator (Eppendorf ThermoMixer C, 800 rpm). After the enzymatic digestion, tissue was passed through a 40 μm cell strainer and washed with PBS/1% FBS. Single cell suspensions were stained for flow cytometry or other downstream applications.

2.4.2. Lung dissociation

Lung enzymatic digestion was prepared using complete RPMI supplemented with 1 mg/mL Liberase TL (Sigma, catalog no.: 5401020001) and 50 μg/mL DNase I (Sigma, catalog no.: 10104159001). Dissected lungs were mechanically dissociated with dissection scissors into fragments of tissue ~1 mm in size. Lung fragments were placed into a 6-well plate fitted with a 40 μm cell strainer and placed in the incubator for 1.5 hours, mixing every 15 minutes. After the incubation, lung tissue was smashed using the end of a 3 mL syringe plunger and washed with 20 mL of RPMI 1640 10% FBS. To separate leukocytes, the cell pellet was resuspended in 5 mL RPMI 1640 (serum-free) and loaded onto 5 mL Lympholyte-M (Cedarlane, catalog no.: CL5035)

and centrifuged at 1,100xg for 20 minutes, 0 brake, 9 acceleration, according to manufacturer's protocol. After centrifugation, lymphocytes at the interface were removed and washed for downstream analysis.

2.4.3. Tumor dissociation

Mouse tumor enzymatic digestion was prepared by adding 2.5 mL of RPMI 1640 or DMEM, 100 µL of Enzyme D, 50 µL of Enzyme R, and 12.5 µL of Enzyme A, using Tumor Dissociation Kit, mouse (Miltenyl, catalog no.: 130-096-730). Bilateral ovarian tumors were dissected and placed in a Petri dish containing ~1 mL of pre-made enzymatic digestion mixture then cut into small fragments of ~1mm in size using a razor blade. Minced tissue mixture was transferred into a gentleMACS C tube containing 1.5 mL of enzymatic digestion mixture and dissociated using the soft/medium program (37C_m_TDK_1). Following tumor dissociation, the enzymatic digestion was quenched by adding ~5mL of PBS/1%BSA and samples are passed through a 40 µm cell strainer and washed with PBS/1% FBS. Single cell suspensions were stained for flow cytometry or other downstream applications.

2.5. Protein analysis

2.5.1. Flow cytometry and fluorescence-activated cell sorting (FACS)

Single cell suspensions from mouse tissues were plated in a 96-well v-bottom plate (1-2x10^6 cells/well) and washed with PBS-1% BSA. The cell suspension was incubated with rat anti-mouse CD16/CD32 (clone 2.4G2, BD Biosciences) for 10 mins at 4°C to block for non-specific binding. Cells were washed and incubated with a cocktail of fluorescently-labelled antibodies (Tables 2.1-2.4) and Zombie NIR™ Fixable Viability Dye (BioLegend, catalog no.: 423106) (1:1000 dilution)

for 30 mins at 4°C. Cells were washed twice with PBS-1% BSA and fixed using eBioscience™ Foxp3 / Transcription Factor Staining Buffer Set (Thermo Fisher Scientific, catalog no.: 00-5523-00) according to the manufacturer's protocol. Following the fixation, cells were stained with fluorescently-labeled antibodies (Tables 2.1-2.4) for intracellular markers for 40 minutes at 4°C. Following incubation cells were washed with 1X Permeabilization Buffer (Thermo Fisher Scientific, catalog no.: 00-5521-00) once then in PBS-1% BSA. Flow acquisition was done using the LSRFortessa (BD Biosciences) or the Aurora (Cytek). Data was analysed using FlowJo (Tree Star Inc.).

2.5.2. Immunofluorescence

Tissues were frozen in optimal cutting temperature (OCT) blocks, cut into 4-6 μm sections using a cryostat (Leica CM1860), and placed on Superfrost plus slides (Thermo Fisher Scientific, catalog no.: 22037246). Sectioned tissue was fixed and permeabilized with 2-4% paraformaldehyde (PFA) for 20 minutes at room temperature. PFA was aspirated and tissue was washed twice with PBS and subsequently blocked with 10% goat serum in 0.2% Triton X-100. Primary antibodies were diluted in 10% goat serum in 0.2% Triton X-100 and added immediately after removal of blocking solution. Sections were incubated with a ST2 primary antibody (Thermo Fisher Scientific, catalog no.: PA5-20077) at 4°C overnight or 1-2 hours at room temperature. Diluted fluorophore-conjugated secondary antibodies (1:1000) and Hoesch stain (Thermo Fisher Scientific., catalog no.: H3570) (1:300) were added and incubated for 1-2 hours at room temperature in the dark. After incubation, the sections were washed three times in PBS for five minutes. Coverslips were mounted onto slides using Immu-Mount™ mounting media (Epredia, catalog no.: 9990402), left to dry overnight at room temperature in the dark, and sealed with nail polish the next day.

2.6. In vitro assays

2.6.1. Cytokine stimulation assay

Lung, ovary, or tumors were dissected and dissociated as described in section 2.4. Single-cell suspensions were plated in a 96-well v-bottom plate in RPMI media containing 5% FBS supplemented with IL-2 (conc.: 1000 U/mL), IL-7 (conc.: 20ng/mL), GolgiStop/GolgiPlug (BD Biosciences, catalog no.: 554724, conc.: 1x). Stimulated groups were additionally supplemented with IL-33 (conc.: 10ng/mL) and PMA (Sigma-Aldrich, catalog no.: P1585, conc.: 20ng/mL) and ionomycin (Thermo Fisher Scientific, catalog no.: I24222, conc.: 1mg/mL). Cells were incubated for 5 hours at 37°C and subsequently stained for intracellular markers and flow cytometry analysis.

2.6.2. Luciferase-release cytotoxicity assay

ILC2s and $CD3^+$ T cells were sorted from ID8*Trp53*$^{-/-}$*Brca1*$^{-/-}$ tumors using FACS (Sony MA900) and plated at various effector:target (E:T) ratios. In a V-bottom plate, effector cells were serially diluted in triplicate wells then 10,000 nanoluciferase-expressing ID8*Trp53*$^{-/-}$*Brca1*$^{-/-}$ cells were plated in each well. Digitonin (Promega, catalog no.: G9441) (conc.: 30 μg/mL) was added to ID8*Trp53*$^{-/-}$*Brca1*$^{-/-}$ cells as a positive control. Contents of each well were thoroughly mixed by pipetting up and down several times, and the assay plate was placed in the incubator at 37°C for 5 hours. After the incubation, 50 μL supernatant from each well was removed and transferred to a new 96-well black flat bottom plate. Coelenterazine (Cedarlane Labs, catalog no.: CZ2.5) substrate mix was prepared (1:200 dilution) and 25μL of substrate mix was added to each well and luminescence was measured using a plate reader. Specific lysis was calculated as follows: % specific lysis = (R<well of interest> - R<targets only>)/ (0-R<targets only>) x 100.

2.7. RNA expression analysis

2.7.1. Nanostring sample preparation and RNA isolation

Prepubescent female C57Bl/6 mice were induced to superovulate via administration of hCG and PMSG (as described in section 2.2.2.). Mice were collected at each stage of the estrus cycle and vaginal smears were sampled as a validation for estrus cycle stage. Ovaries were collected and dissociated (as described in section 2.4.1), followed by cell lysis and RNA extraction using GenElute™ Mammalian Total RNA Miniprep Kit (Sigma, catalog no.: RTN70-1KT). The hybridization reaction was performed according to manufacturer's protocol (nCounter® Nanostring™) and samples were run on the nCounter® MAX/FLEX machine (Ottawa Heart Institute).

2.7.2. scRNA-seq sample preparation

Female C57Bl/6 mice received intrabursal injection of $0.3x10^6$ ID8*Trp53*$^{-/-}$*Brca1*$^{-/-}$ syngeneic cells to form orthotopic tumors. Mice were subsequently treated with 500ng of PBS, IL-25, IL-33, αPD-1, or IL-33+αPD-1 for five days (as described in section 2.2.5). Bilateral tumors were collected on day 45 and $CD45^+$ live cells were sorted using FACS (Sony MA900). Sorted $CD45^+$ live cells were fixed using 10x Fixation of Cells & Nuclei for Chromium Fixed RNA Profiling (catalog no.: 1000414). Samples were sent to StemCore Laboratories (OHRI) for library preparation using the for 10x Genomics Chromium X platform and sequencing (Illumina NovaSeq X).

2.8. Bioinformatic analyses

Single-cell transcriptomic data were processed and analyzed using Seurat (v4.x). After quality control filtering and normalization, dimensionality reduction was performed using principal component analysis (PCA) followed by UMAP embedding for two-dimensional visualization. Unsupervised graph-based clustering was used to identify transcriptionally distinct cell populations, which were subsequently annotated as immune cell types based on canonical marker gene expression. Cell type identities were assigned to the following populations: T cells, γδ T cells (ydT), NK cells, B cells, plasma cells, macrophages, neutrophils, eosinophils, ILC2s, plasmacytoid dendritic cells (pDC), and conventional dendritic cells (cDC1 and cDC2). Gene expression across cell types was visualized by dot plot. Dot size represents the percentage of cells within each cluster expressing the gene, and dot color reflects the scaled average expression level (blue: low/negative; red: high).

2.9. Reproducibility and Statistical Analysis

All in vivo mouse studies were performed at least twice, unless otherwise stated. All statistical analyses in this study were performed using GraphPad Prism version 10. Appropriate statistical tests were used based on experimental design, and included unpaired two-sample Student's t tests, one-way ANOVA, and Mantel Cox log rank test. The number of biological replicates (n value) for each analysis is indicated in the figure legends. Error bars in the figures signify standard error of the mean (SEM). The significance levels for the statistical tests were as follows: not significant (ns) for $p>0.05$, *$p<0.05$, *$p<0.05$, **$p<0.01$, ***$p<0.001$, ****$p<0.0001$. These thresholds were consistently applied to assess the statistical relevance of the findings.

Table 2.1. ILC2 Functionality Flow Cytometry Panel

Marker	Fluorophore	Manufacturer	Clone	Catalog no.	Dilution Factor
Viability	Zombie NIR	BioLegend	N/A	423106	1:500
Amphiregulin	Biotin-SA-PE-CF594	R&D Systems	polyclonal	BAF989	1:400
*CD3	PE-Cy5	BioLegend	145-2C11	100310	1:500
*CD19	PE-Cy5	BioLegend	115510	6D5	1:500
CD45	BUV496	BD Biosciences	30-F11	569673	1:200
CTLA4	PE-Fire 810	BioLegend	UC10-4B9	106335	1:200
*F4/80	PE-Cy5	BioLegend	BM8	123112	1:500
GATA3	AF488	BD Biosciences	L50 823	560163	1:200
GM-CSF	APC/Fire™ 750	BioLegend	MP1-22E9	505424	1:200
IL-5	APC	BD Biosciences	TRFK5	562048	1:200
IL-13	PE-Cy7	Thermo Fisher Scientific	eBio13A	25-7133-80	1:200
Ki67	BV786	BD Biosciences	B56	563756	1:300
KLRG1	BV605	BD Biosciences	2F1	564013	1:200
MHC-II	BUV737	BioLegend	M5/114.15	107641	1:200
*NK1.1	PE-Cy5	BioLegend	PK136	108716	1:500
PD-1	BV750	BioLegend	135263	135263	1:200
ST2	PE	BD Biosciences	U29-93	566311	1:200

* markers included in dump channel gate

Table 2.2 Lymphoid Flow Cytometry Panel

Marker	Fluorophore	Manufacturer	Clone	Catalog no.	Dilution Factor
Viability	Zombie NIR	BioLegend	N/A	423106	1:500
CD3	BB700	BD Biosciences	500A2	742099	1:500
CD4	BUV661	BD Biosciences	GK1.5	612974	1:200
CD8	BUV615	BD Biosciences	53-6.7	613004	1:200
CD19	BV510	BD Biosciences	1D3	562956	1:500
CD20	APC-Fire750	BioLegend	SA271G2	152118	1:200
CD25	BV605	BD Biosciences	PC61	563061	1:200
CD44	BV650	BD Biosciences	IM7	740455	1:200
CD45	BUV496	BD Biosciences	30-F11	569673	1:200
CD49b	AF647	BioLegend	DX5	108912	1:200
CD62L	BUV737	BD Biosciences	MEL-14	612833	1:200
CD69	PE-Cy7	BD Biosciences	H1.2F3	552879	1:200
CTLA4	PE-Fire 810	BioLegend	UC10-4B9	106335	1:200
FoxP3	AF700	BioLegend	MF-14	126422	1:200
GATA3	AF488	BD Biosciences	L50 823	560163	1:200
iCOS	PE-Cy5	BioLegend	15F9	107708	1:200
Ki67	BV786	BD Biosciences	B56	563756	1:300
KLRG1	BUV563	BD Biosciences	2F1	741343	1:200
LAG3	BUV805	BD Biosciences	C9B7W	748540	1:200
NK1.1	BV711	BD Biosciences	PK136	740663	1:200
OX40	BV421	BD Biosciences	OX-86	740061	1:200
OX40L	APC	BioLegend	RM134L	108812	1:200
PD-1	BV750	BioLegend	135263	135263	1:200
PD-L1	BUV395	BD Biosciences	10F.9G2	568308	1:200
ST2	PE	BD Biosciences	U29-93	566311	1:200
TIGIT	PE-Dazzle594	BioLegend	1G9	142110	1:200

Table 2.3 Myeloid Flow Cytometry Panel

Marker	Fluorophore	Manufacturer	Clone	Catalog no.	Dilution Factor
Viability	Zombie NIR	BioLegend	N/A	423106	1:500
Arginase-1	PE-Cy7	ThermoFisher	A1exF5	25-3697-82	1:200
*CD3	PE-Cy5	BioLegend	145-2C11	100310	1:500
CD11b	BUV661	BioLegend	m24	565080	1:200
CD11c	BUV563	BD Biosciences	N418	749040	1:200
*CD19	PE-Cy5	BioLegend	115510	6D5	1:500
CD27	BB700	BD Biosciences	LG.3A10	742135	1:200
CD45	BUV496	BD Biosciences	30-F11	569673	1:200
CD80	BV510	BioLegend	16-10A1	104741	1:200
CD86	BV786	BD Biosciences	PO3	740900	1:200
CD103	BV711	BD Biosciences	M290	564320	1:200
CD206	BV650	BioLegend	C068C2	141723	1:200
CCR5	BUV615	BD Biosciences	C34-3448	752321	1:200
CCR7	BUV805	BD Biosciences	4B12	742065	1:200
F4/80	BV421	BioLegend	BM8	123137	1:500
GATA3	AF488	BD Biosciences	L50 823	560163	1:200
Gr1	BV605	BD Biosciences	RB6-8C5	563299	1:200
iNOS	APC	BioLegend	W16030C	696808	1:200
MHC-II	BUV737	BioLegend	M5/114.15	107641	1:200
*NK1.1	PE-Cy5	BioLegend	PK136	108716	1:500
PD-1	BV750	BioLegend	135263	135263	1:200
PD-L1	BUV395	BD Biosciences	10F.9G2	568308	1:200
Siglec-F	NovaFluor™ Blue 610-70S	ThermoFisher	1RNM44N	M042T03B 06-A	1:200
ST2	PE	BD Biosciences	U29-93	566311	1:200

* markers included in dump channel gate

Table 2.4 B cell Flow Cytometry Panel

Marker	Fluorophore	Manufacturer	Clone	Catalog no.	Dilution Factor
Viability	Zombie NIR	BioLegend	N/A	423106	1:500
CD45	BUV496	BD Biosciences	30-F11	569673	1:200
CD19	PE-Cy5	BioLegend	115510	6D5	1:500
B220	AF700	Thermo Fisher Scientific	RA3-6B2	56-0452-82	1:200
IgM	Biotin-SA PerCP-Cy5.5	BioLegend	RMM-1	406503	1:200
IgG1	Super Bright 436	Thermo Fisher Scientific	M1-14D12	62-4015-82	1:200
IgD	BV711	BioLegend	11-26c.2a	405731	1:200
CD43	PE-Dazzle 594	BioLegend	S11	143218	1:200
CD5	BV480	BD Biosciences	53-7.3	746485	1:200
CD21/35	BV510	BioLegend	7E9	123437	1:200
CD23	FITC	BioLegend	B3B4	280.101605	1:200
GL7	PE	BioLegend	GL7	144608	1:100
CD138	AF647	BioLegend	281-2	142526	1:200
Fas	PerCP Fire 780	BioLegend	SA367H8	152628	1:200
CD69	PE-Cy7	BD Biosciences	H1.2F3	552879	1:200
MHC-II	BUV737	BioLegend	M5/114.15	107641	1:200
PD-L1	BUV395	BD Biosciences	10F.9G2	568308	1:200
CD11b	BV605	BD Biosciences	M1/70	563015	1:200
CD20	APC-Fire750	BioLegend	SA271G2	152118	1:200
CXCR5	BV650	BD Biosciences	2G8	563981	1:200
Ki67	BV786	BD Biosciences	B56	563756	1:300

Chapter 3

Ovarian ILC2s are regulated by estrus cycling and androgen signalling

3. Ovarian ILC2 abundance is regulated by estrus cycling and androgen signalling

3.1. Introduction and rationale

The ovary presents a unique immunological environment characterized by cyclical, tightly regulated inflammatory events. Through the progression of the estrus cycle, the ovary undergoes repeated episodes of follicle growth and rupture, wound healing, and stromal remodelling. Ovulation is a well-established inflammatory event, invoking leukocyte recruitment, cytokine production, vascular remodelling, and tissue repair. Despite this inflammatory landscape, the contribution of ILC2s to ovarian homeostasis has not yet defined.

ILC2s are now recognized as key mediators of immunological homeostasis due to their roles in wound healing, inflammation, and epithelial barrier maintenance. However, while ILC2s have been extensively characterized in barrier tissues including the lung, gut, and skin, their presence and function in the ovary have not yet been described. Particularly, the phenotypic and functional characterization of ovarian ILC2s and their regulation through the progression of the estrus cycle requires further investigation. Thus, we aimed to characterize ILC2s in the mouse ovary as a foundation for understanding their role in ovarian physiology.

3.2. ILCs are present in the mouse female reproductive tract and ovaries

To determine the presence of ILCs in the female reproductive tract, we performed flow cytometry analyses to quantify subsets in the ovaries, oviduct, and uterus of cycling female C57BL/6 mice. ILC2s were defined here and throughout the thesis as lineage$^-$ (Lin$^-$)(CD3$^-$CD19$^-$F4/80$^-$) and NK1.1$^-$ST2$^+$GATA3$^+$CD45$^+$ live cells. As tissue-resident cells, ILC2s were not detected in the spleen, but were present at comparable frequencies across all female reproductive tissues examined (Figure 3.1A). Specifically, ILC2s represented approximately 2-4% of total leukocytes (Figure 3.1C), with slightly higher frequencies observed in the oviduct (4-5% of CD45$^+$ live).

ILC1 and NK cells, defined as CD45$^+$Lin$^-$NK1.1$^+$NKp46$^+$ cells, collectively represented 5-10% of leukocytes in the ovaries, oviduct, and uterus (Figure 3.1B). In the ovaries, conventional NK (cNK) cells (defined as CD49a$^-$Eomes$^+$) predominated amongst other ILC1 and NK cell subsets, consistent with their distribution in the spleen. In contrast, the oviduct and uterus exhibited higher frequencies of tissue-resident NK (trNK) cells (defined as CD49a$^+$Eomes$^-$ cells) (Figure 3.1B-C).

Overall, all major ILC subsets, with the exception of ILC3s (data not shown), were detected in the ovaries, oviduct, and uterus, comprising 2-6% of total leukocytes. Together, these findings identify ILC2s as a distinct and novel population of cells in the mouse female reproductive tract and ovaries.

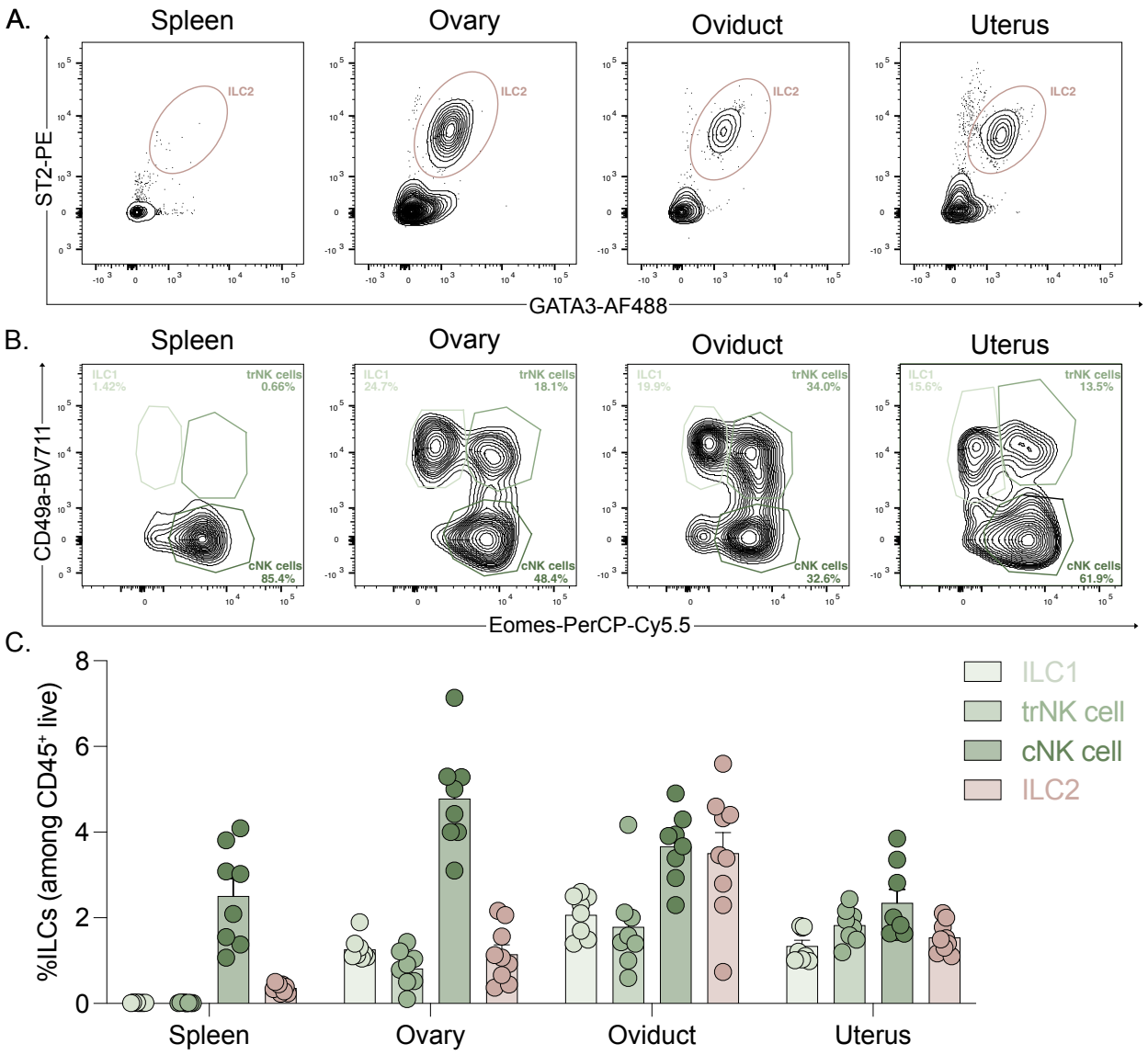

Figure 3.1: ILCs are present in the mouse female reproductive tract and ovaries. Spleen, ovary, oviduct, and uteri were collected from female C57BL/6 mice for flow cytometry analysis. (A) Flow cytometry plots depicting ILC2s across various tissues. ILC2s are gated as lineage negative ($CD3^-CD19^-F4/80^-$) and $ST2^+GATA3^+$. (B) ILC1 and NK cells subsets, are defined as $CD3^-CD19^-F4/80^-NKp46^+NK1.1^+$. ILC1 are further gated as $CD49a^+Eomes^-$, tissue-resident NK (trNK) cells as $CD49a^+Eomes+$ and conventional NK (cNK) cells are defined as $CD49b^-Eomes^+$. (C) ILC1, ILC2, and NK cell frequencies among all leukocytes across various tissues. Results shown are compiled from three independent experiments. N = 8-9/group.

3.3. Ovarian ILC2s respond to epithelial-derived cytokines, IL-25 and IL-33

Having identified the presence of ILC2s in the female reproductive tract and ovaries, we next focused our investigations solely on ovarian ILC2s. To this end, we administered IL-33, IL-25, or PBS vehicle control to female C57Bl/6 mice daily for five days. Following in vivo stimulation, ovaries were collected and processed for flow cytometry staining and analysis.

Ovarian ILC2 expanded in response to both IL-25 or IL-33 stimulation, albeit with a more pronounced effect observed with IL-33 (Figure 3.2A). Notably, IL-33 stimulation resulted in greater than a 10-fold increase in frequency and abundance of ILC2s compared to PBS controls (Figure 3.2B). Expression of KLRG1, a canonical marker of ILC2 activation (*86*), increased with IL-25 and IL-33 stimulation compared to baseline levels observed in PBS controls. In addition, proliferation of ovarian ILC2s was observed following cytokine stimulation as evidenced by Ki67 staining (Figure 3.2C). Together, these data show that ovarian ILC2s become activated and proliferate in response to cytokine stimulation, with a preferred responsiveness to IL-33 over IL-25.

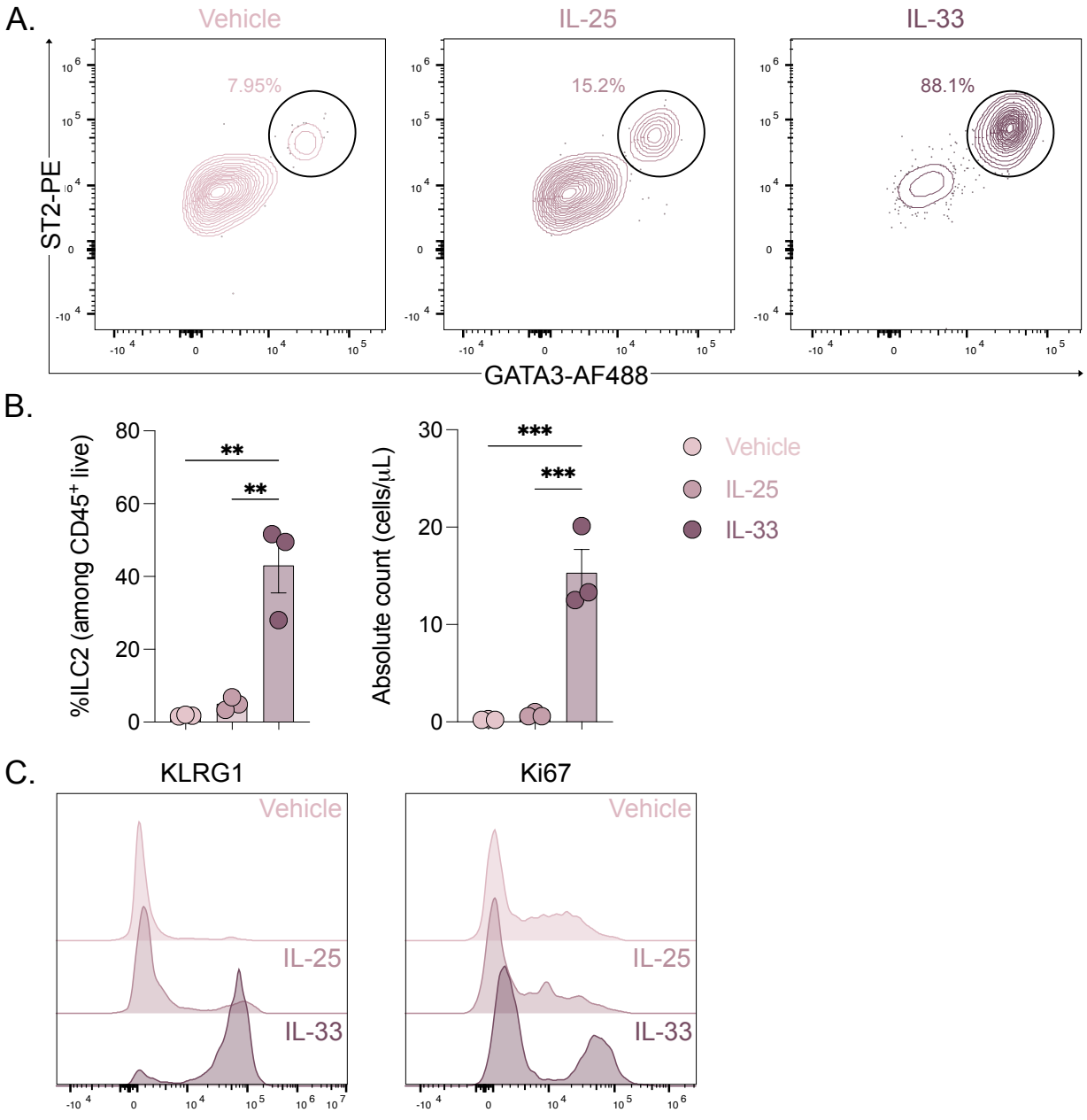

Figure 3.2: Ovarian ILC2s respond to IL-25 and IL-33 stimulation. Female C57BL/6 mice were administered 500ng IL-25, IL-33, or PBS vehicle control i.p. daily for five days, and ovaries were subsequently collected for flow cytometry analysis. (A) Flow cytometry plots depicting ILC2s in PBS, IL-25, or IL-33-treated mice. (B) Frequency and absolute count of ILC2s, and (C) KLRG1 and Ki67 expression on ILC2s in response to cytokine treatments. Experiments depicted are representative of two performed. *N*= 3/group. One-way ANOVA. *p<0.05, **p<0.01, ***p<0.001, ****p<0.0001.

To assess the functional capacity of ovarian ILC2s, mice were treated with IL-33 or PBS, and ovaries were collected for ex vivo stimulation followed by intracellular flow cytometry staining. IL-33 stimulation markedly increased IL-5 and IL-13 expression in ovarian ILC2s compared to PBS vehicle controls (Figure 3.3A), with approximately 10-15% of IL-33-stimulated ILC2s co-expressing these cytokines versus 1-4% in PBS controls (Figure 3.3A). These results further confirm ovarian ILC2s responsiveness to IL-33 stimulation, with their expansion tightly linked to enhanced effector function.

Beyond these type 2 canonical cytokines, ILC2s can produce other effector molecules such as GM-CSF and amphiregulin (Areg), which contribute to innate immunity by driving inflammatory responses and supporting tissue repair (*87, 88*). We observed high expression of GM-CSF and Areg on IL-33 stimulated ILC2s compared to PBS controls (Figure 3.3B). Lastly, we observed that concomitantly with cellular activation, IL-33 treatment induced the expression of checkpoint molecules PD-1 and CTLA-4, with approximately 15% of ILC2s co-expressing both molecules, whereas baseline co-expression was absent (Figure 3.3C). Expression of PD-1 and CTLA-4 on activated ILC2s positions them as potential targets for checkpoint blockade, and provides a rationale for harnessing these cells for immunotherapy in future investigations (Chapter 4).

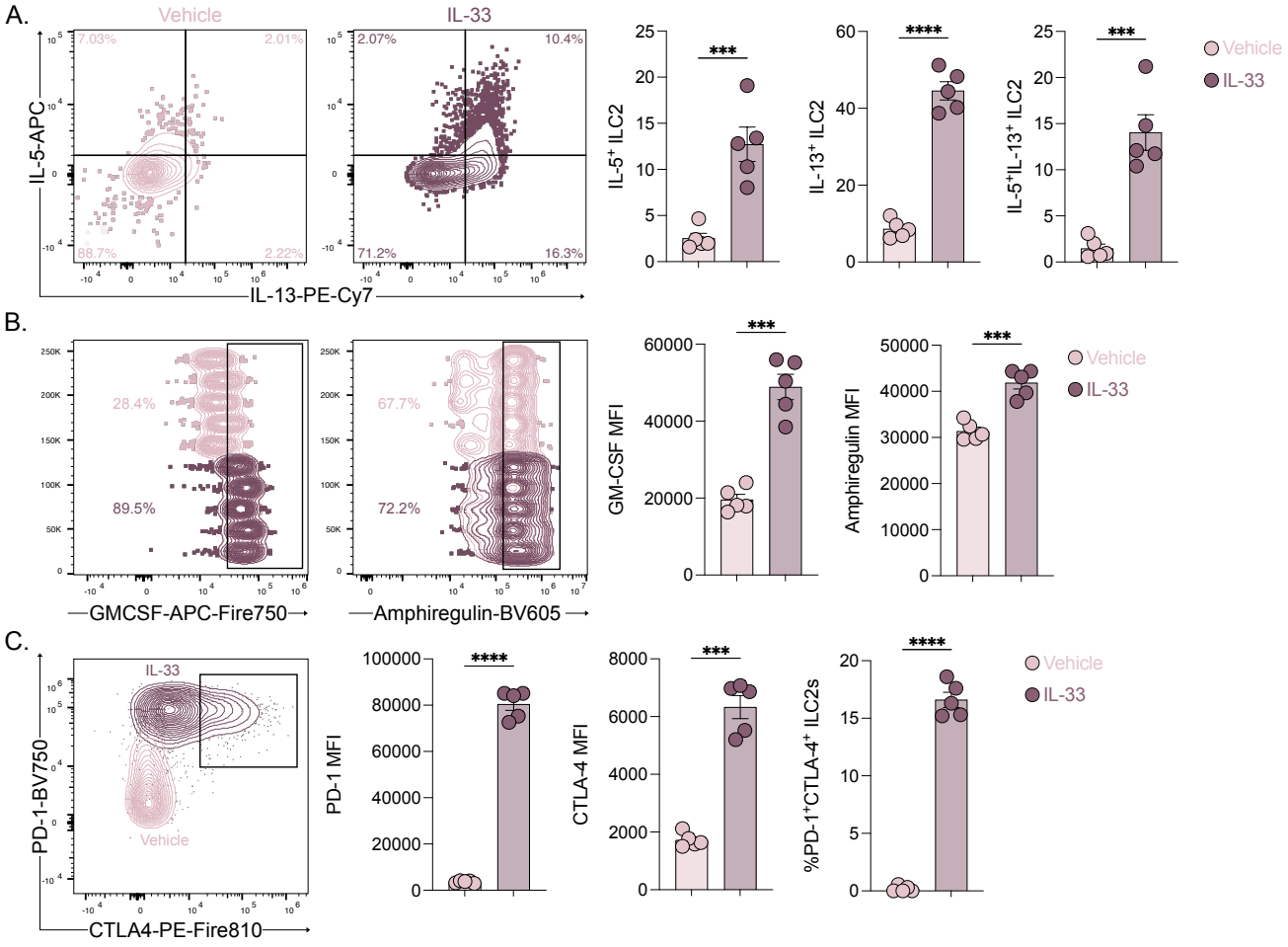

Figure 3.3: IL-33 increases expression of ILC2 effector molecules in the ovary. Female C57BL/6 mice were administered 500ng IL-33 or PBS vehicle control daily for five days. PBS or IL-33-treated ovaries were collected and stimulated ex vivo with PMA/ionomycin for 5 hours followed by intracellular flow cytometry staining. (A) Flow cytometry contour plots depicting IL-5 and IL-13 expression on ILC2s and frequencies of IL-5$^+$, IL-13$^+$, or IL-5+IL-13$^+$ ILC2s. (B) Flow cytometry contour plots and mean fluorescence intensity (MFI) of GM-CSF and amphiregulin intracellular staining in ILC2s. (C) Flow cytometry plots and corresponding MFI of PD-1 and CTLA-4 expression on ILC2s. Experiments depicted are representative of one performed. *N*= 5/group. Unpaired t test. *p<0.05, **p<0.01, ***p<0.001, ****p<0.0001.

Collectively, these data show that IL-33-stimulation leads to an enhanced ILC2 functional state, with the capacity to express key molecules associated with type 2 inflammation and tissue repair, including IL-5, IL-13, GM-CSF, and Areg (Graphical Abstract 1.1). Collectively, these cytokines induce tissue inflammation, which, in the ovary, may reflect tissue-specific roles, such as supporting ovulation.

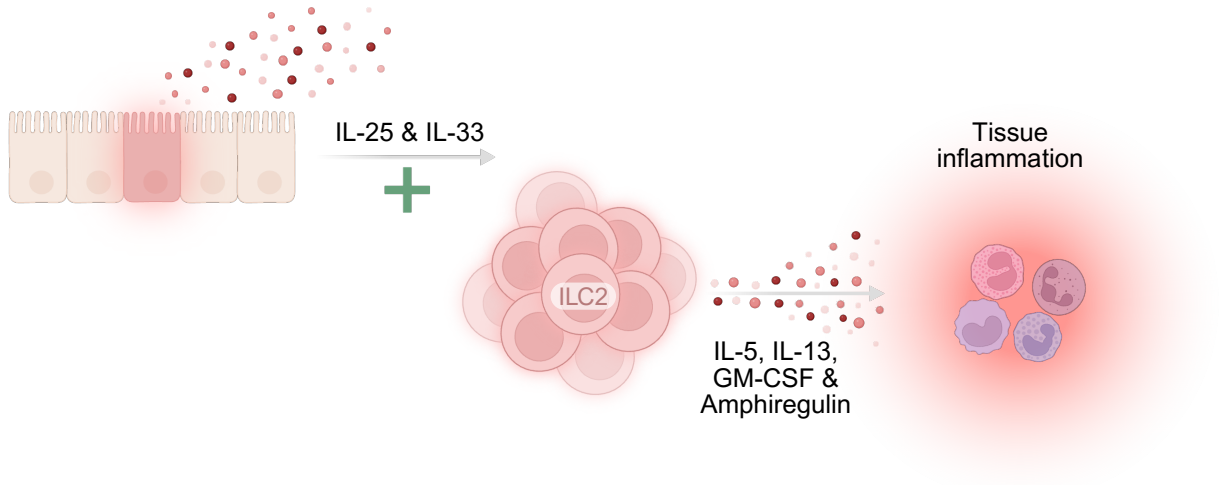

Graphical Abstract 1.1: Epithelial-derived cytokines activate ovarian ILC2s. IL-25 and IL-33 cytokines stimulate ovarian ILC2s, leading to their activation and proliferation. Activated ILC2s, express IL-5, IL-13, GM-CSF, and amphiregulin, collectively contributing to type 2 inflammatory environment.

3.4. ILC2-associated genes, *Areg* and *Il33*, are upregulated pre-ovulation

Ovulation, one of the ovary's most critical functions, is a well-established inflammatory event. ILC2s are key drivers of tissue inflammation and wound healing. As tissue resident cells in the ovary with the capacity to respond to tissue alarmins, we hypothesized that ovarian ILC2s may play a role in ovulation. Therefore, to contextualize the cytokine milieu of the ovary pre- and post-ovulation, we performed transcriptional analysis using the NanoString nCounter® platform to assess the inflammatory profile of each stage of the estrus cycle. The NanoString nCounter® platform is highly sensitive and allows for the precise quantification of genes from a customizable gene set. We constructed a 127 gene probe set that incorporated several cytokine and chemokine genes, as well as several ovulation-associated genes. To collect mouse ovaries at each stage of the estrus cycle, we leveraged the use of a superovulation model in rodents by administration of exogenous hormones. In a superovulation cycle, mice ovulate a greater number of oocytes in a time-predictable manner while allowing for estrus cycle synchronization. To this end, we administered pregnant mare's serum gonadotropin (PMSG) followed by human chorionic gonadotropin (hCG) i.p to prepubertal female mice 44 hours later to induce ovulation (Figure 3.4A). Ovaries were collected at various timepoints corresponding to proestrus, estrus, metestrus, and diestrus stages of the cycle (Figure 3.4A).

Analysis using the NanoString nCounter® technology revealed the top 20 differentially expressed genes between the pre-ovulatory (proestrus) and post-ovulatory (estrus) stage of the estrus cycle. Of note, expression of *Areg*, which encodes for amphiregulin, was found to be the most significantly down-regulated gene between proestrus and estrus (Figure 3.4B). Interestingly, gene expression analysis of individual cytokines revealed that *Il33* also decreased post-ovulation,

although expression of ILC2 effector genes, such as *Il5* and *Il13* remained unchanged throughout the estrus cycle (Figure 3.4C). Although this analysis limits us from delineating the cell source of gene expression, these data may implicate ILC2 biology during the estrus cycle. For example, peak transcriptional expression of *Areg* and *Il33* in proestrus, and its significant reduction post-ovulation during estrus, may indicate the presence of ILC2s during ovulation. Furthermore, these data may suggest the existence of an IL-33-ILC2-Areg axis in the ovary and provide the rationale to investigate its presence and role in maintaining ovarian homeostasis and ovulation.

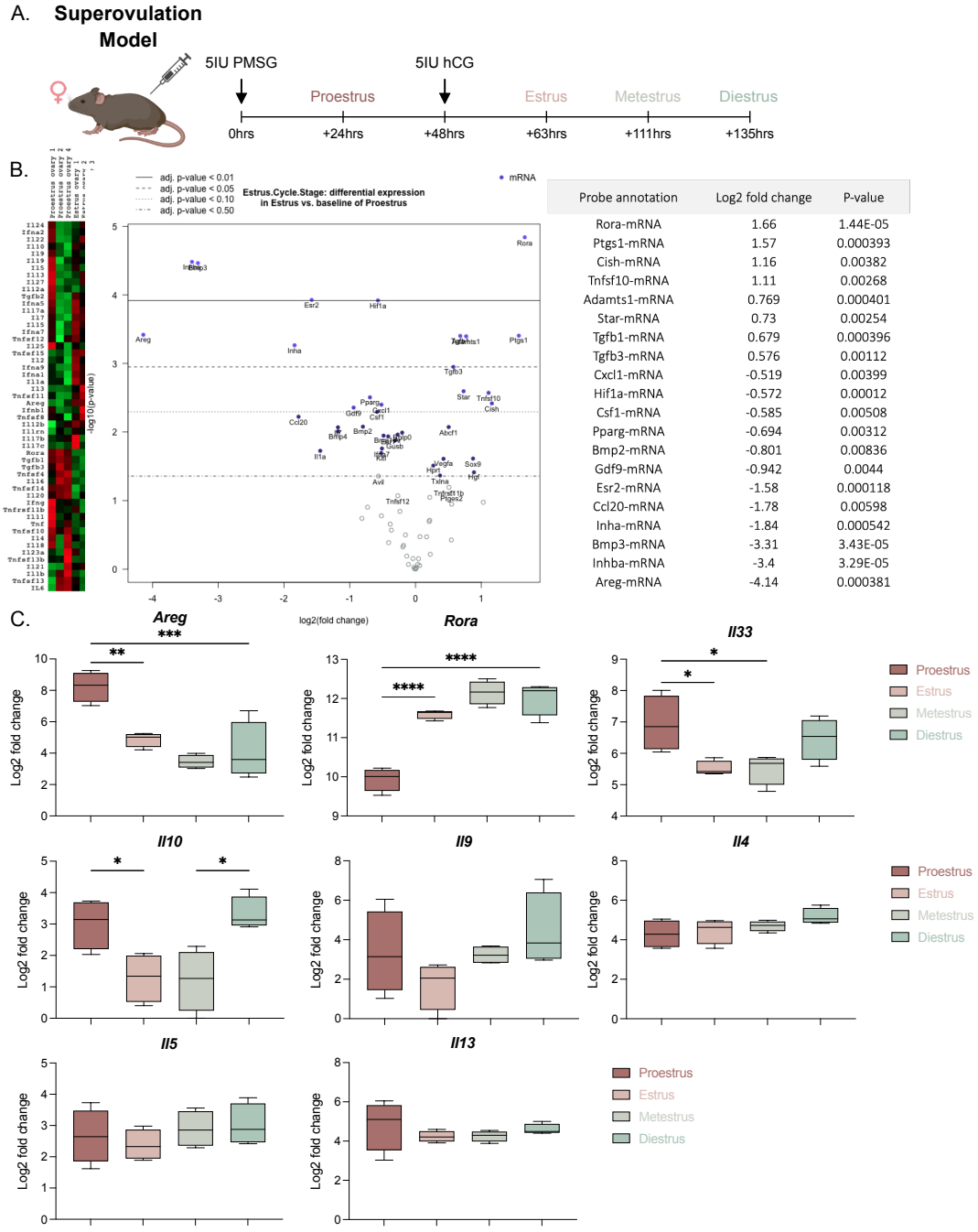

Figure 3.4: ILC2-associated genes, *Areg* and *Il33*, are upregulated pre-ovulation. (A) Immature female C57BL/6 mice were induced to superovulate with PMSG and hCG hormones. Ovaries were collected at each stage of the estrus cycle and total RNA was purified to perform gene expression analysis using NanoString nCounter® technology. (A) Top differentially expressed genes between proestrus (pre-ovulatory stage) and estrus (post-ovulatory stage) of the estrus cycle. (B) Gene expression of selected cytokines or factors during the estrus cycle. Data were normalized to housekeeping genes and presented as ± SEM. *N*=3/group. One-way ANOVA. *p<0.05, **p<0.01, ***p<0.001, ****p<0.0001.

3.5. ILC2s are abundant in the pre-ovulatory stage of the estrus cycle

Based on our phenotypic and functional characterization of mouse ovarian ILC2s, and our transcriptional analysis of mouse ovaries, we next sought to investigate the abundance of ILC2s through the progression of the estrus cycle. To this end, mice were superovulated and ovaries were collected at each stage of the estrus cycle for flow cytometry analysis (Figure 3.5A).

Ovarian ILC2s fluctuated between 2-3% of all leukocytes in line with our previous observations, and remained stable in numbers through estrus, metestrus, and diestrus stages of the estrus cycle. ILC2s were distinctly abundant in proestrus, the preovulatory stage of the estrus cycle (Figure 3.5B). Intriguingly, we observed a significant decrease in the frequency and number of ILC2s between proestrus and estrus phase (Figure 3.6C), following a similar pattern of expression for *Il33* and *Areg* observed in our transcriptomic analysis (Figure 3.4). As key mediators of tissue inflammation and wound healing, the observed changes in ILC2 abundance may indicate their possible role in the inflammatory response during ovulation.

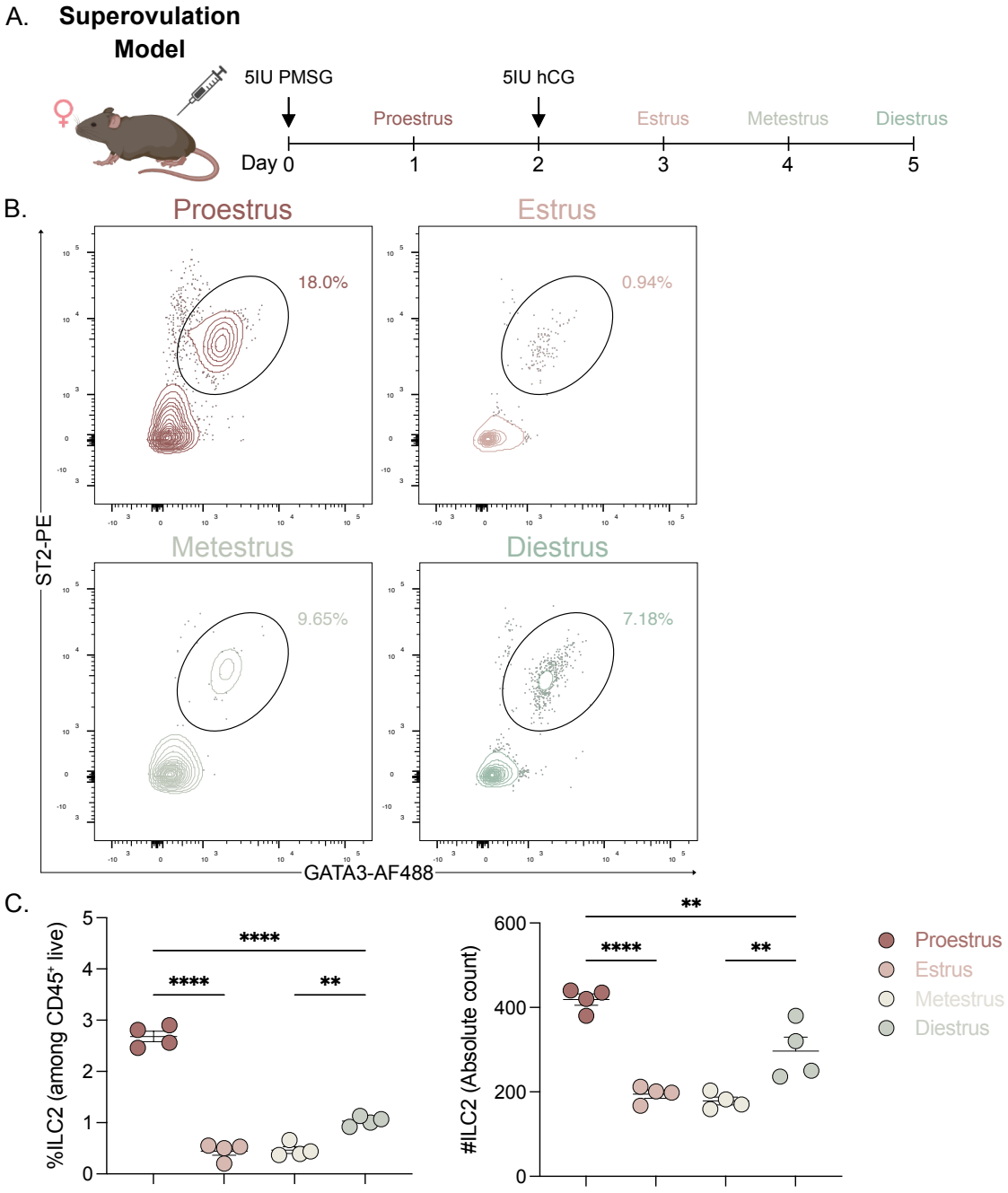

Figure 3.5: ILC2s are abundant during the preovulatory stage of the estrus cycle. (A) Prepubescent female C57Bl/6 mice were superovulated with i.p. injection of 5 IU pregnant PMSG then 5 IU hCG 44 hours later. Ovaries were collected at each stage of the estrus cycle for flow cytometry staining and analysis. (B) Flow cytometry contour plots and depicting ovarian ILC2s at each stage of the estrus cycle. (C) Frequency and absolute count of ILC2s in the ovary at each stage of the estrus cycle. Experiment depicted is representative of four performed. *N*=4/group. One-way ANOVA. **p<0.01, ***p<0.001, ****p<0.0001.

3.6. Aromatase inhibition restores ILC2 frequencies in superovulation cycles

The cyclic levels of steroidogenic sex hormones including 17β-estradiol, progesterone, and testosterone during the estrus cycle facilitate many reproductive functions, including follicular maturation, ovarian atresia, and ovulation. Levels of circulating estrogen peak during ovulation and decrease thereafter, paralleling the fluctuation of ILC2 frequencies in the ovaries. Based on these observations, we initially hypothesized that ovarian ILC2s were positively regulated by estrogen, as previously described in uterine ILC2s (*89, 90*).

To investigate the hormonal regulation of ovarian ILC2s, we treated immature female C57BL/6 mice with an aromatase inhibitor, letrozole, then induced them to ovulate with PMSG and hCG hormones (Figure 3.6A). Letrozole blocks the aromatase enzyme which converts testosterone into estrogen, the rate-limiting step of estrogen biosynthesis (Figure 3.6B). In control mice, levels of ILC2 significantly decreased in the estrus phase, in line with our previous observations (Figure 3.5). However, this effect was abrogated in mice treated with letrozole, with a slight upwards trend in ILC2 frequencies in the transition to estrus (Fig. 3.6C). Therefore, by blocking estrogen production, ILC2 levels in the post-ovulatory stage remain stable, suggesting that estrogen may suppress ILC2 levels in the ovary. Alternatively, the buildup of testosterone, which occurs when letrozole effectively blocks its conversion to estrogen, may also contribute to this observed effect.

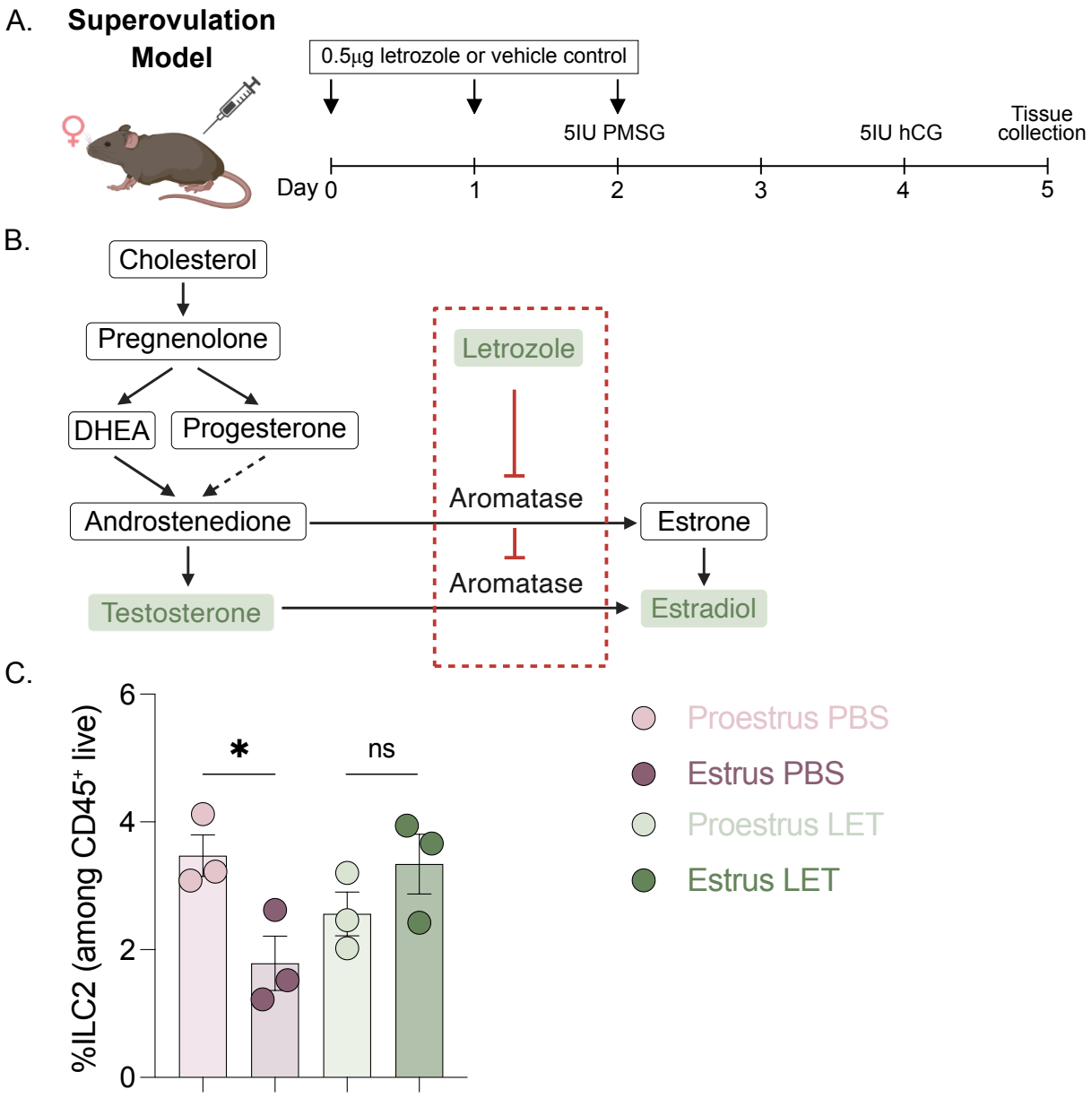

Figure 3.6: Aromatase inhibition restores ILC2 frequencies in superovulation cycles. (A) C57BL/6 mice were administered letrozole (LET) once daily for 3 days and were induced to superovulate with 5IU PMSG and 5IU hCG. (B) schematic depicting the estrogen biosynthesis pathway and letrozole's mechanism of action. (C) Frequencies of ILC2s in the transition from proestrus to estrus in superovulated mice treated with PBS or letrozole. Experiment depicted is representative of two performed. *N*= 3/group. (B) Unpaired t test. **P* < 0.05.

3.7. Androgen signalling regulates ILC2 abundance in the ovary

Hormonal regulation, particularly through androgen signalling, has been reported to attenuate ILC2 function in mouse models of airway inflammation (*91-93*). Analysis of single-cell RNA sequencing previously generated in the Vanderhyden lab revealed that ovarian ILC2s express high levels of the androgen receptor, but not estrogen and progesterone receptors (Figure 3.7A). This data provides an important clue for the hormonal regulation of ovarian ILC2s and offers a potential explanation for our earlier observation that elevated levels of testosterone, resulting from letrozole-mediated aromatase inhibition, may regulate ILC2 abundance in the ovary.

Thus, we hypothesized that androgen signalling positively regulates ILC2 levels in the ovary. To this end, we treated female mice with an androgen antagonist, flutamide, and collected ovaries to assess ILC2 levels using flow cytometry (Figure 3.7B). As a control, we collected lungs where the role of androgen signalling in negatively regulating ILC2 in the lungs in the context of allergic asthma has been well-established. Whereas flutamide treatment led to an increase in lung ILC2s, we observed a ~50% reduction in the number and frequency of ILC2s in the ovaries (Figure 3.7C). These data provide further evidence that androgen signalling positively regulates ILC2 numbers in the mouse ovary.

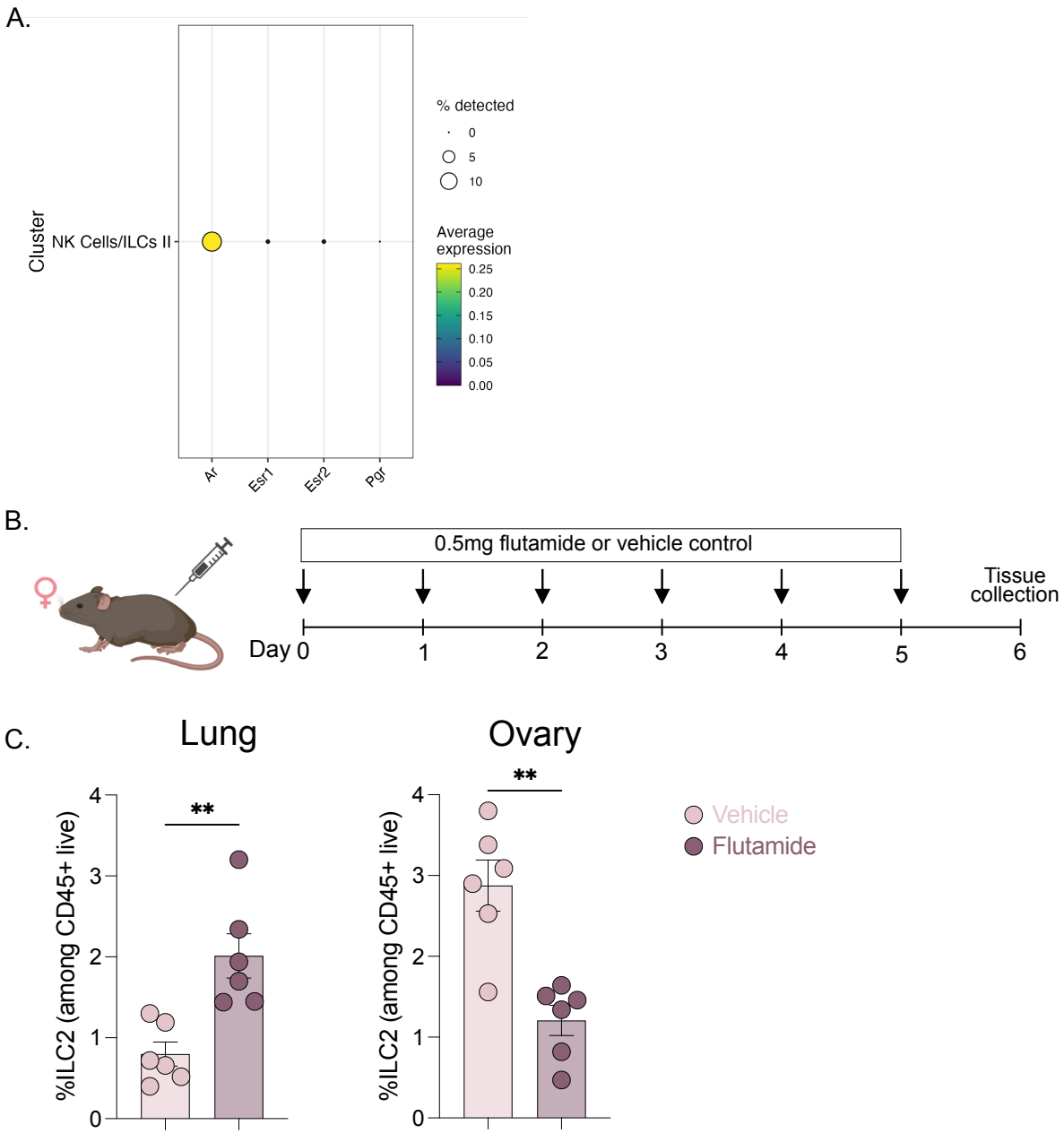

Figure 3.7: Androgen signalling regulates ILC2 levels in the ovary. (A) Androgen receptor (Ar) is highly expressed on ovarian ILC2s. (B) Female C57BL/6 mice were treated with 0.5mg of flutamide daily for six days followed by tissue collection and flow cytometry staining and analyses. (C) Androgen signalling inhibition by flutamide increased ILC2 frequencies in the lung, but decreased ILC frequencies in the ovary. Experiment depicted is representative of two performed. *N*= 6/group. (B) Student's *t* test. $^{**}P < 0.01$.

Thus far, we have identified ILC2s in the mouse ovary, which represent 2-4% of total leukocytes, and broadly characterized their phenotypic and functional properties. Given the tissue-specific nature of ILC2s, we next performed transcriptional profiling of the mouse ovary to better define the inflammatory environment across the stages of the estrus cycle. This analysis revealed that *Il33* and *Areg*, genes associated with ILC2 biology, were highly expressed during the pre-ovulatory stage of the estrus cycle and significantly decreased post-ovulation. Consistent with this pattern, ILC2s were most abundant during the pre-ovulatory stage of the estrus cycle and contracted significantly thereafter. We also investigated an additional layer of hormonal regulation of ovarian ILC2s and found that these cells express high levels of the androgen receptor, and pharmacological inhibition of this receptor reduced ILC abundance in the ovary (Graphical Abstract 1.2). Building on these findings describing the phenotype, function, and regulation of ovarian ILC2s, we next sought to uncover their role in ovarian health and disease. More specifically, we aimed to investigate the role of ILC2s in ovulation and in a model of mouse polycystic ovarian syndrome (PCOS).

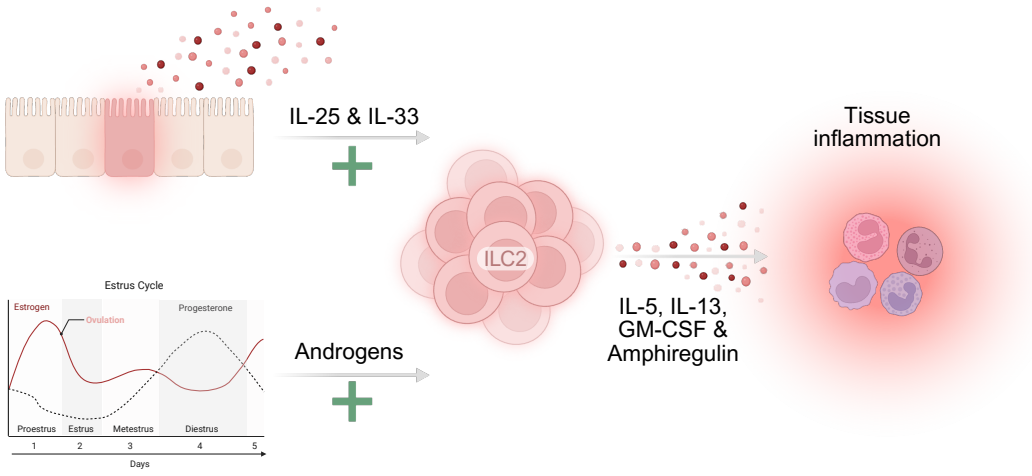

Graphical Abstract 1.2: Cytokine and hormonal regulation of ovarian ILC2s. Epithelial derived cytokines and androgen signalling positively regulates ILC2 abundance in the ovary.

3.8. The IL-33 receptor is localized to the periphery of oocytes

Given the high and transient expression of *Il33* during proestrus, we next assessed the spatial localization of its receptor, ST2, within the ovarian architecture. Ovaries were isolated from mice 14-hours post-hCG to capture the expression pattern of ST2 in the peri-ovulatory stage of the estrus cycle using immunofluorescence. We found a specific, localized expression of ST2 around the perimeter of oocytes, and was evident in mature ovulating follicles as well as primary and secondary follicles (Figure 3.8). This finding suggests that ST2 expression in the mouse ovary follows a localized and organized pattern that does not appear to originate from ILC2s, however this warrants further investigation using multiplex imaging techniques. Together, these data suggest that IL-33 signalling is intricately tied to the developing oocyte, where ILC2s may be involved.

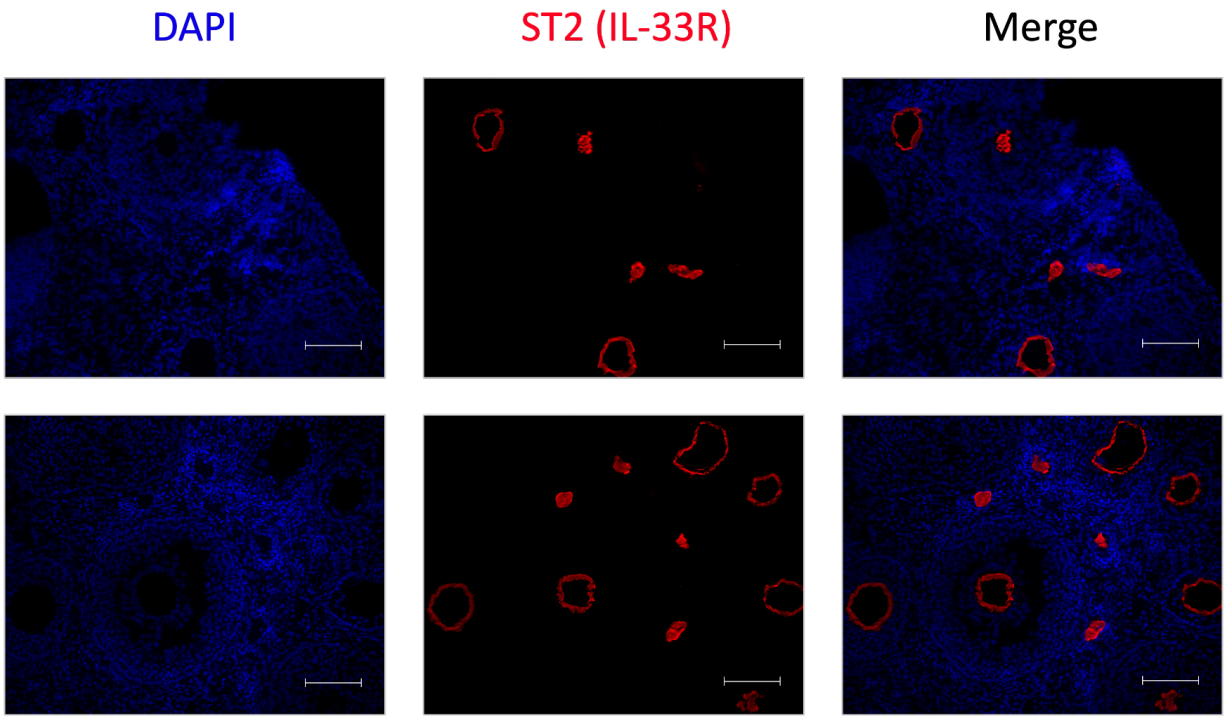

Figure 3.8: Ovarian ST2 (IL-33R) expression is localized at the periphery of oocytes. Prepubertal female mice were induced to superovulate by i.p. administration of 5IU PMSG followed by 5IU hCG 48 hours later. Mouse ovaries were collected 14-hours post-hCG administration and stained for ST2 (red), and counterstained with Hoechst for immunofluorescence imaging. IL-33R localization is restricted to the periphery of oocytes in follicles at various stages of development. Scale bars, 50μm.

3.9. IL-33R (ST2) blockade reduces ovulation efficiency

Thus far, our findings show ILC2s are most abundant in the ovaries during the pre-ovulatory stage of the estrus cycle and significantly decrease thereafter. In parallel to this, we observed transient and high expression of *Il33* at the proestrus stage of the estrus cycle, and that the IL-33 receptor ST2 is localized to the periphery of the oocyte. These data implicate an IL-33-ST2 axis in ovulation, potentially involving ILC2s. We therefore investigated whether blocking IL-33-ST2 signalling affects ovulation by measuring the number of MII oocytes recovered from the oviduct as a direct readout of ovulation efficiency. To this end, we treated $Rag1^{-/-}$ (Rag1 KO) mice, which lack adaptive immune cells, with anti-ST2 or IgG1 k isotype control once daily for 2 days and subsequently superovulated the mice with PMSG and hCG (Figure 3.9A). $Rag1^{-/-}$ mice were used to eliminate potential confounding effects from adaptive immune cells, such as Th2 cells, which may respond intrinsically to ST2 blockade. MII ovulated oocytes were isolated from oviducts 16-hours post-hCG injection and were enumerated (Figure 3.9A).

On average, mice in the C57Bl/6 background ovulate 26-40 oocytes in a superovulation cycle, which we found to be similar in $Rag1^{-/-}$ mice (Figure 3.9B). Under ST2 blockade, we observed a significant impairment in ovulation, with approximately 50% reduction in ovulated oocytes compared to isotype controls (Figure 3.9C). Our data corroborates another study where Carlock et al. found that neutralization of IL-33 in female mice induced to superovulate led to a reduction in oocyte number but did not prevent ovulation (*39*). Whether ILC2s contribute to this abrogated effect is still under active investigation, and will be addressed in future studies using ILC2 deficient mice. Together, these data indicate that IL-33 signalling plays an important role in supporting ovulation in mice.

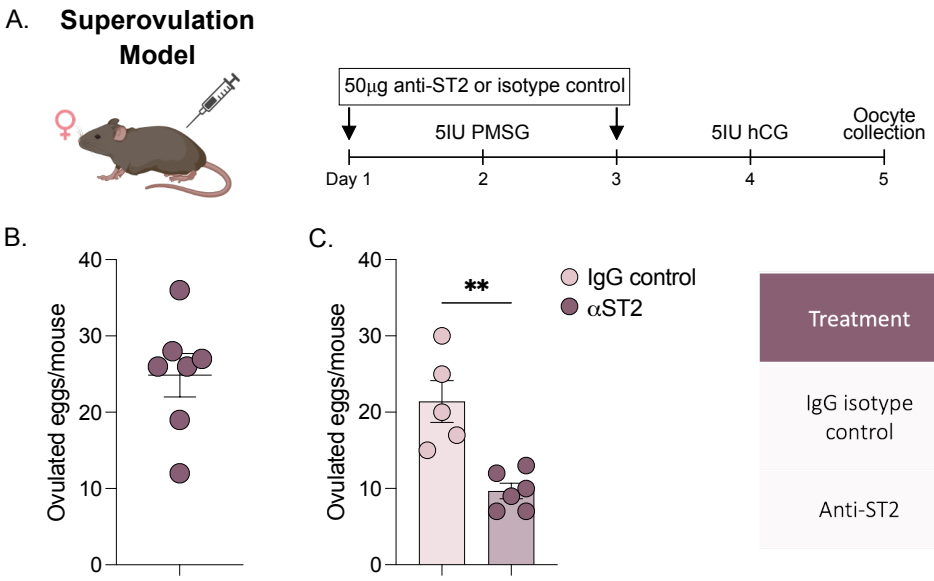

Treatment	Average # of ovulated MII oocytes
IgG isotype control	22
Anti-ST2	10

Figure 3.9: ST2 blockade reduces ovulation efficiency. (A) C57Bl/6 mice were administered i.p. injections of 50 μg αST2 or isotype control once daily for two days. Mice were subsequently induced to superovulate by i.p. administration of 5 IU PMSG followed by 5 IU hCG 48 hours later. (B) Average number of ovulated oocytes per C57Bl/6 mouse in a superovulation cycle. (C) Number of ovulated oocytes in mice treated with ST2 blockade compared to isotype control. Experiment depicted is compiled from two independent experiments. N=5–6/group. Student's t test. $^{**}P < 0.01$.

3.10. Testing the role of ILC2s in a PCOS model

ILC2s are important regulators of tissue inflammation at steady state, but can also contribute to the immunopathology of several diseases associated with inflammation and fibrosis (*94-96*). Polycystic ovarian syndrome (PCOS) is a condition characterized by ovarian cysts, hyperandrogenism, and low-grade inflammation (*97*). Despite the clear link between PCOS and low-grade inflammation, the immunological basis of PCOS remains unclear with some reports indicating a link between pro-inflammatory markers and immune dysfunction (*98*).

Given our findings that ovarian ILC2s highly express the androgen receptor, and their known role in fibrosis, we hypothesized that androgen-responsive ILC2s contribute to the pathogenesis of PCOS by promoting tissue inflammation. To this end, we leveraged the use of a mouse model of PCOS that involves the implantation of a slow-release letrozole pellet (*99*). Letrozole blocks the aromatase enzymes thereby preventing the conversion of androgens into estrogens (Figure 3.6 schematic), and creating a hyperandrogenic environment. The administration of a continuous slow-release letrozole pellet in mice has been reported to lead to the formation of ovarian cysts, acyclic estrus cycles, and dysregulated hormone levels including elevated testosterone and luteinizing hormone (LH) and decreased estradiol levels (*99, 100*). This mouse model of PCOS is clinically relevant as it recapitulates many of the metabolic features of PCOS including obesity, increased fat mass, and elevated basal glucose levels and impaired glucose tolerance (*101*).

At 4 weeks of age (pre-pubertal), female mice were subcutaneously implanted with letrozole (LET) (50μg/day) or vehicle control 60-day continuous release pellet (Figure 3.10A). Body weight was monitored weekly, and insulin and glucose tolerance tests was done to confirm the

development of PCOS (Figure 3.10B). Mice were collected at week 6, and ovaries were collected for flow cytometry staining and analysis. In our flow cytometry analysis, we observed no differences in immune cell subsets, with a slight trending increase in ILC2s, however this was not statistically significant (Fig 3.10C). Current and future investigations will optimize the establishment of this model in our lab and then determine if ILC2 abundance and frequency is altered in this model.

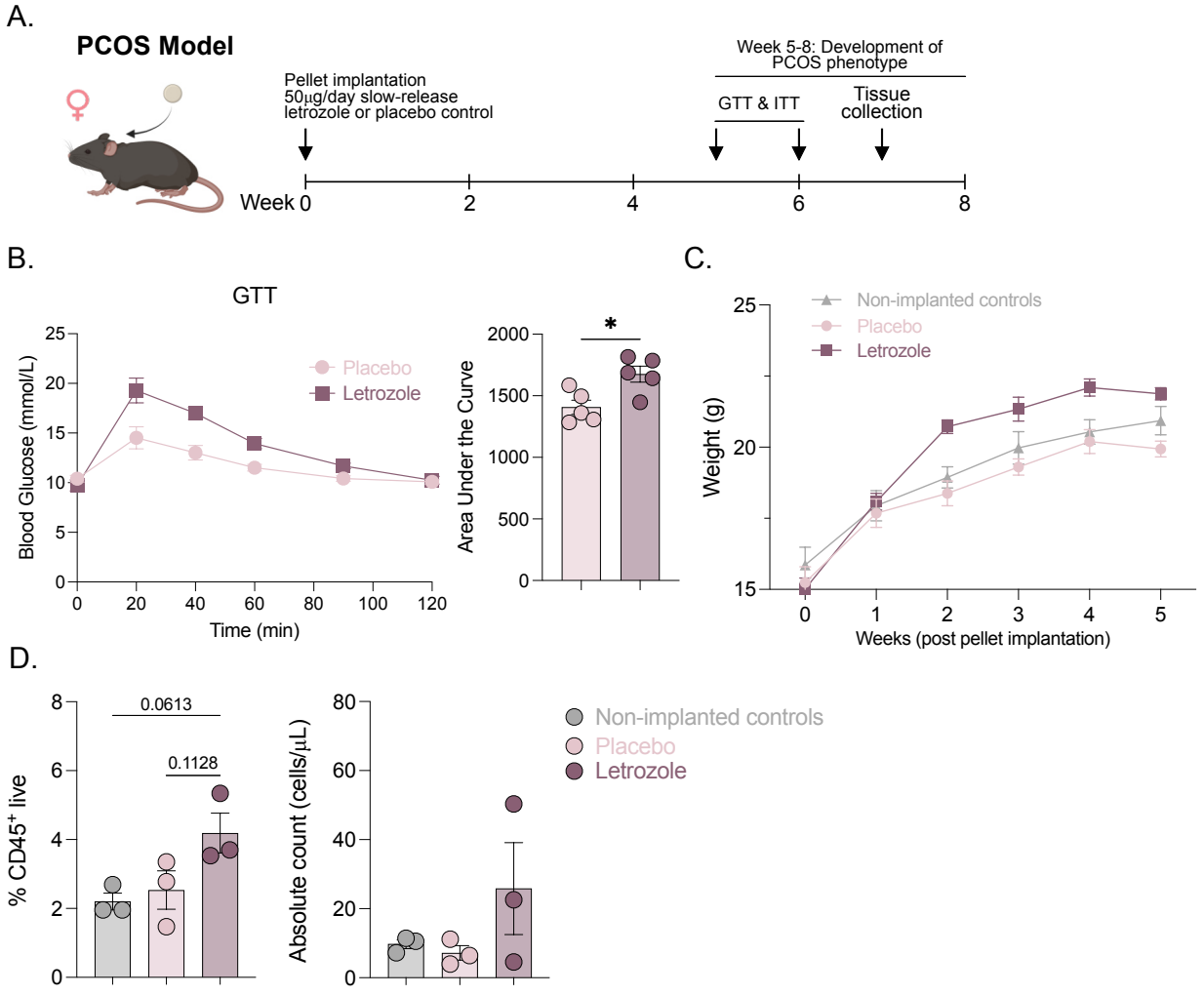

Figure 3.10: ILC2s may increase in abundance in a mouse PCOS model. (A) Female C57Bl/6 mice were subcutaneously implanted with placebo or letrozole slow-release pellets to generate a PCOS mouse model. (B) Diagnostic GTT and weight measurements indicate metabolic dysfunction in letrozole mice. (C) Frequency and absolute counts of ILC2s in mice implanted with placebo or letrozole pellets. Experiment depicted is representative of 2 performed. Data presented as ± SEM. *N*=3/group. One-way ANOVA. *p<0.05.

Together, we identified ILC2s in the mouse ovary and found that these cells are a dynamic population regulated by epithelial-derived cytokines and steroid hormone signalling (Graphical Abstract 1.3). Phenotypic and functional analyses revealed that these cells are highly responsive to IL-33 and androgen signalling, with potential roles in ovulation and PCOS. Although the precise role of ovarian ILC2s in these contexts remains to be fully elucidated, our work provides a novel and foundational characterization of this population.

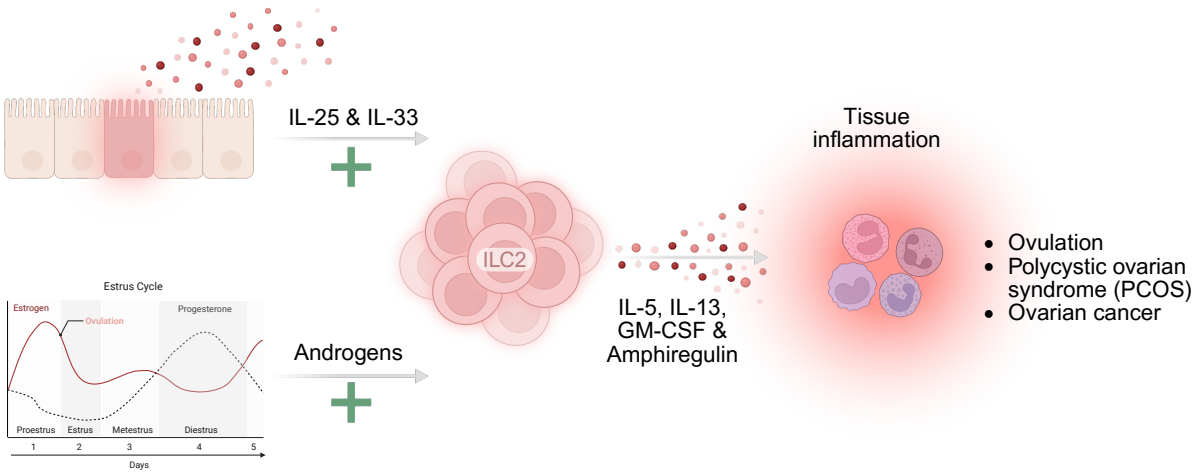

Graphical Abstract 1.3: Epithelial-derived cytokines activate ovarian ILC2s. IL-25, IL-33, and androgens increase ILC2 abundance in the ovary. Upon activation, ILC2s proliferate, and express canonical type 2 molecules, IL-5, IL-13, GM-CSF, and amphiregulin, leading to tissue inflammation. ILC2-driven type 2 inflammation may have important implications in ovulation, PCOS, or ovarian cancer.

Chapter 4

Harnessing ILC2s for immunotherapy in ovarian cancer

4. Harnessing ILC2s for immunotherapy in ovarian cancer

4.1. Introduction and rationale

In recent years, an increasing body of literature has implicated ILC2s in cancer, albeit with conflicting reports regarding their pro- or anti-tumoral roles across different models. Depending on the context, ILC2s can coordinate with other immune cells to actuate anti-tumoral responses or maintain a tumor permissive environment. The functional duality and tissue specificity of ILC2s in cancer emphasizes the need to expand our study of ILC2s in other tumor settings, such as ovarian cancer.

Having identified ILC2s in the naïve mouse ovary, we next sought to extend our studies to ovarian cancer, where the role of ILC2s remain undefined. Earlier, we observed that ovarian ILC2s highly upregulate PD-1 on their cell surface upon IL-33 stimulation (Figure 3.3), thus positioning ILC2s as potential cellular targets for αPD-1 therapy. Based on this observation, we hypothesized that IL-33+αPD-1 combination treatment will provide enhanced therapeutic efficacy by simultaneous activation and disinhibition of ILC2s to unlock their full anti-tumor potential. Checkpoint blockade, including αPD-1 therapy, have historically shown poor responses in clinical and preclinical models of ovarian cancer, likely due to an immunosuppressive, and immunologically "cold" tumor microenvironment. We therefore hypothesized that IL-33 will sensitize ovarian tumors to αPD-1 therapy by converting immunologically "cold" tumors to a more inflamed, "hot" state.

4.2. Ovarian tumor-infiltrating ILC2s respond to IL-25 and IL-33 stimulation

To investigate the presence and responsiveness of ILC2s in ovarian cancer, we leveraged the use of a clinically relevant mouse model of ovarian cancer. To this end, we injected ID8*Trp53*$^{-/-}$*Brca1*$^{-/-}$ mouse ovarian cancer cells under the ovarian bursa of C57Bl/6 female mice. This ovarian orthotopic model forms small primary tumors that aggressively metastasize to the peritoneal cavity and omentum (*102*), recapitulating key clinical features of ovarian cancer, such as peritoneal metastasis and ascites accumulation. Moreover, orthotopic implantation of tumor cells is essential to our goal of studying tissue-specific ILC2s in their original anatomical location. Following tumor inoculation, mice were treated with IL-25 or IL-33, to establish the presence and responsiveness of ILC2s to these cytokines (Figure 4.1A). In some mice, tumor cells were injected unilaterally to assess whether tumor-infiltrating ILC2s respond differently or acquire distinct characteristics from ovarian ILC2s within the same biological setting. Following cytokine treatment, tumors, ovaries, lungs, and peritoneal lavages were collected and processed for flow cytometry analysis.

ILC2s were present in primary tumors, representing 2-4% of all leukocytes (Figure 4.1B), in frequencies similar to what was observed in normal lung and ovarian tissue. In the ovaries, lung, and tumors, IL-25 had a modest effect on ILC2 abundance, however, IL-33 robustly expanded ILC2s across all tissues, with nearly a 10-fold expansion in the tumor (Figure 4.1C). Thus, in the ID8*Trp53*$^{-/-}$*Brca1*$^{-/-}$ orthotopic model, we confirmed the presence of ILC2s and observed a robust expansion in response to IL-33, but not IL-25, stimulation. This preferential responsiveness to IL-33 was also observed in the lungs and ovaries, indicating shared attributes of ILC2s across these tissues.

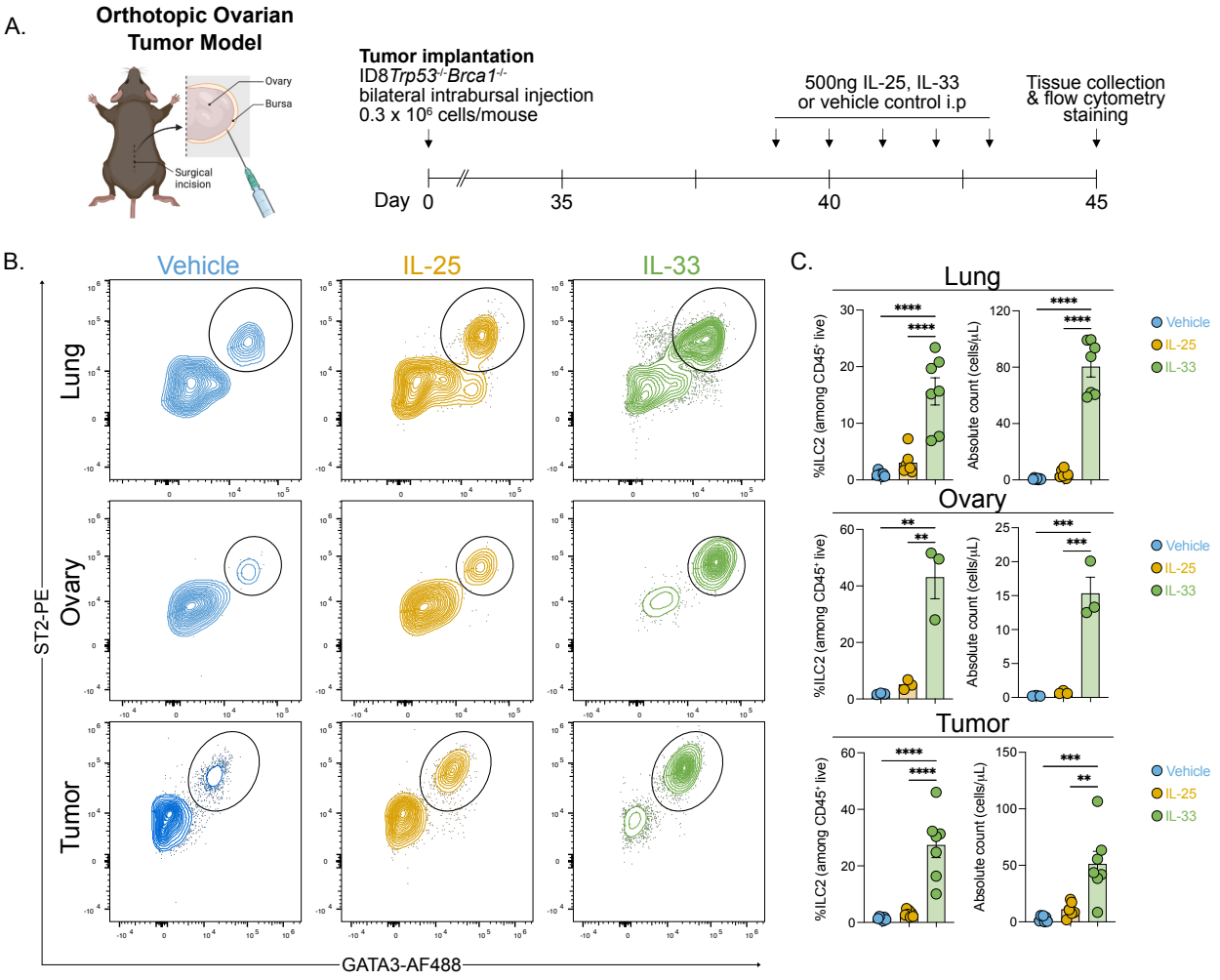

Figure 4.1: ILC2s in ovarian tumors are activated by IL-25 and IL-33. (A) 0.3x10^6 ID8*Trp53*$^{-/-}$*Brca1*$^{-/-}$ syngeneic cells were intrabursally injected to form orthotopic tumors. Mice were subsequently treated with 500ng of IL-25, IL-33 or PBS vehicle control daily for five days and on day 45, tumors, ovaries, lung, and peritoneal lavage was collected for flow cytometry staining and analyses. (B) Flow cytometry plots depicting abundance of ILC2s in response to IL-25 and IL-33 across several tissues and (C) frequencies and absolute number of ILC2s. Data presented as ± SEM. *N*=3-7/group. One-way ANOVA. *p<0.05, **p<0.01, ***p<0.001, ****p<0.0001.

4.3. Activated intratumoral ILC2s co-express checkpoint receptors PD-1 and CTLA-4

Beyond the canonical activation markers, IL-33 activation of ILC2s also induces PD-1 expression, which functionally constrains ILC2 proliferation and secretion of Th2 cytokines (*23, 103*). We also observed that tumor-infiltrating ILC2s expressed moderate levels of PD-1 at baseline, however, upon stimulation with IL-25 and IL-33, ILC2s co-expressed the checkpoint receptors PD-1 and CTLA-4 (Figure 4.2A). In IL-33-treated tumors, ILC2s emerged as the highest-expressing cells for PD-1 among other lymphocytes including $CD8^+$ and $CD4^+$ T cells (Figure 4.2B). On the other hand, IL-25 induced higher expression of CTLA-4 on ILC2s compared to IL-33, providing a rationale for investigating the combination treatment of IL-25+αCTLA-4 in this tumor model. These findings further validate ILC2s as potential immunotherapeutic targets for PD-1 checkpoint blockade. This is a significant distinction, as it challenges the long-standing dogma that T cells are the main targets for checkpoint blockade therapy.

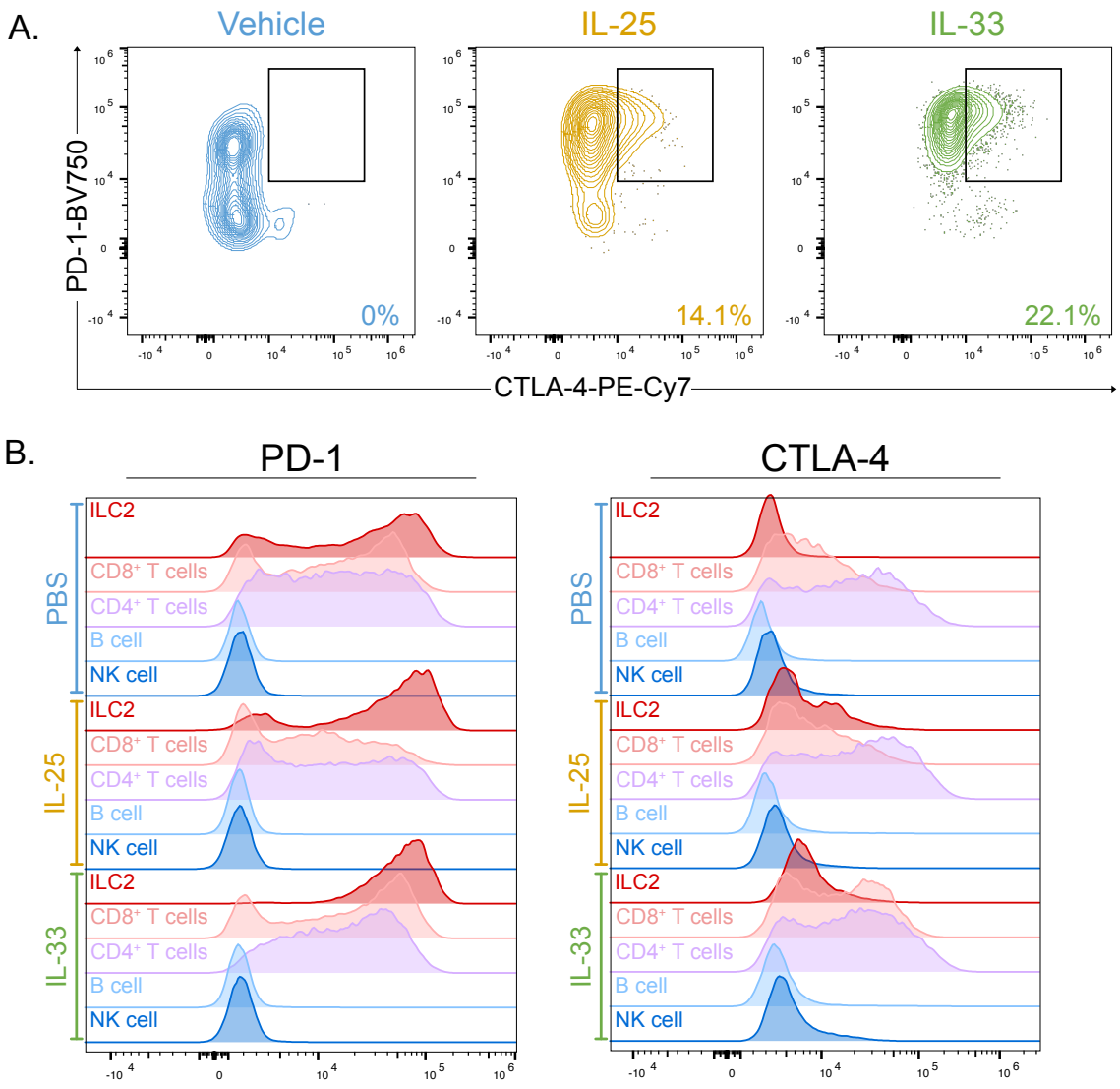

Figure 4.2: Activated tumor ILC2s co-express checkpoint receptors PD-1 and CTLA-4. $0.3x10^6$ ID8*Trp53*$^{-/-}$*Brca1*$^{-/-}$ syngeneic cells were intrabursally injected to form orthotopic tumors. Mice were subsequently treated with 500ng of IL-25, IL-33 or PBS vehicle control daily for five days and on day 45, tumors, were collected and stained for flow cytometry analysis. (A) Flow cytometry contour plots depicting tumor ILC2 co-expression of PD-1 and CTLA-4. (B) Expression of PD-1 and CTLA-4 in PBS, IL-25, or IL-33-treated mice across several immune cell types.

4.4. ILC2 are present in the peritoneal ascites fluid as distinct subpopulations

In ovarian cancer, ascites – the abnormal buildup of fluid in the abdomen – is a sign of advanced and metastatic stages of cancer. This fluid contains disseminated immune cells that can remodel the tumor microenvironment and influence treatment response and disease outcomes (*102, 104*). Given that ILC2s are largely tissue-resident cells and rarely detected in circulation or bodily fluids, we became interested in determining if ILC2s were present in the ascites fluid. In ID8*Trp53*$^{-/-}$ *Brca1*$^{-/-}$ tumor-bearing mice, ILC2s represented 2-4% of all leukocytes in the ascites; however, following IL-25 or IL-33 treatment, these cells expanded to comprise 20-30% of all leukocytes, representing a 30-90-fold increase in absolute numbers (Figure 4.3A).

In response to IL-25 and IL-33 stimulation, ovarian ILC2s uniquely separated into distinct ST2^{dim}GATA3^{dim} and ST2^{bright}GAT3^{bright} subpopulations (Figure 4.3B). Delineation of these peritoneal ILC2 subpopulations revealed variegated expression of checkpoint receptors PD-1 and CTLA-4 (Figure 4.3B). The ST2^{bright}GAT3^{bright} ILC2 subpopulation in the ascites had higher expression of PD-1, KLRG1, and Ki67, while the ST2^{dim}GATA3^{dim} subpopulation distinctively had higher expression of CTLA-4. The presence of inducible ILC2 subpopulations has been reported in the literature, specifically IL-25-induced inflammatory ILC2s (iILC2s) (*86*). Distinct from natural ILC2s (nILC2s) that respond to IL-33 and are present at steady state, iILC2s arise under inflammatory conditions such as IL-25 stimulation or helminth infection, where they migrate from the gut to distal sites of inflammation in the body (*105*). Inflammatory ILC2s are ST2$^{lo/-}$ and KLRG1^{hi} while nILC2s are ST2^{+}KLRG1^{int} (*22*). However, based on our analyses, we cannot conclusively determine whether the populations we observed correspond to the subsets

described in the literature. Moreover, it remains unclear whether these cells expand locally or are also recruited from hematopoietic sources or the gut.

Together, these data show that ILC2s accumulate in primary ovarian tumors and disseminate in the peritoneal cavity during metastatic spread, which is further amplified by IL-25 or IL-33 stimulation. Notably, these activated ILC2s highly express the checkpoint receptors CTLA-4 and PD-1, positioning them as promising cellular targets for checkpoint blockade therapy (Graphical Abstract 2.1).

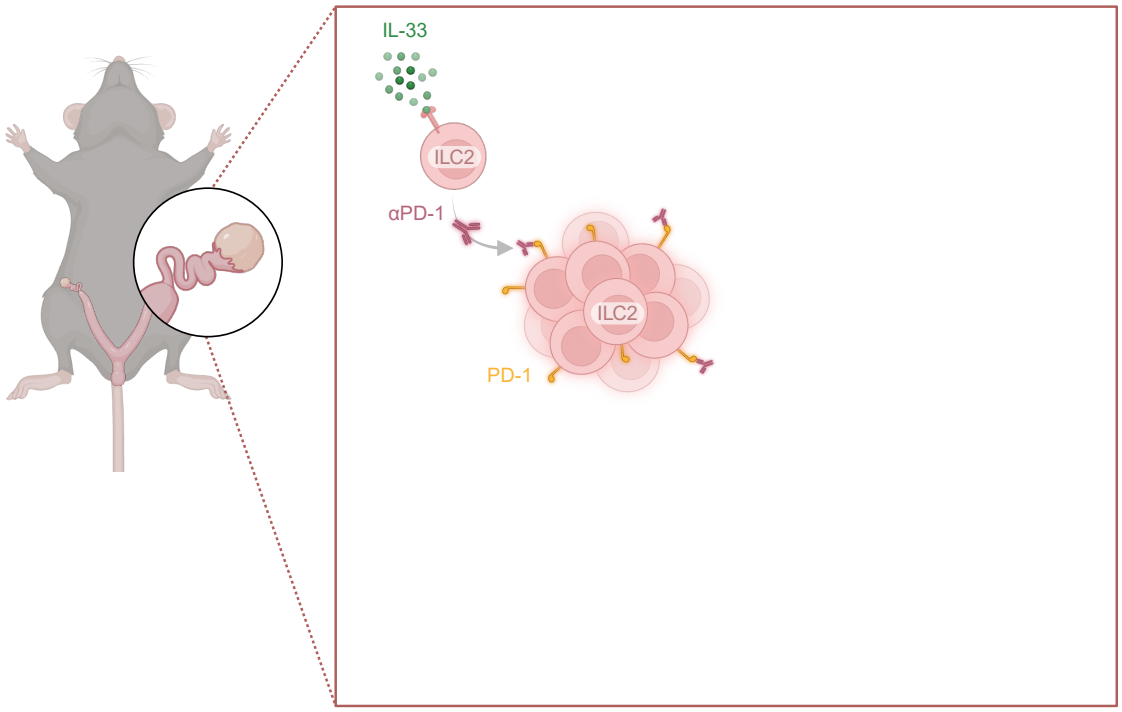

Graphical Abstract 2.1: Tumor-infiltrating ILC2s accumulate in mouse orthotopic tumors. IL-33 stimulation robustly simulates ILC2s, leading to their activation, proliferation, and increased expression of checkpoint receptor PD-1.

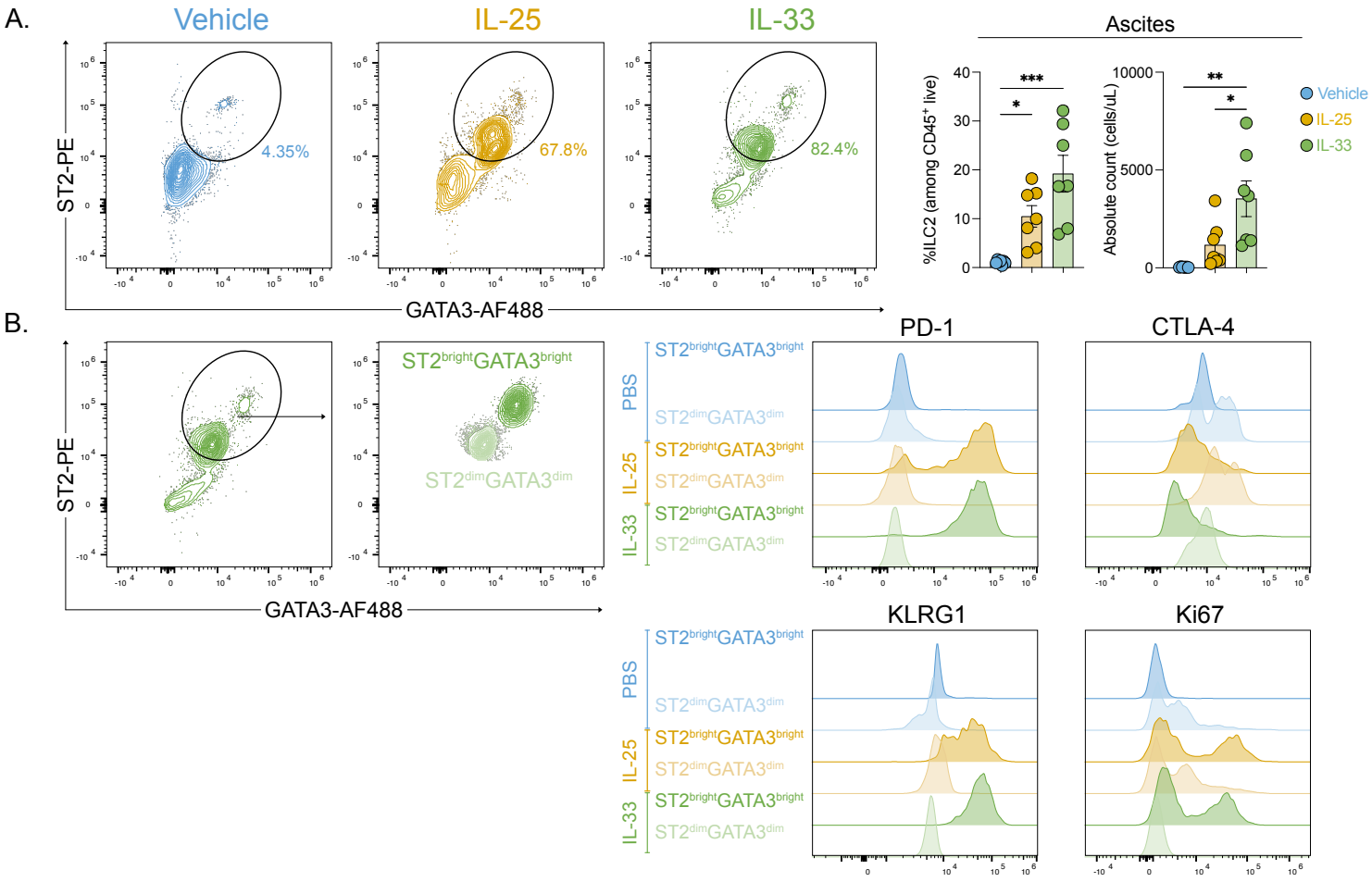

Figure 4.3: ILC2 are present in the peritoneal ascites fluid in distinct subpopulations. $0.3x10^6$ ID8*Trp53*$^{-/-}$*Brca1*$^{-/-}$ syngeneic cells were intrabursally injected to form orthotopic tumors. Mice were subsequently treated with 500ng of IL-25, IL-33 or PBS vehicle control daily for five days and on day 45, tumors, were collected and stained for flow cytometry analysis. (A) Flow cytometry contour plots depicting ascitic ILC2s and corresponding frequencies and absolute counts. (B) Flow cytometry contour plots depicting delineation of ILC2 subpopulations and their expression of various markers on histogram plots. Data presented as ± SEM. *N*=7/group. One-way ANOVA. *p<0.05, **p<0.01, ***p<0.001.

4.5. IL-33 treatment improves the therapeutic efficacy of PD-1 blockade.

To determine the therapeutic efficacy of IL-33+αPD-1 therapy, we employed the ID8*Trp53*$^{-/-}$ *Brca1*$^{-/-}$ orthotopic model, which has previously shown limited sensitivity to αPD-1 therapy (*106, 107*). Following orthotopic tumor implantation, mice were treated with daily i.p. injections of IL-25 or IL-33 for 7 days, then every 2 days thereafter, followed by 250μg αPD-1, αCTLA-4 or vehicle control every day for 5 days (*65*) (Figure 4.4A).

Treatment of IL-25 alone provided no therapeutic benefit (median survival 60d.) compared to untreated controls (median survival 64d.) (Figure 4.4B). As we observed earlier, IL-25 stimulation had a limited effect on the expansion of ILC2s in this model (Figure 4.1B). Moreover, IL-25 has been reported to drive an immunosuppressive ILC2 program via an IL-25-ILC2-MDSC circuit in colorectal cancer (*51*), which may explain the survival outcome observed here. Treatment with αCTLA-4 alone, or in combination with IL-25 also provided no therapeutic benefit. These findings indicate that IL-25 does not offer any therapeutic potential, and furthermore, IL-25 does not sensitize the tumor microenvironment to CTLA-4 therapy, as we also hypothesized. Conversely, but in line with clinical data (*108*), treatment with IL-33 or αPD-1 alone yielded a modest, albeit statistically significant, improvement in survival (both median survivals 71d.) compared to vehicle control (median survival 64d.). Strikingly, the combination of IL-33 and αPD-1 provided an additive effect to substantially delay mouse mortality (median survival 83d.), with 25% of mice found to be tumor-free post-mortem analysis. Finally, we observed that the novel triple combination of IL-33+αPD-1+αCTLA-4 provided a superior survival benefit (median survival 90d.) compared to IL-33+αPD-1, with 50% of the mice found to be tumor-free upon postmortem analysis on day 100 (Figure 4.4C). The combinations of IL-33+αPD-1 or IL-33+αPD-1+αCTLA-

4 provided improved survival outcomes compared to IL-33 and αPD-1 alone (Figure 4.4C), showing that combination immunotherapy can be an effective strategy for overcoming the limitations of single-agent treatments. Collectively, these data show that the ID8*Trp53*$^{-/-}$*Brca1*$^{-/-}$ orthotopic tumors, which are largely refractory to checkpoint blockade therapy, can be sensitized by IL-33 to substantially improve its efficacy.

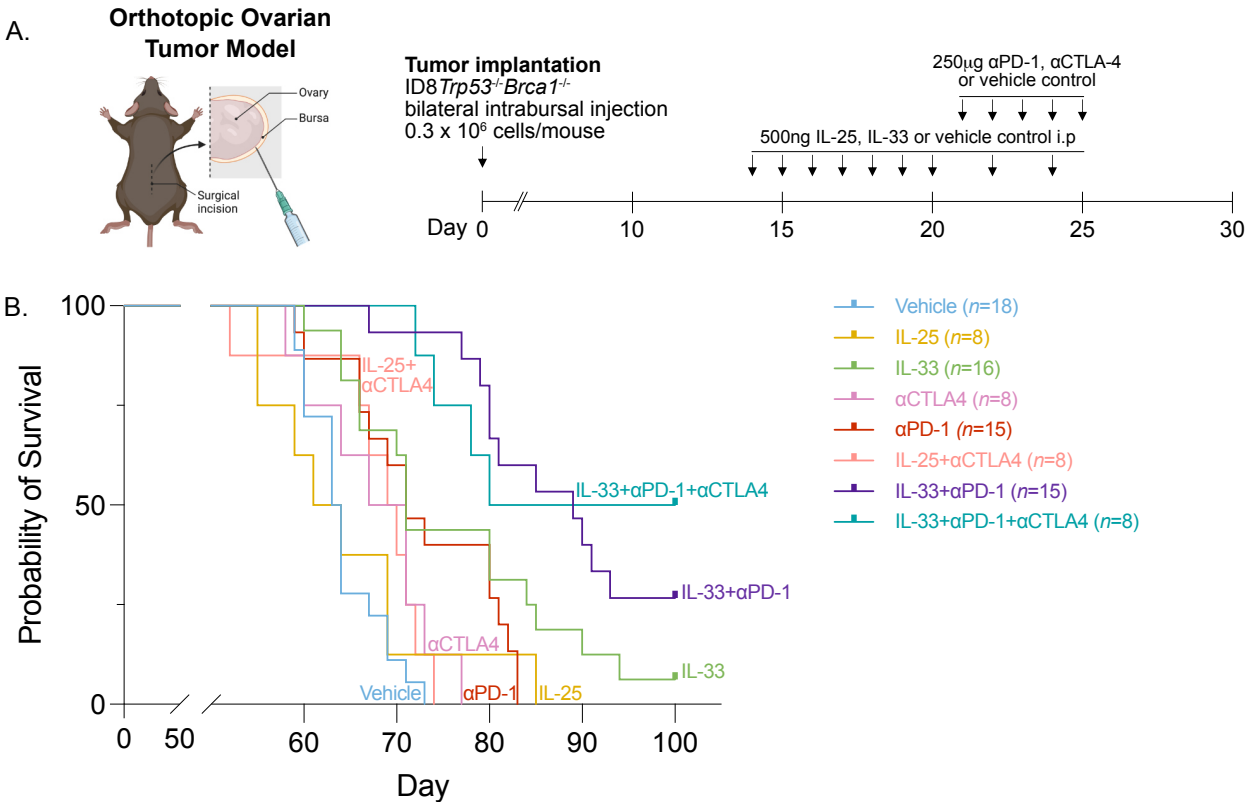

C.

Treatment	Log-rank (Mantel-Cox) test	Significance
Vehicle vs. IL-33	*P*=0.0001	***
Vehicle vs. αPD-1	*P*=0.0006	***
Vehicle vs. IL-33+αPD-1	*P*<0.0001	****
Vehicle vs. IL-33+αPD-1+αCTLA-4	*P*<0.0001	****
IL-33 vs. IL-33+αPD-1	*P*=0.0272	*
IL-33 vs. IL-33+αPD-1+αCTLA-4	*P*=0.0312	*
αPD-1 vs. IL-33+αPD-1	*P*=0.0003	***
αPD-1 vs. IL-33+αPD-1+αCTLA-4	*P*=0.0136	*
IL-33+αPD-1 vs. IL-33+αPD-1+αCTLA-4	*P*=0.5938	ns

Figure 4.4: IL-33 treatment improves the therapeutic efficacy of PD-1 blockade. (A) ID8*Trp53*$^{-/-}$*Brca1*$^{-/-}$ ovarian cancer cells were orthotopically implanted in C57Bl/6 female mice. Following tumor inoculation mice were treated with 500ng of IL-25, IL-33, or PBS vehicle control, followed by αPD-1 or αCTLA-4 treatment. (B) Kaplan-Meir curve depicting survival of ovarian-tumor bearing mice treated with single- or combination therapies. (C) Statistical test results of relevant treatment group comparisons. Results depicted are combined from three independent experiments. *N*=7-18/group. Log-rank (Mantel-Cox) test. *p<0.05, **p<0.01, ***p<0.001, ****p<0.0001.

4.6. IL-33 selectively and robustly activates ILC2s in ID8*Trp53*$^{-/-}$*Brca1*$^{-/-}$ tumors

Next, we employed high-parameter spectral flow cytometry to characterize the immune landscape of tumors, draining lymph node (dLN) and peritoneal lavage of ID8*Trp53*$^{-/-}$*Brca1*$^{-/-}$ tumor-bearing mice treated with PBS, αPD-1, IL-33, or IL-33+αPD-1. ILC2s accumulated in the tumors, dLNs, and peritoneal lavage upon IL-33 or IL-33+αPD-1 treatment at significantly elevated levels compared to vehicle or αPD-1 treated mice (Figure 4.5A). Notably, ILC2s underwent a significant expansion and activation upon IL-33, but not αPD-1 treatment. This observation may disprove our initial hypothesis that ILC2 tumor activity can be modulated with αPD-1 therapy, as we did not observe any ILC2 cell-intrinsic activation upon αPD-1 treatment.

In addition to a robust and selective expansion of tumor-infiltrating ILC2s upon IL-33 treatment, we observed a pronounced shift toward a more inflammatory and proliferative phenotype (Figure 4.5B). IL-33-activated ILC2s express canonical markers of activation including KLRG1, CD44, CD25, CD69, ICOS and Arginase-1 (Figure 4.5C). Collectively, these markers define a distinct activated and inflammatory subset of ILC2s.

Further sub-clustering of ILC2s revealed that IL-33-driven proliferation, as evidenced by Ki67 expression, is accompanied by reduced CD69 expression, consistent with a loss of tissue-residency (Figure 4.5C). CD69 is a marker of early activation on lymphocytes, and its expression can influence the sensing of sphingosine 1-phosphate 1 (S1P) gradient that directs lymphocytes between tissues and lymph nodes (*109*). This pattern supports a model where IL-33 activates ILC2s in situ, then with reduced CD69 expression, licenses their trafficking to distal tissues, such as the draining lymph node (*110, 111*).

Interestingly, we observe an inverse expression of checkpoint receptors PD-1 and CTLA-4 on activated ILC2s, with PD-1 expression evident in resting ILC2s, and CTLA-4 expression appearing in a later, more proliferative subset of ILC2s (Figure 4.5C). This evidence suggests that the expression of checkpoint receptors on tumor-infiltrating ILC2s is temporally restrained which can provide insight into refined therapeutic strategies targeting ILC2s. Collectively, these data show that treatment of IL-33, but not necessarily αPD-1, strongly activates ILC2s and increases their abundance in the tumor, dLN, and peritoneal cavity.

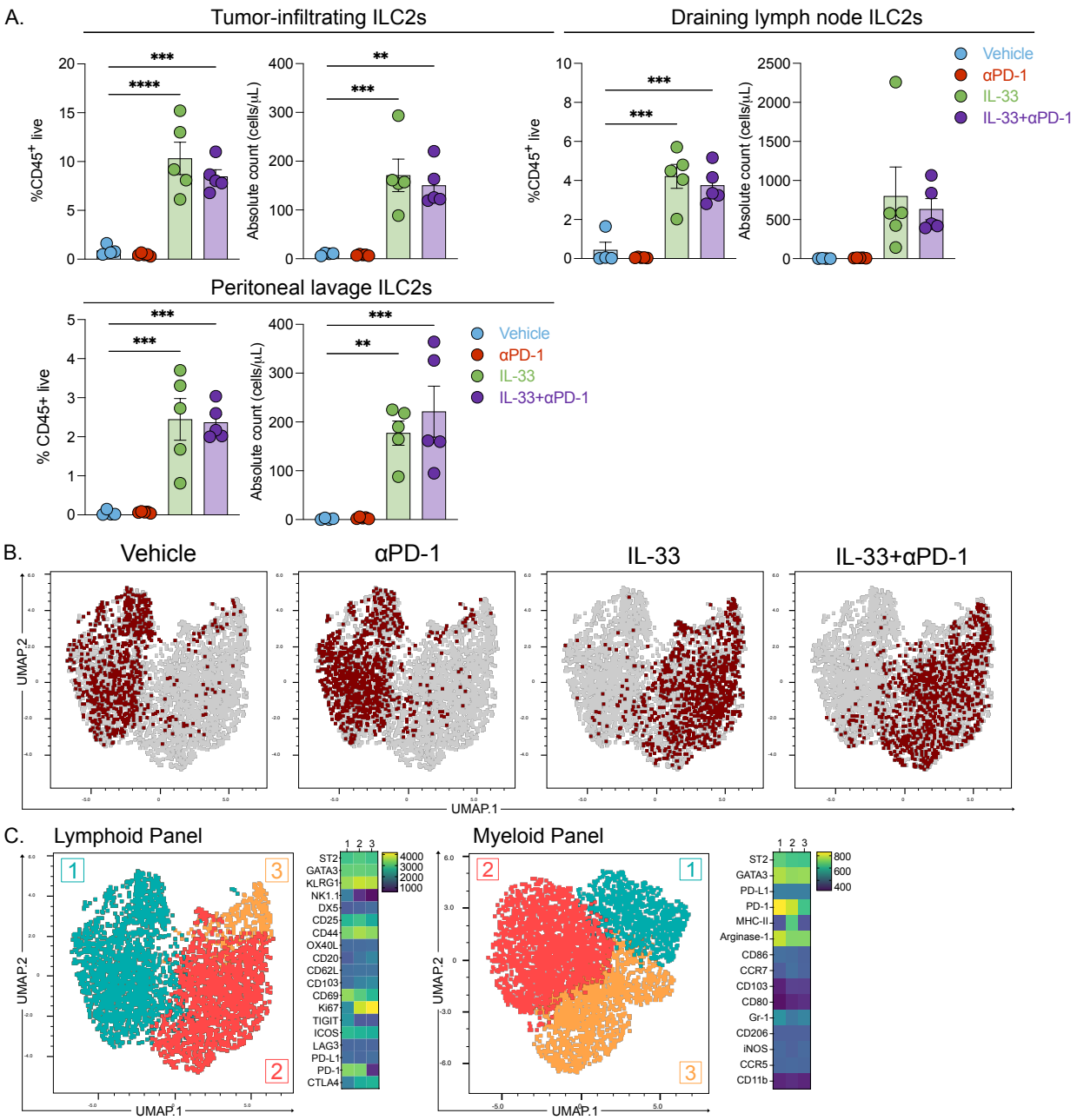

Figure 4.5: IL-33 selectively and robustly activates ILC2s. ID8*Trp53*$^{-/-}$*Brca1*$^{-/-}$ ovarian cancer cells were orthotopically implanted in C57Bl/6 female mice. Mice were subsequently treated with 500ng of IL-33 or PBS every day for five days with 250 μg αPD-1 or vehicle control every other day. Primary tumors, draining lymph node, and peritoneal lavage were collected on day 45 for flow cytometry staining and analysis. (A) Frequencies and absolute counts of ILC2s in the tumor, draining lymph node, and peritoneal lavage of tumor bearing mice. (B) Uniform manifold approximation and projection (UMAP) plots depicting tumor ILC2s in ID8*Trp53*$^{-/-}$*Brca1*$^{-/-}$mice. (C) FlowSOM analysis depicting ILC2 subsets identified using a lymphoid panel and myeloid panel and corresponding marker expression. Data presented as ± SEM. *N*=5/group. One-way ANOVA. *p<0.05, **p<0.01, ***p<0.001, ****p<0.0001.

4.7. IL-33 skews the lymphoid immune compartment to favour type 2 immunity

Beyond its effects on ILC2s, IL-33 or IL-33+αPD-1 treatment globally skewed the tumor microenvironment to favour type 2 immunity. Treatment with αPD-1 had the largest impact on the T cell repertoire, with increased frequency and number of $CD8^+$ and $CD4^+$ T cells in the tumor (Figure 4.6A). IL-33 diminished the effects of αPD-1 by decreasing the overall abundance of T cells in the tumor. However, within the $CD4^+$ T cell population, IL-33 and IL-33+αPD-1 treatments selectively expanded Th2 cells in the tumor, as expected, given their expression of ST2 (Figure 4.6B). In contrast, intratumoral NK cells decreased in abundance following IL-33 or IL-33+αPD-1 treatment, an effect that is also driven by IL-33. IL-33 treatment may have increased B cells frequencies, but additional phenotypical analyses was not done at this stage to determine which subset of B cells were affected here, but was followed up later in the thesis.

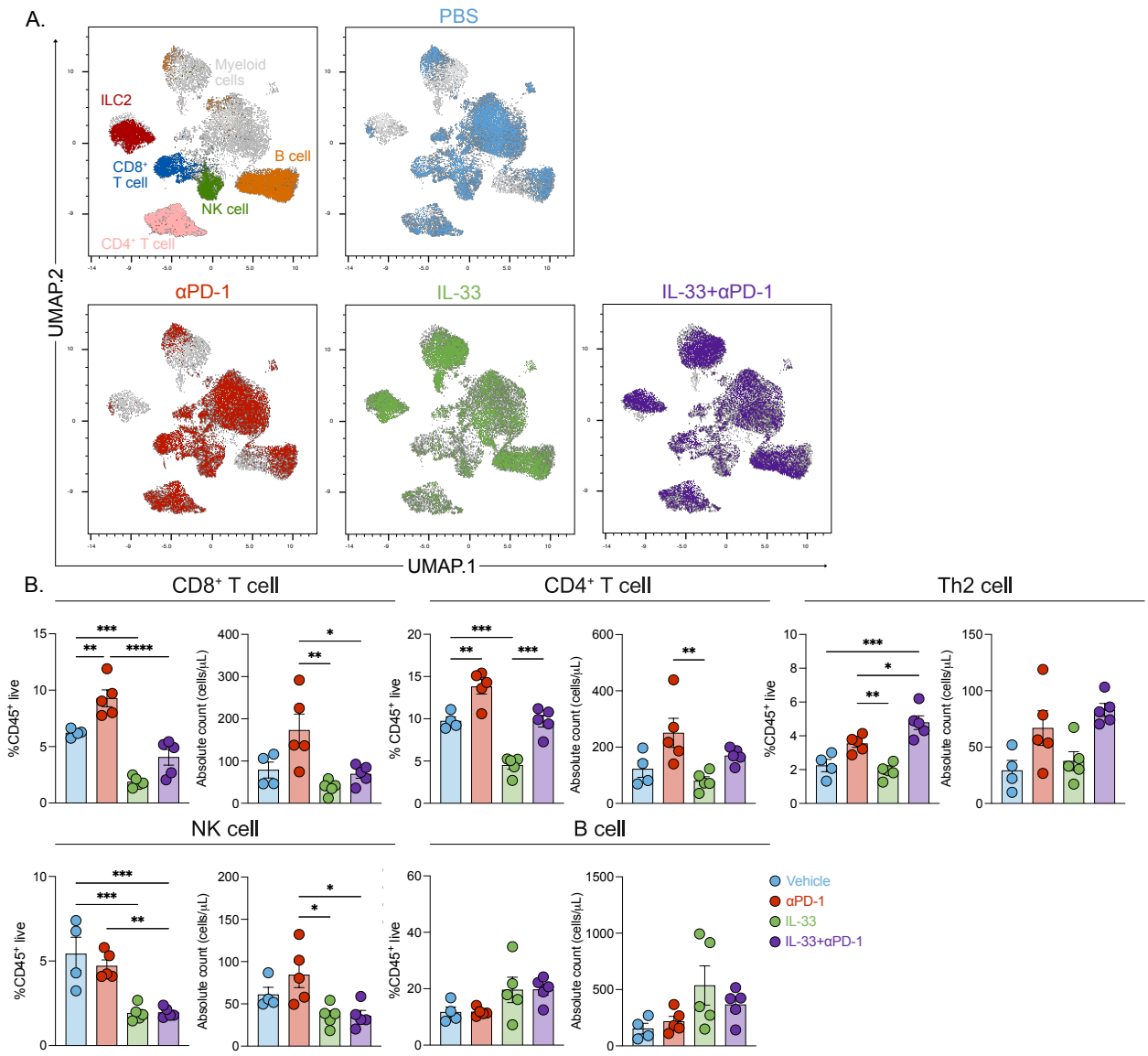

Figure 4.6: IL-33 skews the ovarian tumor microenvironment towards type 2 immunity. ID8*Trp53*$^{-/-}$*Brca1*$^{-/-}$ ovarian cancer cells were orthotopically implanted in C57Bl/6 female mice. Mice were subsequently treated with 500ng of IL-33 or PBS every day for five days with 250 μg αPD-1 or vehicle control every other day. Primary tumors, draining lymph node, and peritoneal lavage were collected on day 45 for flow cytometry staining and analysis. (A) UMAP plots depicting the lymphoid immune cell compartment in ID8*Trp53*$^{-/-}$*Brca1*$^{-/-}$ tumors. (B) Frequencies and absolute counts of tumor-infiltrating lymphocytes. Data presented as ± SEM. *N*=5/group. One-way ANOVA. *p<0.05, **p<0.01, ***p<0.001, ****p<0.0001.

In the dLN (the mesenteric lymph node in this model), we did not observe substantial changes in overall T cell abundance, with the exception of Th2 cells, which were most abundant following IL-33+αPD-1 treatment (Figure 4.7A). Since T cell levels in the lymph node are maintained – even showing a slight upward trend – with IL-33 or αPD-1 treatment, these data suggest that antigen priming, and tumor-specific T cell responses are still being generated despite reduced intratumoral T cell abundance. In the peritoneal lavage, we observed a similar trend in the tumor, where αPD-1 treatment increased the abundance of $CD8^+$ and $CD4^+$ T cells, while IL-33 treatment decreased the abundance of T cells and NK cells (Figure 4.7B). Together, these data suggest that IL-33 drives a type 2 specific tumor microenvironment, with predominantly ILC2 and Th2 cells in abundance.

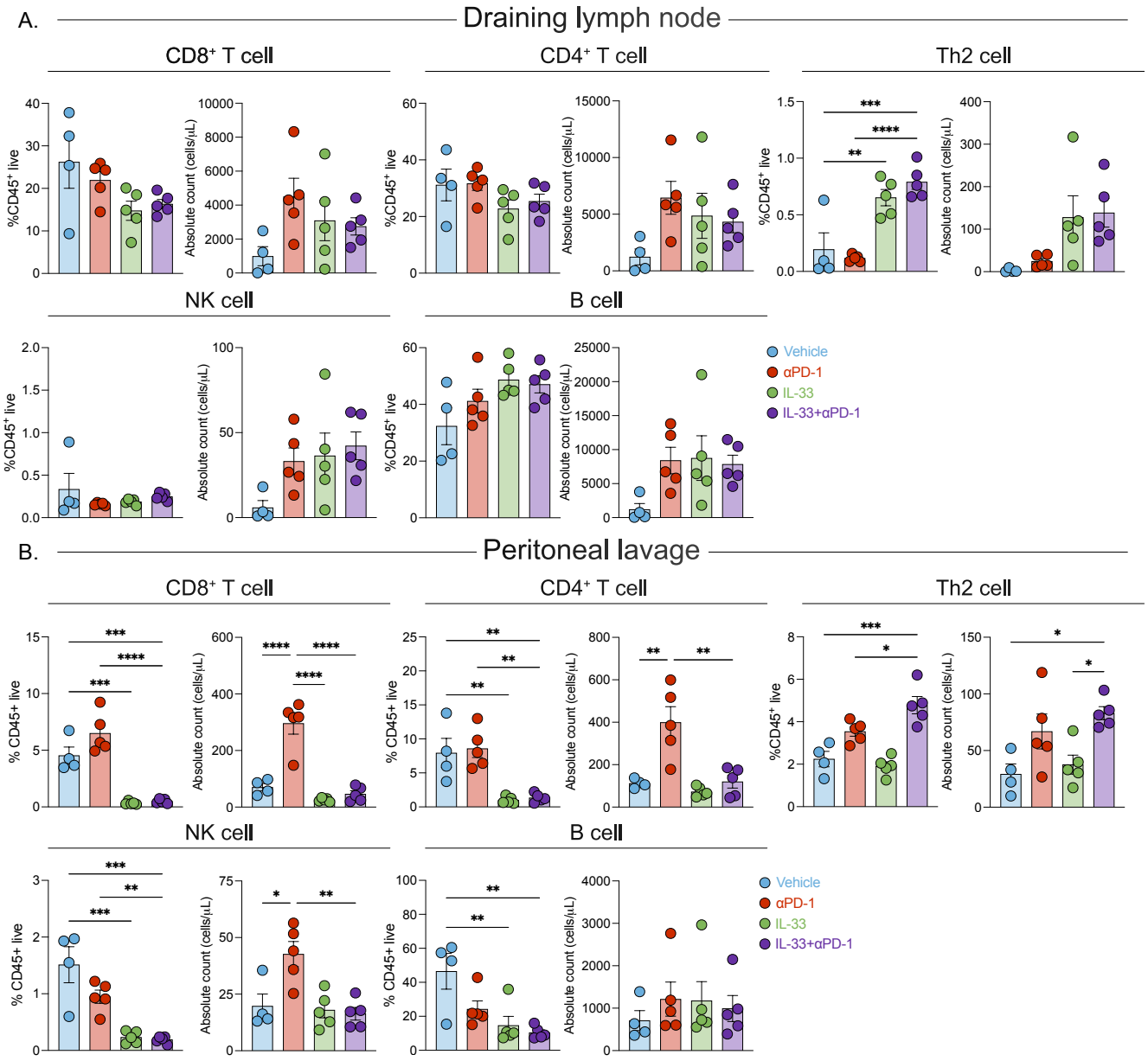

Figure 4.7: IL-33 globally enriches for type 2 immune cells. ID8*Trp53*$^{-/-}$*Brca1*$^{-/-}$ ovarian cancer cells were orthotopically implanted in C57Bl/6 female mice. Mice were subsequently treated with 500ng of IL-33 or PBS every day for five days with 250 μg αPD-1 or vehicle control every other day. Primary tumors, draining lymph node, and peritoneal lavage were collected on day 45 for flow cytometry staining and analysis. Frequencies and absolute counts of lymphocytes in the (A) draining lymph node and (B) peritoneal lavage. Data presented as ± SEM. *N*=5/group. One-way ANOVA. *p<0.05, **p<0.01, ***p<0.001, ****p<0.0001.

4.8. IL-33 expands eosinophils and mast cells in the myeloid compartment

IL-33 can directly activate myeloid cells, such as eosinophils and mast cells, that can degranulate to release immunomodulatory compounds and shape tumor immunity. Moreover, ILC2-derived IL-5 promotes eosinophilia, providing an indirect mechanism through which IL-33 further activates eosinophils (*47, 112*). The relevance of ILC2-mediated eosinophilia in the tumor context has been highlighted in recent studies; eosinophils can antagonize NK cell metabolism and promote tumor growth (*47*), or be recruited by ILC2-derived GM-CSF to orchestrate anti-melanoma immune responses (*49*). Therefore, as main effector cells of ILC2s, eosinophils represent a key mechanism through which IL-33 can exert its effects.

Globally, the myeloid compartment in the tumor was most affected by IL-33 treatment, with distinct accumulation of ILC2s and eosinophils (Figure 4.8A). Specifically, IL-33 or IL-33+αPD-1 treatment induces eosinophilia in tumors, dLN, and peritoneal lavage. Parallel to this, mast cells, which represent a small subset of immune cells (~1-2% of all leukocytes), also expand in response to IL-33 treatment (Figure 4.8A). Although intratumoral macrophages and dendritic cells decrease upon IL-33 stimulation, we observed an increase in macrophages in the dLN and peritoneal lavage (Figure 4.9A-B). Overall, IL-33+αPD-1 treatment shifted the tumor microenvironment to favour type 2 immunity (i.e. ILC2s, eosinophils, mast cells, and Th2 cells) while supressing type 1 immunity (i.e. $CD8^+$ T cells and NK cells).

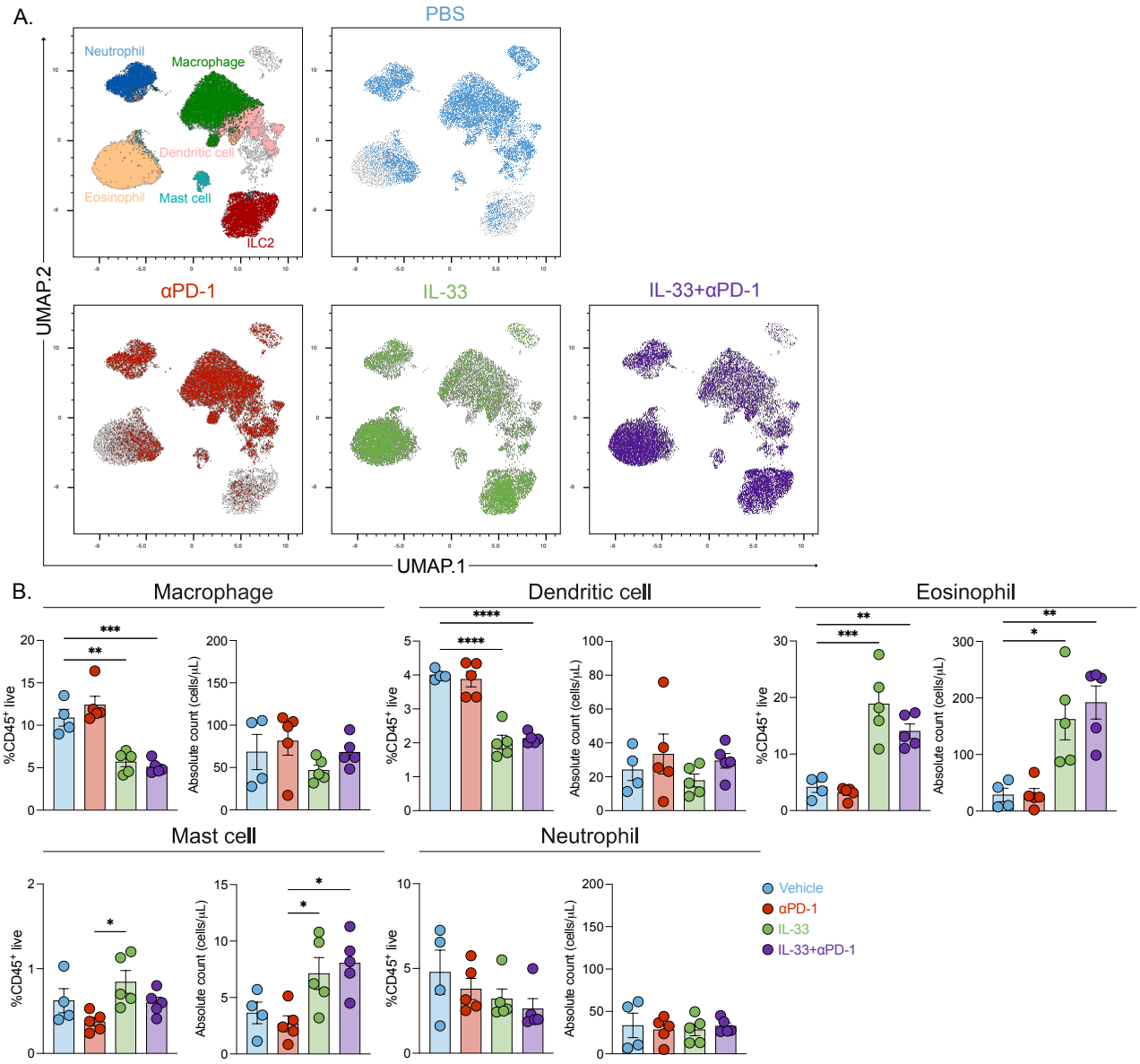

Figure 4.8. IL-33 expands eosinophils and mast cells in ovarian tumors. ID8*Trp53*$^{-/-}$*Brca1*$^{-/-}$ ovarian cancer cells were orthotopically implanted in C57Bl/6 female mice. Mice were subsequently treated with 500ng of IL-33 or PBS every day for five days with 250 μg αPD-1 or vehicle control every other day. Primary tumors, draining lymph node, and peritoneal lavage were collected on day 45 for flow cytometry staining and analysis. (A) UMAP plots depicting changes in the myeloid compartment of ovarian tumors with different treatments. (B) Frequencies and absolute counts of tumor-infiltrating myeloid cells. Data presented as ± SEM. *N*=5 for each group. One-way ANOVA. *p<0.05, **p<0.01, ***p<0.001, ****p<0.0001.

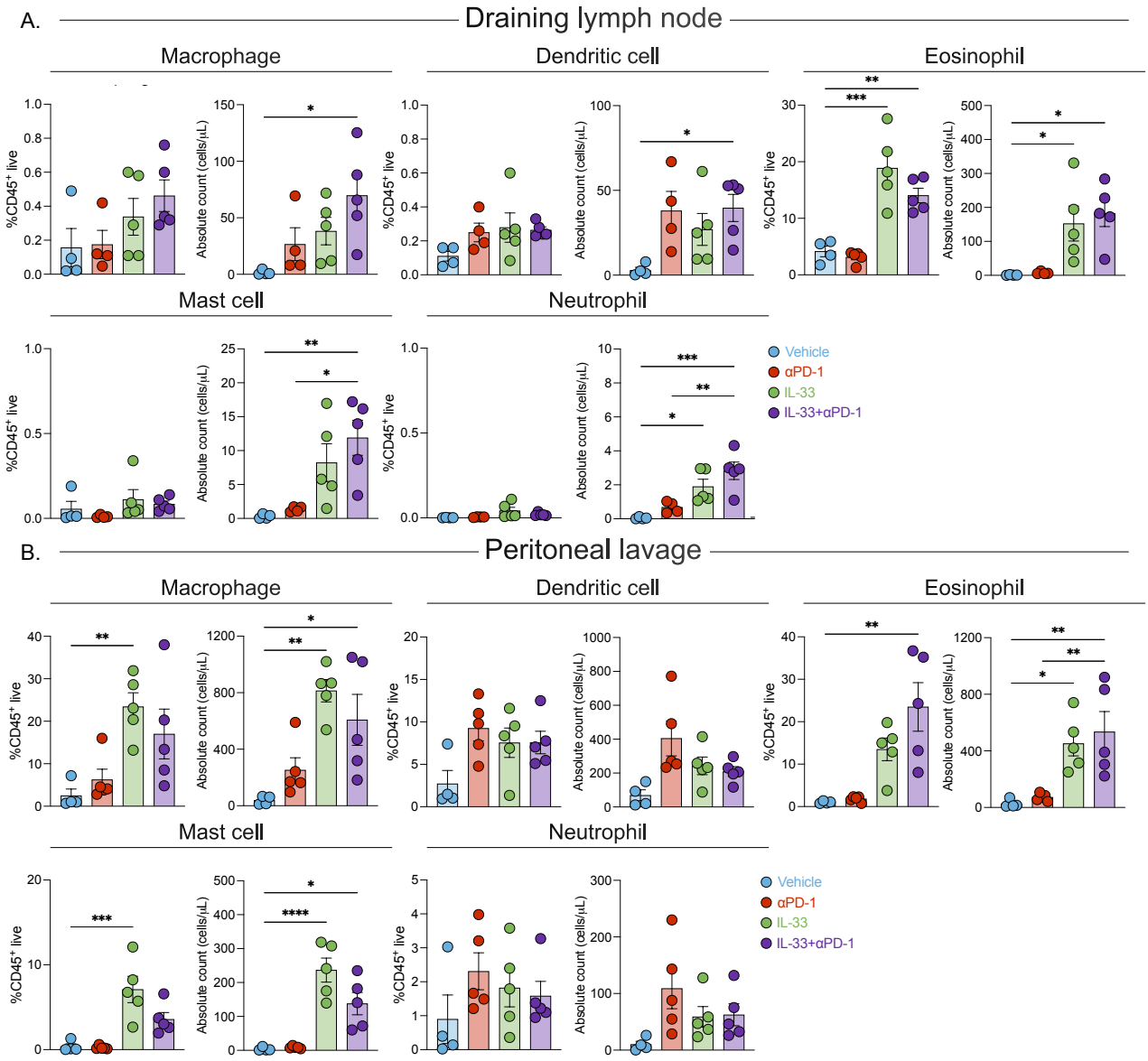

Figure 4.9. IL-33 globally expands type 2 myeloid cells. ID8*Trp53*$^{-/-}$*Brca1*$^{-/-}$ ovarian cancer cells were orthotopically implanted in C57Bl/6 female mice. Mice were subsequently treated with 500ng of IL-33 or PBS every day for five days with 250 μg αPD-1 or vehicle control every other day. Primary tumors, draining lymph node, and peritoneal lavage were collected on day 45 for flow cytometry staining and analysis. Frequencies and absolute counts of myeloid cells in the (A) draining lymph node and (B) peritoneal lavage. Data presented as ± SEM. *N*=5 for each group. One-way ANOVA. *p<0.05, **p<0.01, ***p<0.001, ****p<0.0001.

4.9. ILC2s abundantly express effector cytokines at the transcriptional level

Thus far we have reported that IL-33 potently and selectively activates ILC2s, and this concomitantly improves survival outcomes in mice. Next, to investigate how ILC2s modulate this antitumor response, we performed scRNA-seq analysis of tumor-infiltrating leukocytes ($CD45^+$ live cells) isolated from ID8*Trp53*$^{-/-}$*Brca1*$^{-/-}$ tumors treated with PBS, IL-25, IL-33, αPD-1, or IL-33+αPD-1. Gene expression analysis of ILC2 from IL-33+αPD-1 tumors reveals exclusive expression of *Il5*, *Il13*, and other well-defined ILC2 effector molecules such as *Csf2* and *Areg* on ILC2s among other immune cells (Figure 4.10B). Other type 2 cytokines, such as *Il4* and *Il6* are less expressed at the transcriptional level in ILC2s, consistent with reports that ILC2s are not the main producers of these cytokines in some contexts (*113, 114*). Interestingly, we observed high expression of *Il9* and in some ILC2s. IL-9 is a non-canonical ILC2 cytokine that has been implicated in promoting the immunosuppressive activity of Tregs in the resolution of inflammation in arthritis. In the context chimeric antigen therapy, IL-9 can rewire T cell fate to enhance tumor infiltration and tumoricidal activity (*115, 116*). ILC2s also express the chemokine receptors *Ccr8* and *Ccr4* (Figure 4.10B), which are selectively expressed on ILC2s based on global transcriptomic analyses, and contribute to ILC2-driven inflammation and tissue-specific functions through autocrine and paracrine signalling (*117, 118*). Collectively, our scRNA-seq analyses revealed several effector molecules expressed on tumor ILC2s that provide mechanistic clues for their downstream function.

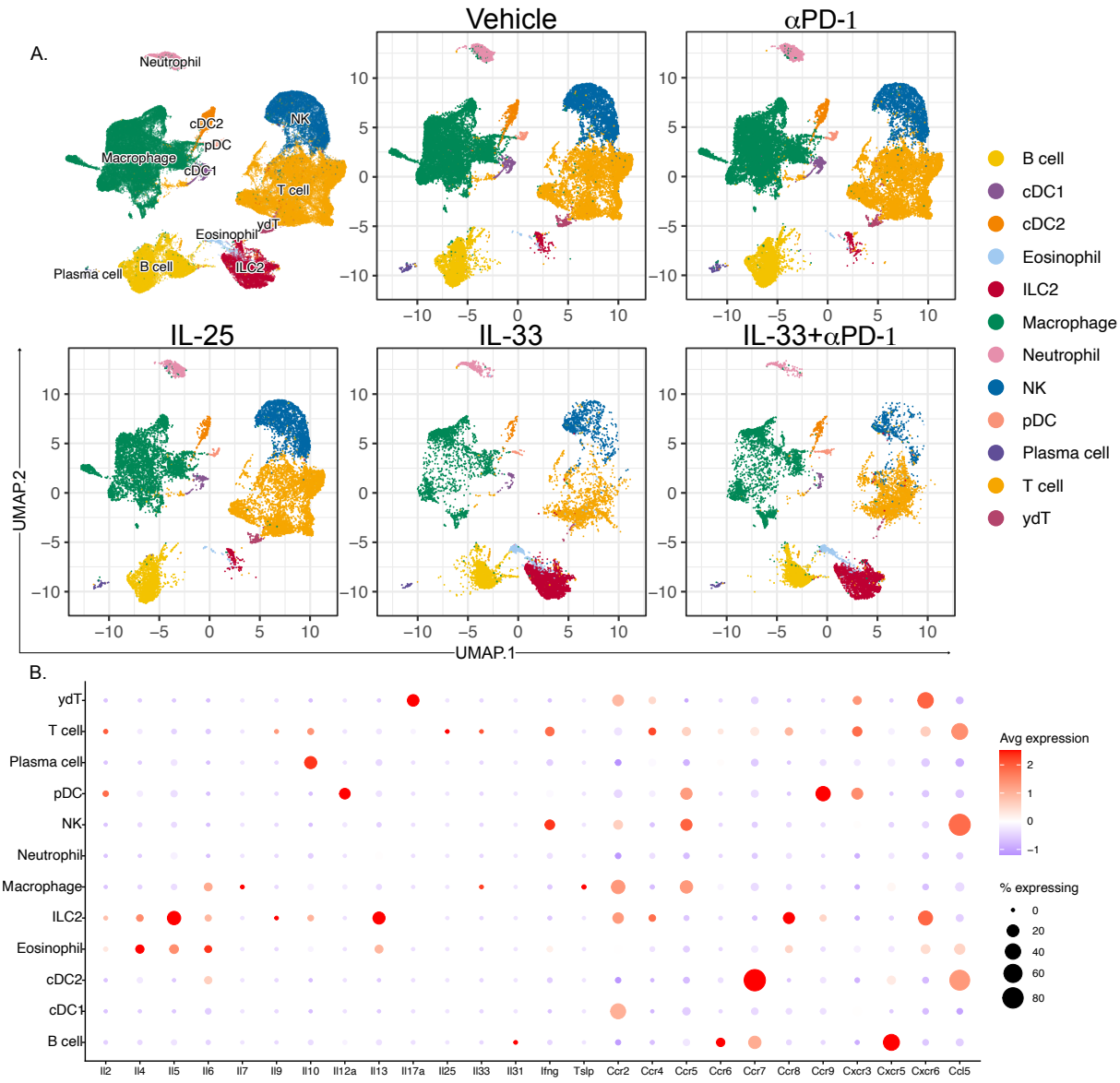

Figure 4.10: ILC2s abundantly express effector cytokines at the transcriptional level. CD45^{+} live cells were sorted from ID8*Trp53*$^{-/-}$*Brca1*$^{-/-}$ tumors treated with PBS, αPD-1, IL-25, IL-33, and IL-33+αPD-1 and analyzed for scRNA-seq. (A) UMAP plots representing immune cell populations in tumors analyzed by scRNA-seq. (B) Dot plots showing average and percent expression of cytokine and chemokine gene for diverse immune cell populations.

4.10. IL-5 and IL-13 are abundant in the ascites fluid of IL-33-treated mice

To determine whether these cytokines were produced at the protein level, we collected the ascites fluid from PBS, IL-25, IL-33, αPD-1, or IL-33+αPD-1-treated mice and conducted a multiplex ELISA using a custom 10-analyte LEGENDplex™ kit to detect various cytokines present in the peritoneal milieu. IL-5 and IL-13 were found at significantly elevated levels in the ascites fluid of mice treated with IL-33 or IL-33+αPD-1 compared to untreated mice, consistent with our finding that *Il5* and *Il13* are highly expressed in ILC2s (Figure 4.11). Interestingly, IL-6 was selectively elevated in IL-25-treated mice, while IL-9 was increased only in IL-33-treated mice, indicating that these cytokines may drive distinct ILC2 programs. Treatment of αPD-1 elicited a strong IFN-γ response, consistent with activation of T cells and NK cells (Figure 4.11). Although IL-4 levels were elevated in IL-33 and IL-33+αPD-1treatments, the levels were at the lower limit of detection, indicating that IL-4 is not found at significant levels in the ascites, while also corroborating our earlier finding that ILC2s are not major producers of IL-4 (Figure 4.10) (*26*).

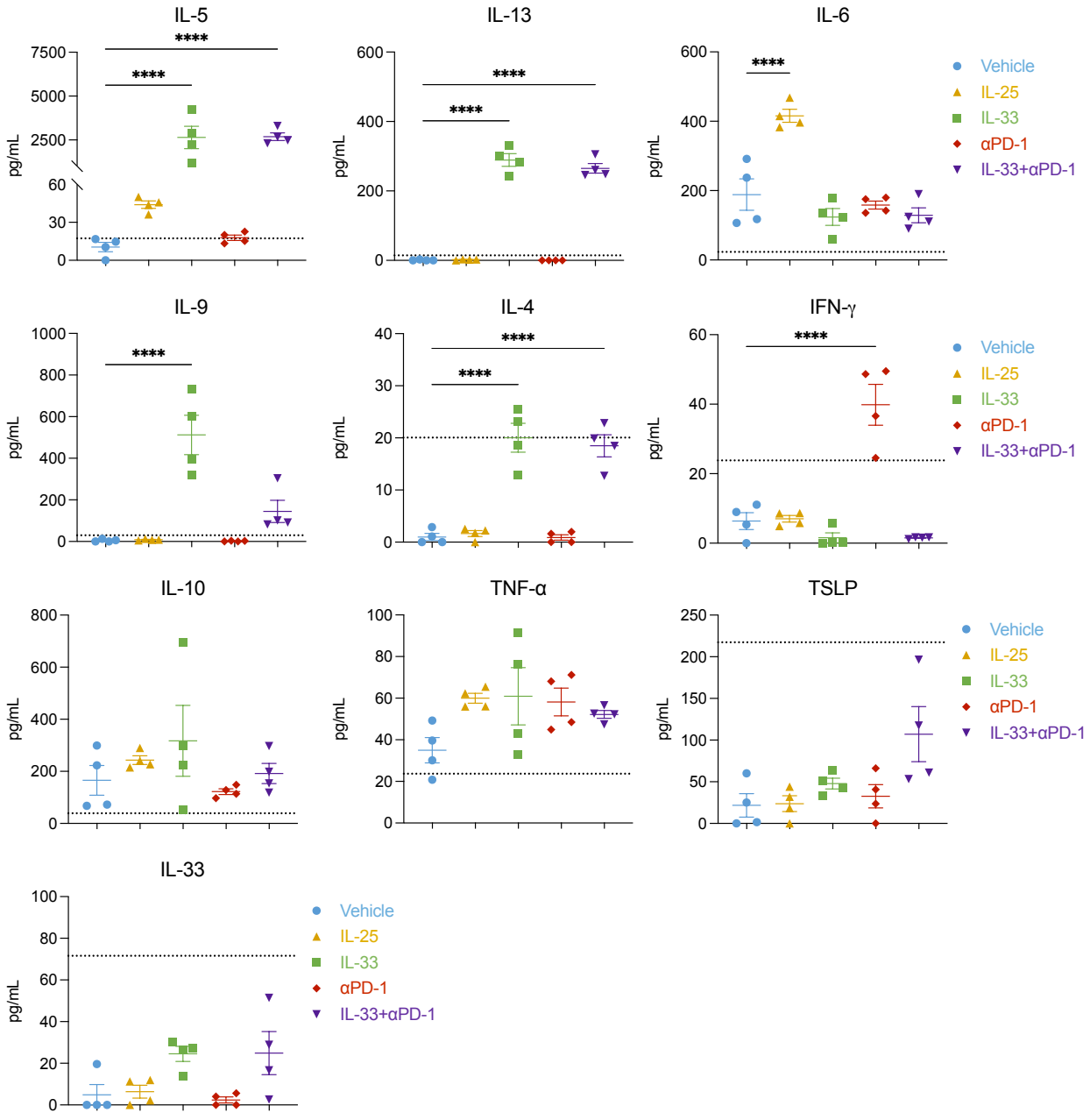

Figure 4.11: IL-5 and IL-13 are abundant in the ascites fluid of IL-33-treated mice. Female C57Bl/6 mice were inoculated with ID8*Trp53*$^{-/-}$*Brca1*$^{-/-}$ ovarian cancer cells and subsequently treated with PBS (vehicle control), IL-25, IL-33, αPD-1, or IL-33+αPD-1. Ascites fluid was collected, and serum was isolated for analysis using a custom 10-probe LEGENDplex™ kit. Data presented as ± SEM. *N*=4/group. One-way ANOVA. *p<0.05, **p<0.01, ***p<0.001, ****p<0.0001.

4.11. IL-33-activated tumor ILC2s abundantly express IL-5 and IL-13

To determine whether the source of these cytokines are intra-tumor ILC2s, we conducted functional analyses experiments. Tumor-infiltrating lymphocytes were isolated from PBS or IL-33-treated mice followed by ex vivo stimulation and flow cytometry analysis to detect intracellular cytokines. IL-33-treated ILC2s expressed significantly higher levels of IL-5 and IL-13 compared to PBS controls, and this expression increased upon ex vivo stimulation (Figure 4.12A). Following ex vivo stimulation, IL-33-activated ILC2s exhibited IL-5 and IL-13 expression in approximately 20% and 50% of cells respectively, with ~20% of tumor-infiltrating ILC2s co-expressing both cytokines (Figure 4.12B). The frequency of GM-CSF^{+} ILC2s was also markedly increased in IL-33 treated ILC2s compared with PBS controls; however, ex vivo stimulation resulted in reduced GM-CSF expression, possibly reflecting a negative regulatory mechanism. We also confirmed that IL-33 stimulation increased frequency of ILC2s, and increased expression of Ki67, KLRG1, and PD-1 upon ex vivo stimulation (Figure 4.12B). These results indicate that treatment with IL-33 induces potent ILC2 activation and that these cells are the main source of IL-5 and IL-13, which are also abundantly detected in the peritoneal ascitic fluid (Graphical Abstract 2.2).

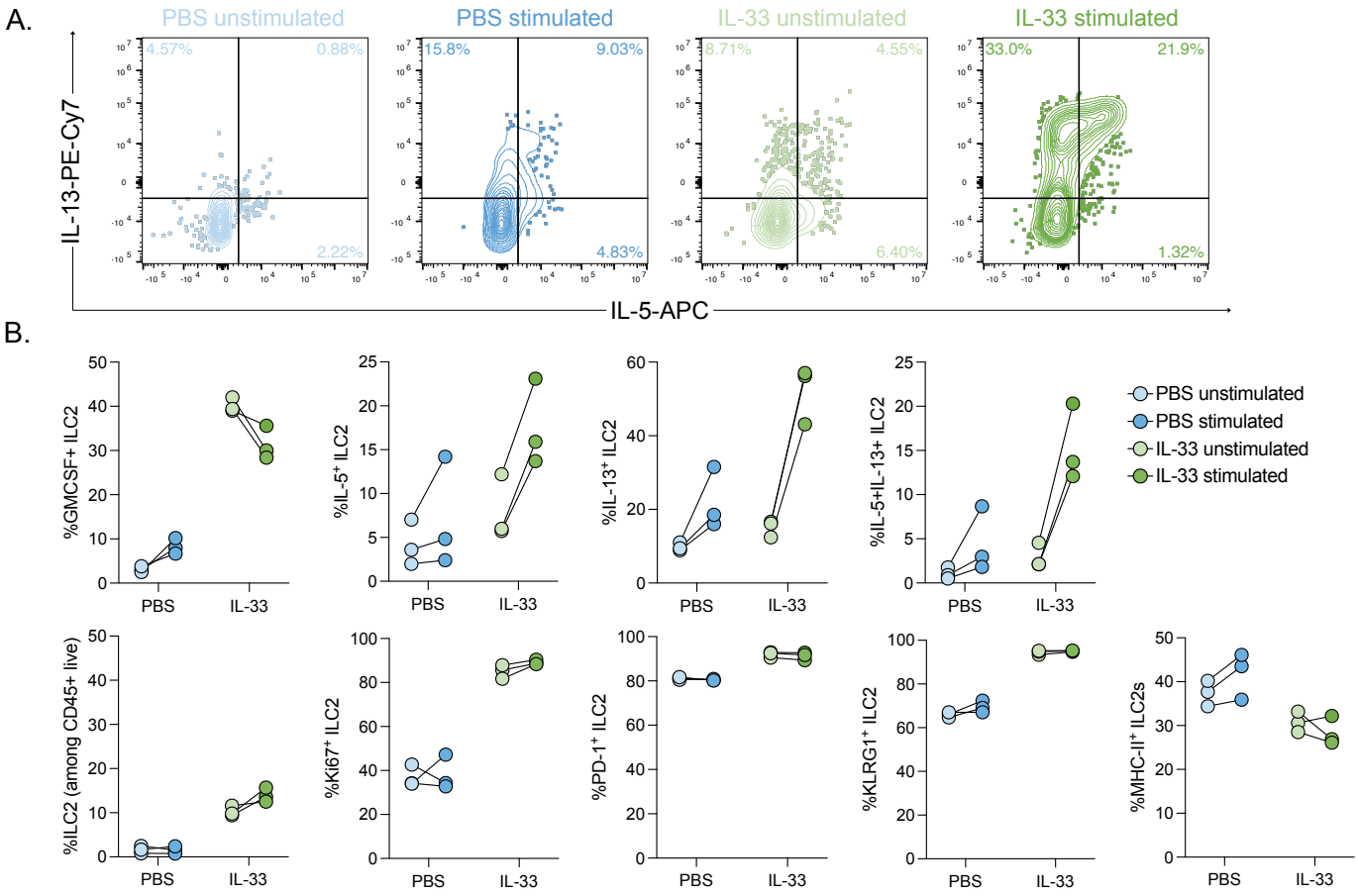

Figure 4.12: IL-33-activated tumor ILC2s abundantly express IL-5 and IL-13. (A) Representative flow cytometry contour plots depicting IL-5 and IL-13 expression on ILC2s stimulated ex vivo from PBS or IL-33-treated ID8*Trp53*$^{-/-}$*Brca1*$^{-/-}$ tumors. (B) Expression of intracellular cytokines on ILC2s from PBS or IL-33-treated ID8*Trp53*$^{-/-}$*Brca1*$^{-/-}$ tumors. Data presented as ± SEM. *N*=3 for each group.

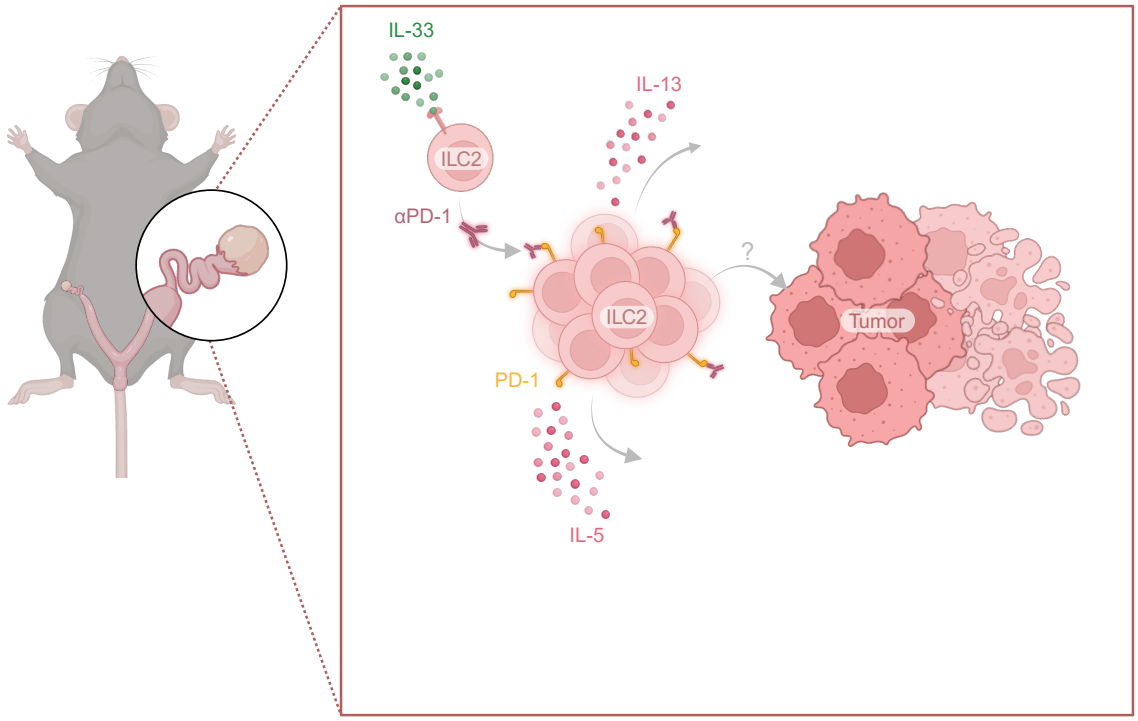

Graphical Abstract 2.2: IL-33+αPD-1 treatment improves survival in mouse ovarian tumors. IL-33+αPD-1 treatment induces an ILC2-dominant tumor microenvironment where ILC2s produce high amounts of IL-5 and IL-13 and exhibit direct tumoricidal activity against tumor cells.

4.12. ILC2s exhibit anti-tumor cytotoxicity

ILC2s can regulate anti-tumor immunity by activating tissue-specific innate and adaptive responses. However, recent reports have shown that tumor-associated ILC2s express cytotoxic factors, including granzyme B and C, suggesting that ILC2s can independently direct tumor cell killing (*53, 119*). To investigate this in our ovarian cancer model, we harvested IL-33-treated primary tumors and isolated ILC2s and $CD3^+$ T cells using FACS. Tumor-derived ILC2s and T cells were co-cultured with ID8*Trp53*$^{-/-}$*Brca1*$^{-/-}$ target cells expressing nanoluciferase for 5 hours. Following the incubation time, nanoluciferase activity was measured as a direct readout for target

cell killing (Figure 4.13A). Tumor-derived ILC2s cultured with target cells alone exhibited tumor-specific killing in a dose-dependent manner, indicating that ILC2 show cytotoxic potential. Moreover, co-culturing ILC2s with $CD3^+$ tumor-infiltrating lymphocytes enhanced tumor cell killing (Figure 4.13B). Whether this observation indicates additive or synergistic effects requires further investigation.

Human ILC2s have been reported to mediate cytotoxicity through DNAM-1, which engages with its cognate ligands CD112/CD155 on acute myeloid leukemia (AML) cells, thereby promoting granzyme secretion and tumor cell killing (*54*). Indeed, in our scRNA-seq analysis, we found that intratumoral ILC2s from IL-33+αPD-1-treated mice expressed *Cd266* which encodes for the DNAM-1 receptor, which we confirmed by flow cytometry, indicating that ovarian ILC2s may mediate tumor killing through a similar mechanism (Figure 4.13C-D). Moreover, ovarian tumor ILC2s express *tnfsf10* (also known as TRAIL) and its receptor *tnfrsf10b* (TRAIL-R2 or DR5), genes that belong to the TNF family of receptors. TRAIL, and its receptor TRAIL-R2, form a critical signalling pathway that can induce apoptosis in tumor cells, representing another possible mechanism by which ILC2s may direct tumor killing. Overall, this experiment suggests that tumor ILC2s are functionally capable of directly killing tumor cells, though the underlying mechanism requires further investigation.

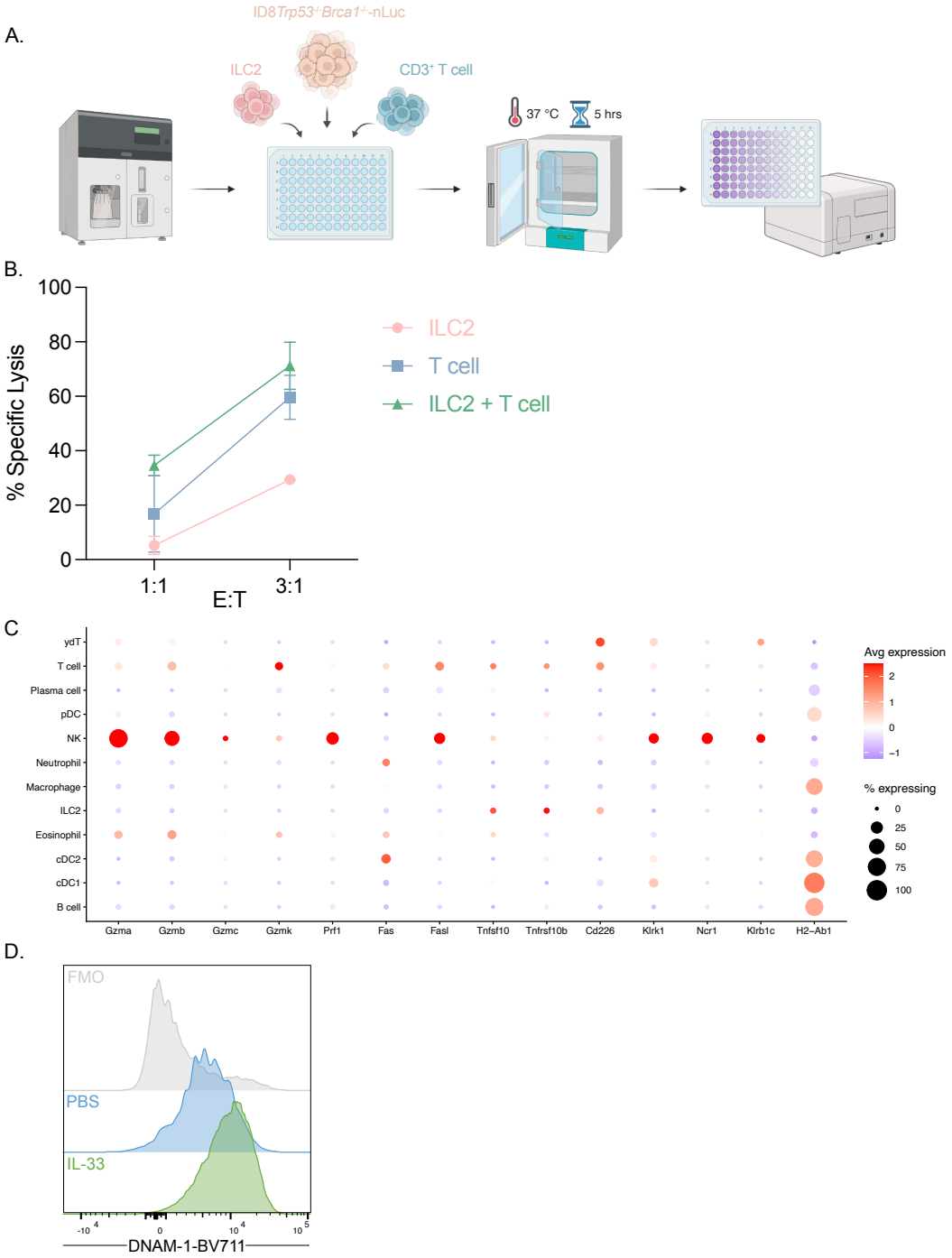

Figure 4.13: Tumor ILC2s exhibit anti-tumor cytotoxicity. (A) Experimental workflow for luciferase-based cytotoxicity assay. (B) Percent specific lysis at increasing effector: target (E:T) ratios. (C) Dot plot analysis showing expression of granzymes and death receptors expression for diverse immune cell subsets in tumors treated with IL-33+αPD-1. (D) expression of DNAM-1 on PBS or IL-33-treated ILC2s.

4.13. IL-33 as a single agent enhances survival in STOSE tumor-bearing mice

After conducting comprehensive phenotyping and functional analyses of the effects of IL-33 on ID8*Trp53*$^{-/-}$*Brca1*$^{-/-}$ tumors, we next sought to determine whether the observed therapeutic response was reproducible in other mouse models. Thus, we extended our survival analyses to the spontaneously transformed ovarian surface epithelial (STOSE) cells, which were orthotopically implanted in FVB/N mice and treated as previously described for the ID8*Trp53*$^{-/-}$*Brca1*$^{-/-}$ model (Figure 4.14A). Although both murine cell lines originate from the ovarian surface epithelium, the STOSE model primarily differs from the ID8*Trp53*$^{-/-}$*Brca1*$^{-/-}$ tumors due to the genetic background of the mice from which it was derived. The STOSE tumors are implanted in FVB/N mice and produce a more immunogenic and inflammatory tumor microenvironment at baseline compared to the ID8*Trp53*$^{-/-}$*Brca1*$^{-/-}$ tumors in C57Bl/6 mice (*102*). Moreover, scRNA-seq analysis previously conducted in the lab revealed that STOSE tumors exhibit higher endogenous expression of *Il33* compared to ID8*Trp53*$^{-/-}$*Brca1*$^{-/-}$ tumors. Interestingly, in this model, IL-33 monotreatment was sufficient to significantly improve survival (median survival 120d.) compared to vehicle control (median survival 80 days), while αPD-1 alone or the IL-33+αPD-1 combination provided a weaker therapeutic benefit (median survival 86d.) (Figure 4.14B).

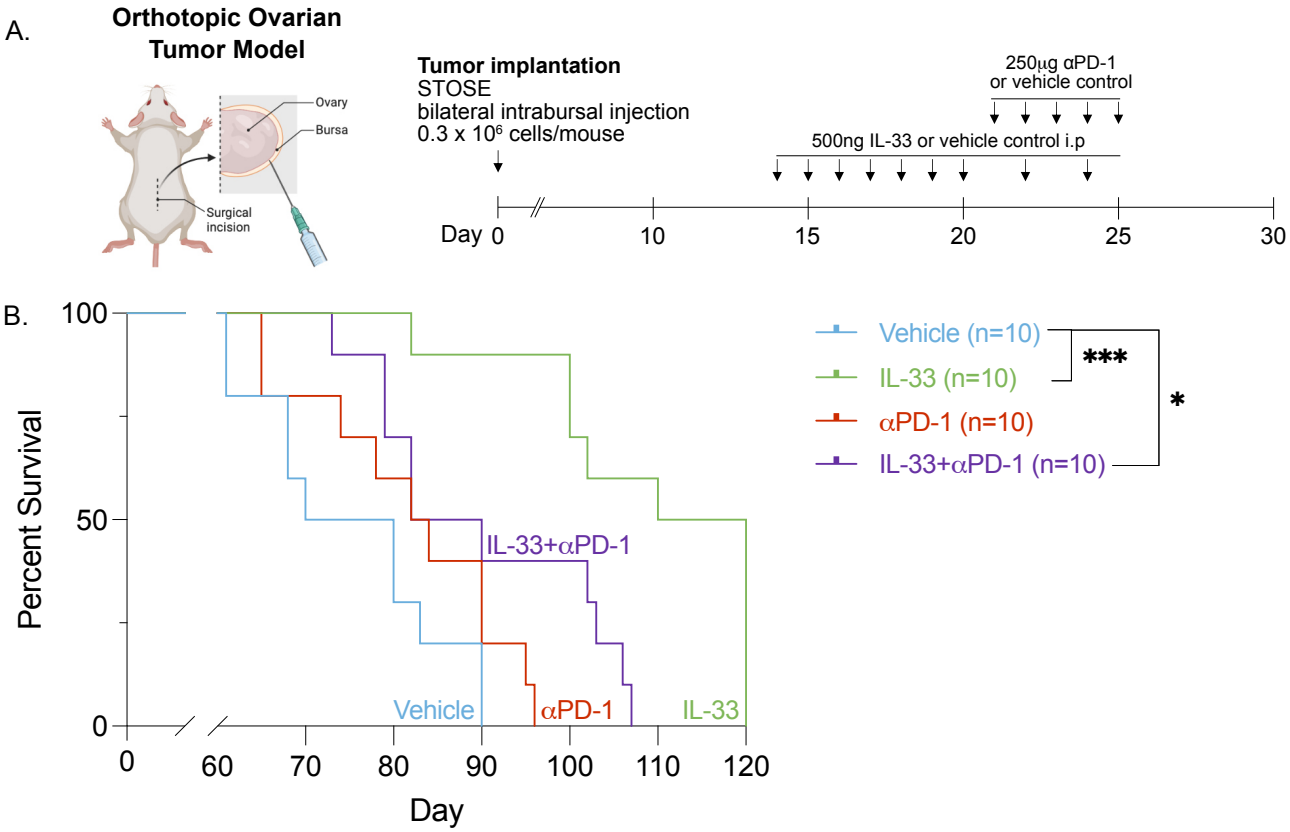

Figure 4.14: IL-33 monotherapy improves survival in STOSE ovarian tumors. (A) STOSE ovarian cancer cells were orthotopically implanted in female FVB/N mice. Following tumor inoculation mice were treated with 500ng of rmIL-33, or PBS vehicle control, then 250 µg of αPD-1 daily for five days. (B) Kaplan-Meier survival curve depicting of STOSE mice. *N*=10/group. Log-rank (Mantel-Cox) test. *p<0.05, **p<0.01, ***p<0.001.

To assess the impact of these treatments on the tumor microenvironment, we performed immune profiling of tumors collected from STOSE tumor-bearing mice treated with PBS, IL-33, αPD-1, or IL-33+αPD-1. UMAP clustering of intratumoral ILC2s revealed a pronounced phenotypic shift with IL-33 or IL-33+αPD-1 treatment, whereas αPD-1 alone did not result in any phenotypic difference compared to vehicle control (Figure 4.15A). Moreover, clustering of the ILC2 populations revealed three distinct subsets: subsets 1 and 3 which arise upon IL-33 stimulation and are marked by increased expression of Sca-1, Ki67, PD-1, and CTLA-4, compared to subset 2 which is mainly observed in the vehicle and αPD-1treatments (Figure 4.15B).

In STOSE tumors, αPD-1treatment markedly increased the proportion of T cells, including both $CD8^+$ and $CD4^+$ subsets. Within the $CD4^+$ T cell compartment, we additionally observed increased frequencies of Th2 and regulatory T cells (Treg) populations (Figure 4.15C). While the overall increase in T cells is consistent with the known effects of αPD-1-mediated T cell disinhibition, the further enrichment of Th2 and Treg populations in the IL-33+αPD-1 groups suggests that IL-33 provides an additional layer of activation in these cells. However, despite the boost in T cell frequencies, αPD-1 treatment did not translate to increased survival in STOSE tumors (Figure 4.14C). Interestingly, frequencies of NK cells were also increased in response to IL-33 or IL-33+αPD-1 treatment, but not αPD-1 alone, indicating that NK cells are more responsive, directly or indirectly, to IL-33 stimulation than PD-1 blockade in this tumor model. Within the myeloid compartment, we observed increased frequencies of eosinophils and mast cells following IL-33 or IL-33+αPD-1 treatment, as expected (Figure 4.14C). Both cell types express ST2 and therefore respond directly to IL-33, while eosinophils may also be recruited indirectly via ILC2-derived IL-5. In contrast, macrophage frequencies were unchanged with IL-33 treatment but showed a modest

decrease following αPD-1 treatment (Figure 4.14C). Overall, αPD-1 treatment in STOSE tumors resulted in a T cell-dominant tumor microenvironment; however, contrary to its canonical role, this increase in T cell proportions did not translate into an improved survival. In contrast, exogenous IL-33, which lead to the strongest therapeutic response, primarily increased intratumoral ILC2 and NK cells populations, implicating these cells as potential mediators of anti-tumor immunity in the STOSE model.

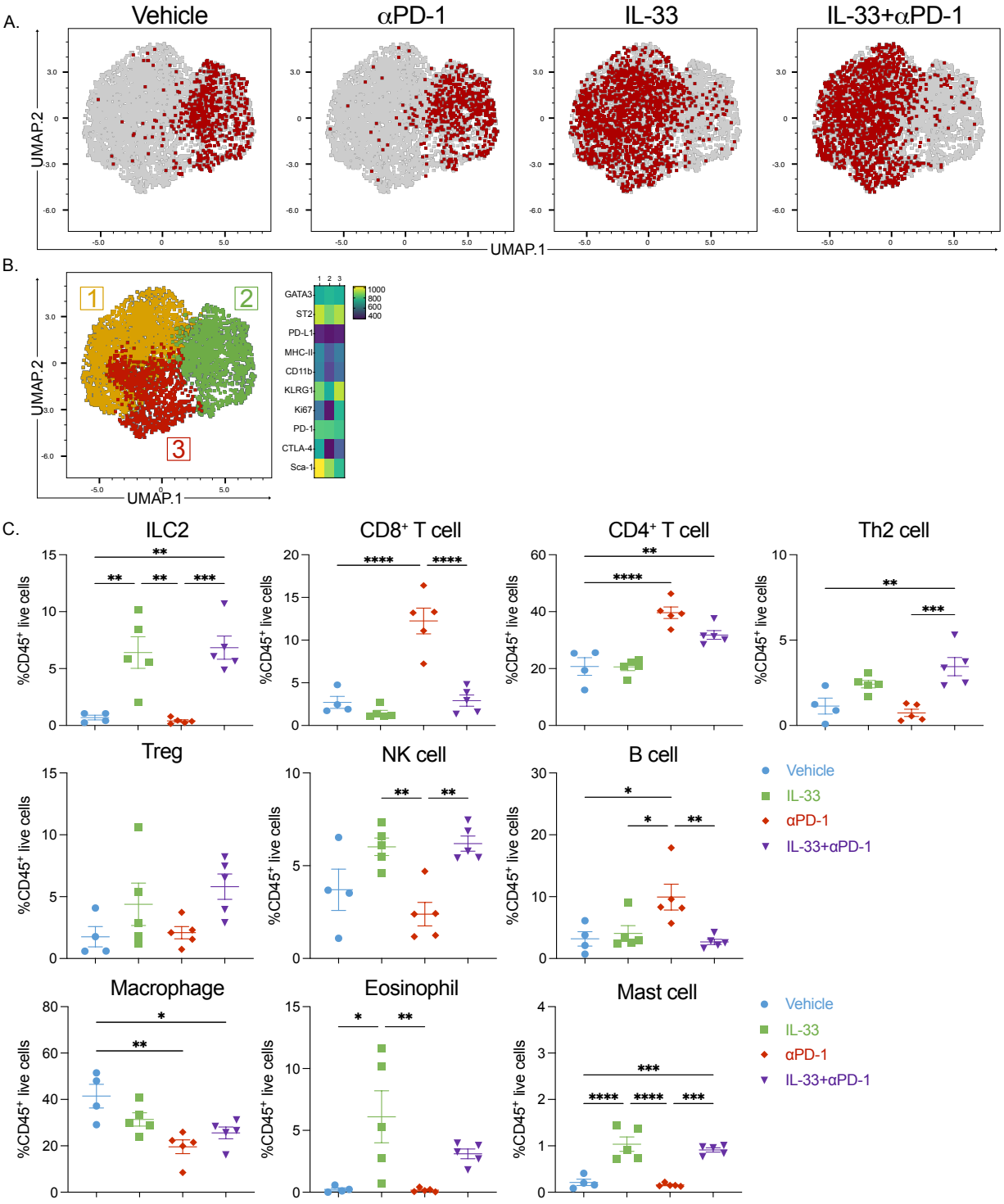
A.
Vehicle
αPD-1
IL-33
IL-33+αPD-1
UMAP.2
UMAP.1
B.
1
2
3
GATA3
ST2
PD-L1
MHC-II
CD11b
KLRG1
Ki67
PD-1
CTLA-4
Sca-1
C.
ILC2
CD8⁺ T cell
CD4⁺ T cell
Th2 cell
Treg
NK cell
B cell
Macrophage
Eosinophil
Mast cell
%CD45⁺ live cells
Vehicle
IL-33
αPD-1
IL-33+αPD-1

Figure 4.15: IL-33 expands ILC2 populations in STOSE tumors. Female FV/BN mice were inoculated with STOSE ovarian cancer cells and subsequently treated with 500ng of IL-33 or PBS every day for five days with 250 μg αPD-1 or vehicle control every other day. Primary tumors, draining lymph node, and peritoneal lavage were collected on day 45 for flow cytometry staining and analysis. (A) UMAP plots depicting phenotypic shifts in tumor ILC2s upon different treatments. (B) FlowSOM analysis representing three ILC2 subpopulations based on differential markers expression. (C) Frequencies and absolute counts of tumor-infiltrating immune cells. Data presented as ± SEM. *N*=4-5/group. One-way ANOVA. *p<0.05, **p<0.01, ***p<0.001, ****p<0.0001.

4.14. VSV-IL-33 offers a new deliverable therapeutic platform

Thus far, our data indicates that IL-33, alone or in combination with αPD-1 treatment, provides a robust therapeutic effect in two orthotopic ovarian tumor models. To extend the clinical application of IL-33+αPD-1 treatment, we designed oncolytic viruses (OVs) in collaboration with the Ilkow and Bell labs at the Ottawa Hospital Research Institute. OV therapy aims to directly infect and induce cell lysis in tumor cells while amplifying the host immune system's anti-tumor responses (*120, 121*). Additionally, OVs have garnered attention as a promising adjuvant for immune checkpoint blockade. We tested one of the most widely used OVs; vesicular stomatitis (VSV) that harbors a deletion in methionine 51 of the matrix (M) protein (VSVΔ51), which supresses the ability of the VSV M protein to block nuclear RNA export, thus allowing infected cells to mount anti-viral immune responses (*122*). Consequently, this VSVΔ51 exhibits attenuated replicative ability in normal cells, but efficiently infects transformed cells that have a comprised anti-viral response (*123*). The VSVΔ51 viral backbone was engineered to express the *Il33* transgene by collaborators and IL-33 expression was validated in the supernatant and cell lysates of VSVΔ51-*Il33*-infected ID8*Trp53*$^{-/-}$*Brca1*$^{-/-}$ cells and clone 3 was selected for in vivo testing (Figure 4.16B).

To this end, mice bearing ID8*Trp53*$^{-/-}$*Brca1*$^{-/-}$ tumors were treated with 1e8 PFU of control or IL-33 expressing-virus every other day for three days followed by 250 μg of αPD-1 daily for five days (Figure 4.16A). VSVΔ51-*Il33* (median survival 56d.) or the VSVΔ51-eGFP control virus (median survival 59d.) did little to improve survival without the co-treatment of αPD-1, although the VSVΔ51-*Il33*+αPD-1 (median survival 78d.) provided superior therapeutic efficacy compared to the VSVΔ51-eGFP+αPD-1 (median survival 64d.) (Figure 4.16C).

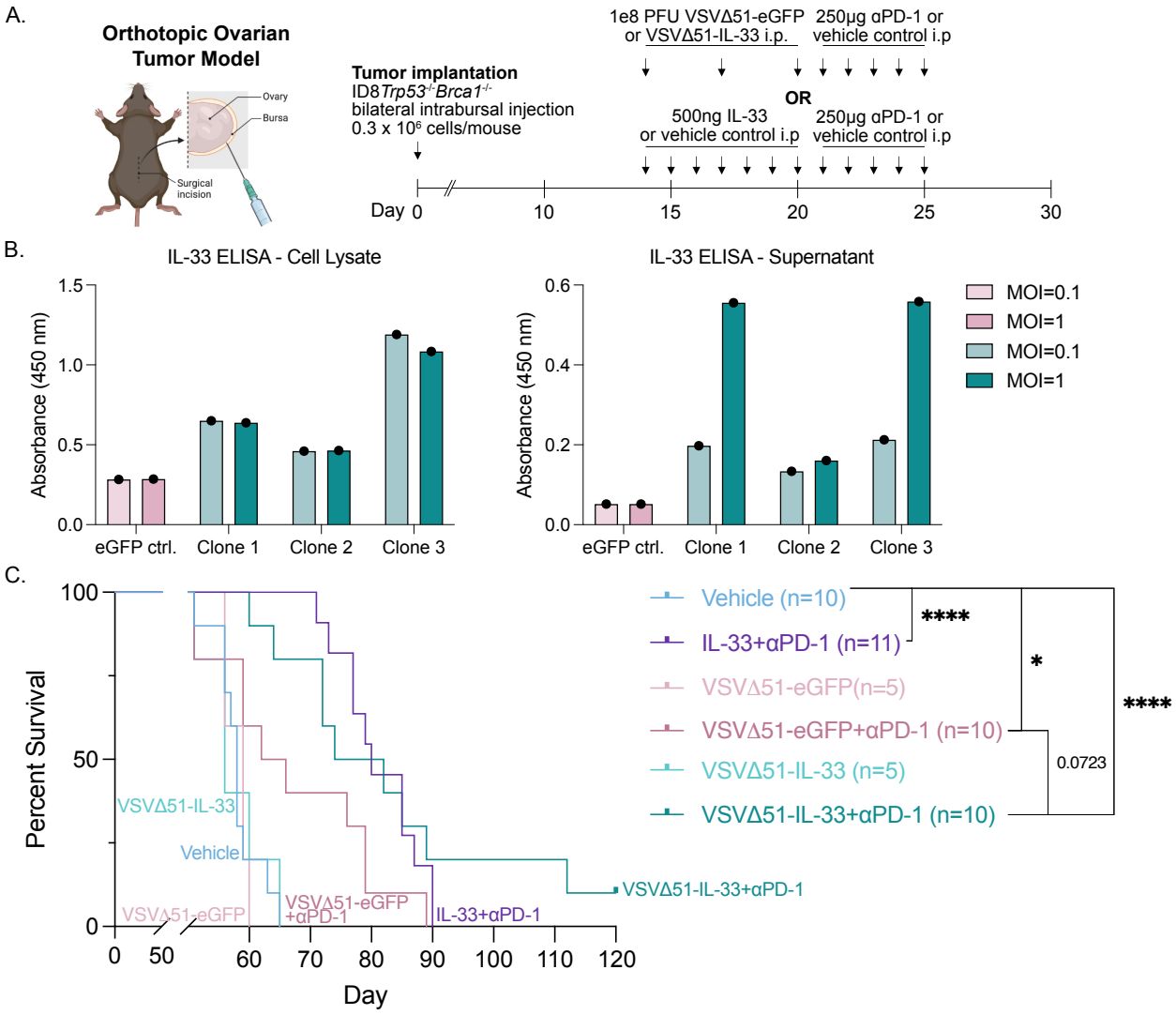

Figure 4.16: αPD-1 enhances the therapeutic effects of VSVD51-IL-33. (A) ID8*Trp53*$^{-/-}$*Brca1*$^{-/-}$ ovarian cancer cells were orthotopically implanted in C57Bl/6 female mice. Following tumor inoculation, mice were treated with 1e8 PFU VSVD51-eGFP or VSVD51-IL-33 on days 14, 16, and 18, then 250 µg αPD-1 for five days. (B) IL-33 expression tested on cell lysate and supernatant samples of VSVΔ51-*Il33* clones (C) Kaplan-Meir curve depicting survival of VSVΔ51-treated mice. The results depicted are representative of 2 independent experiments combined. *n*=5-11/group. Log-rank (Mantel-Cox) test. *p<0.05, **p<0.01, ***p<0.001, ****p<0.0001.

To investigate the immune mechanisms underlying these survival outcomes, we performed an immunoprofiling experiment to uncover the effects of the OV therapy on the ovarian tumor microenvironment. VSVΔ51 infection, particularly with the co-treatment of αPD-1, predominantly elicited T cell responses as reflected by increased frequencies of $CD8^+$ and $CD4^+$ T cells, paralleled with a decreased proportion of NK cells (Figure 4.17). These results were expected because VSVΔ51 infection elicits an inflammatory response which attracts T cells and can be further amplified with the addition of αPD-1 (*124*). However, levels of intratumoral ILC2s did not increase in response to VSVΔ51-eGFP or VSVΔ51-*Il33* treatment, thus confirming that any therapeutic effect observed with this treatment was likely not mediated by ILC2s (Figure 4.17). VSVΔ51 is a lytic virus that has a very short therapeutic window in which the transgene is expressed, as oncolysis clears most cells expressing the transgene. Thus, we hypothesize that VSVΔ51 may not be a suitable OV platform for the delivery of IL-33 to induce ILC2 infiltration into the tumor, and perhaps other OV strategies can address this issue. Current and future investigations in the lab are focused on testing new OV platforms, such as modified vaccine virus Ankara (MVA)-*Il33*, to find an ideal candidate that works in our pre-clinical model. MVA is a highly attenuated, replication deficient poxvirus vector that has been safely used in humans for vaccination (*125*). As an OV therapy, MVA platform has been broadly used to deliver transgene with minimal oncolysis, making the use of MVA-*Il33* a suitable strategy therapeutic IL-33 delivery.

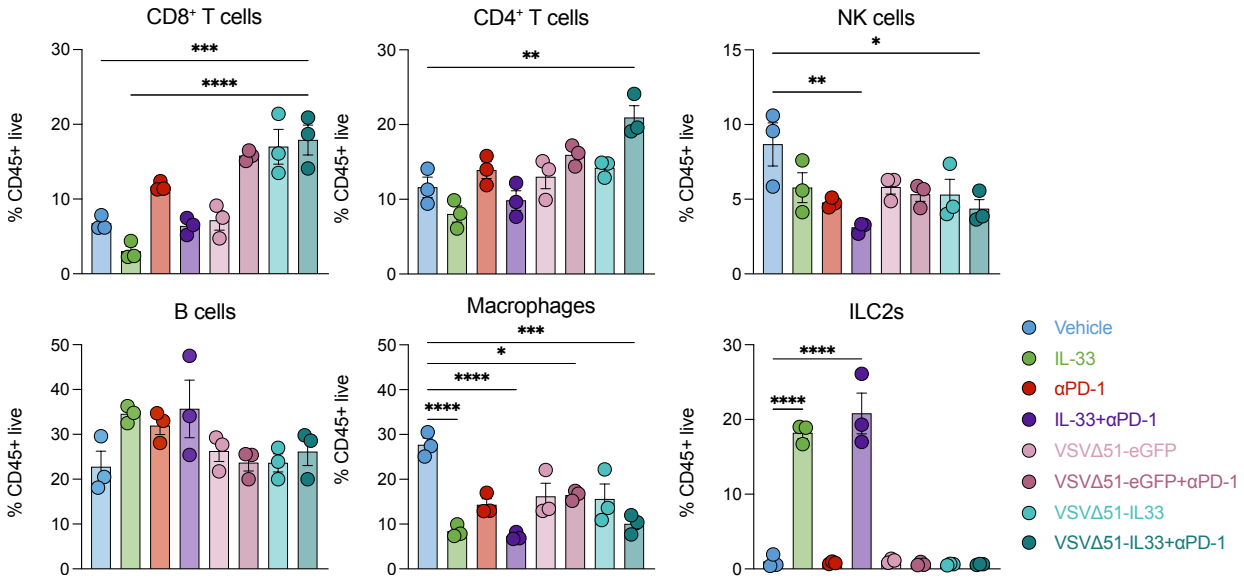

Figure 4.17: VSVΔ51-IL-33 increases T cell, but not ILC2, abundance. (A) ID8*Trp53*$^{-/-}$*Brca1*$^{-/-}$ ovarian cancer cells were orthotopically implanted in C57Bl/6 female mice. Following tumor inoculation, mice were treated with 1e8 PFU VSVΔ51-eGFP or VSVΔ51-*Il33* on days 14, 16, and 18, then 250 μg αPD-1 for five days. On day 45 after tumor implantation, primary tumors were collected for flow cytometry staining and analysis. Frequency of immune cells among live leukocytes depicted. Data presented as ± SEM. *N*=4/group. One way ANOVA, *p<0.05, **p<0.01, ***p<0.001, ****p<0.0001.

Chapter 5:

Beyond ILC2s: uncovering the therapeutic mechanism of IL-33+αPD-1 therapy

5. Beyond ILC2s: uncovering the therapeutic mechanism of IL-33+αPD-1 therapy

5.1. Introduction and rationale

Our data thus far indicates that IL-33 boosts the efficacy of αPD-1 treatment in pre-clinical models of ovarian cancer. IL-33 is a pleiotropic cytokine with multiple cellular targets across both immune and stromal compartments which extend beyond ILC2s alone. For instance, multiple reports indicate that IL-33 can signal directly through human ovarian cancer cells to enhance proliferation and inhibit their apoptosis (*55, 126*). However, we have investigated the expression of ST2 on ID8*Trp53*$^{-/-}$*Brca1*$^{-/-}$ cells and found no expression at the protein level, confirming that IL-33 has no direct impact on tumor cells in this model.

We have previously shown that IL-33 or IL-33+αPD-1 treatment selectively leads to the accumulation of ILC2s in the tumor, dLN, and peritoneal gavage, with notable increases in eosinophils and Th2 cells. Crosstalk between IL-33-activated ILC2s and Th2, eosinophils, or other myeloid cells have been reported to promote tumor killing (*65, 125*). Thus, we hypothesize that IL-33+αPD-1 therapy works through an ILC2-centered axis in this model. However, ILC2s alone are unlikely to account for the full therapeutic efficacy observed. While ILC2s mount rapid and robust responses, they lack antigen specificity, potent cytotoxicity, or phagocytic ability – features that are essential for durable anti-tumor responses. Thus, our next set of investigative studies were aimed at uncovering the contribution of ILC2s, and other immune cells, to the therapeutic efficacy of IL-33+αPD-1.

5.2. IL-33+αPD-1 therapy is still efficacious in Rag1$^{-/-}$ mice

Thus far, the ID8*Trp53*$^{-/-}$*Brca1*$^{-/-}$ tumor model has provided the most consistent and reproducible therapeutic phenotype in response to IL-33+αPD-1 treatment. Moreover, because this model is established in C57BL/6 mice, it enables future studies using transgenic strains on the same background. For these reasons, we exclusively focused on the ID8*Trp53*$^{-/-}$*Brca1*$^{-/-}$ syngeneic model for subsequent investigation in this project.

To uncover the contribution of the adaptive immune system to the therapeutic effect of IL-33+αPD-1, we performed survival analyses in Rag1$^{-/-}$ mice, which lack functional T cells and B cells. Due to availability and breeding limitations, we limited this study to mice treated with either vehicle control, IL-33+αPD-1, or IL-33+αPD-1+αCTLA-4 (Figure 5.1A). Intriguingly, IL-33+αPD-1 treatment still proved to be efficacious in Rag1$^{-/-}$ mice, with a median survival of 74 days compared to 60 days in untreated mice (Figure 5.1B). Moreover, the addition of αCTLA-4 did not confer a survival advantage compared to just IL-33+αPD-1 (median survival 72.5 days), suggesting that αCTLA-4 may be acting through a T cell axis. Nevertheless, all mice still succumbed to the tumor with no long-term survivors as seen in immunocompetent mice. Therefore, since the IL-33+αPD-1 survival phenotype was preserved in the Rag1$^{-/-}$ mice, it suggests that this therapeutic mechanism does not entirely rely on the adaptive immune system, and rather points to an essential role of the innate immune system.

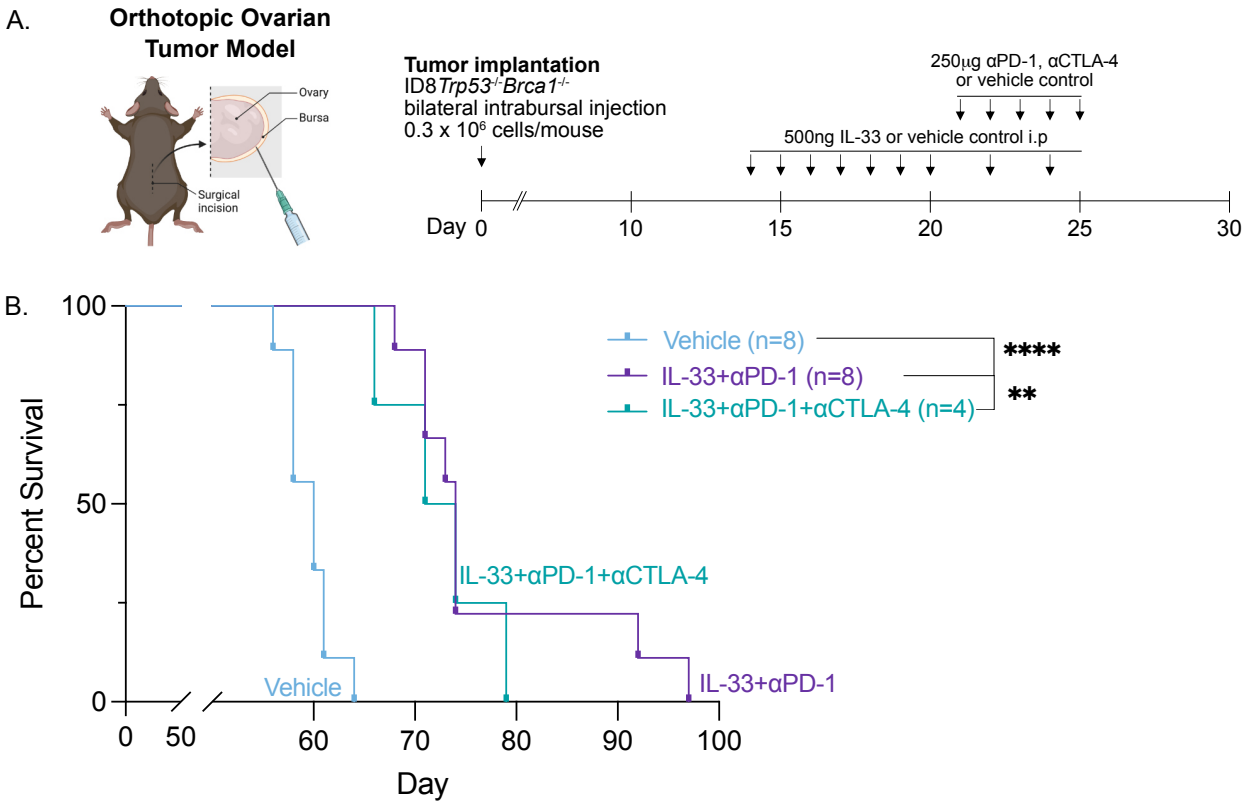

Figure 5.1: IL-33+αPD-1 therapy is still efficacious in Rag1$^{-/-}$ mice. (A) ID8*Trp53*$^{-/-}$*Brca1*$^{-/-}$ ovarian cancer cells were orthotopically implanted in female Rag1$^{-/-}$ mice. Following tumor inoculation, mice were treated with 500ng of rmIL-33, or PBS vehicle control, then 250 µg of αPD-1 daily for five days. (B) Kaplan-Meier curve depicting survival of treated mice. *N*=4-8/group. Log-rank (Mantel-Cox) test. *p<0.05, **p<0.01, ***p<0.001, ****p<0.0001.

5.3. Depletion of NK cells or T cells impairs survival in IL-33+αPD-1-treated mice

To understand the contribution of key immune cells to the therapeutic effect of IL-33+αPD-1, we conducted a survival analysis using various depleting/blocking antibodies. Following tumor implantation, untreated (PBS vehicle control) or treated (IL-33+αPD-1) mice were administered αNK1.1, αCD4/αCD8, or Ig control antibodies, on day -1, 0 of treatment followed by weekly maintenance doses (Figure 5.2A), and successful depletion was verified on day 25 by saphenous blood sampling (Figure 5.2B)

Depletion of NK cells, or $CD4^+$/$CD8^+$ T cells did not affect overall survival in untreated mice (Figure 5.2C). The depletion was initiated two weeks after tumor implantation, before the treatment window, which may explain why the depletion of these immune cells did not affect overall survival. In treated mice, depletion of NK cells led to a severe impairment of survival, suggesting that NK cells are crucial to the therapeutic effect of IL-33+αPD-1. Depletion of $CD4^+$ and $CD8^+$ T cells also led to decreased survival compared to undepleted mice, however to a lesser extent, suggesting that T cells are less necessary than NK cells for this treatment response (Figure 5.3C). This finding corroborates our earlier observation in $Rag1^{-/-}$ mice, where IL-33+αPD-1 treatment was still found to be efficacious without the presence of T cells but with intact NK cells (Figure 5.2).

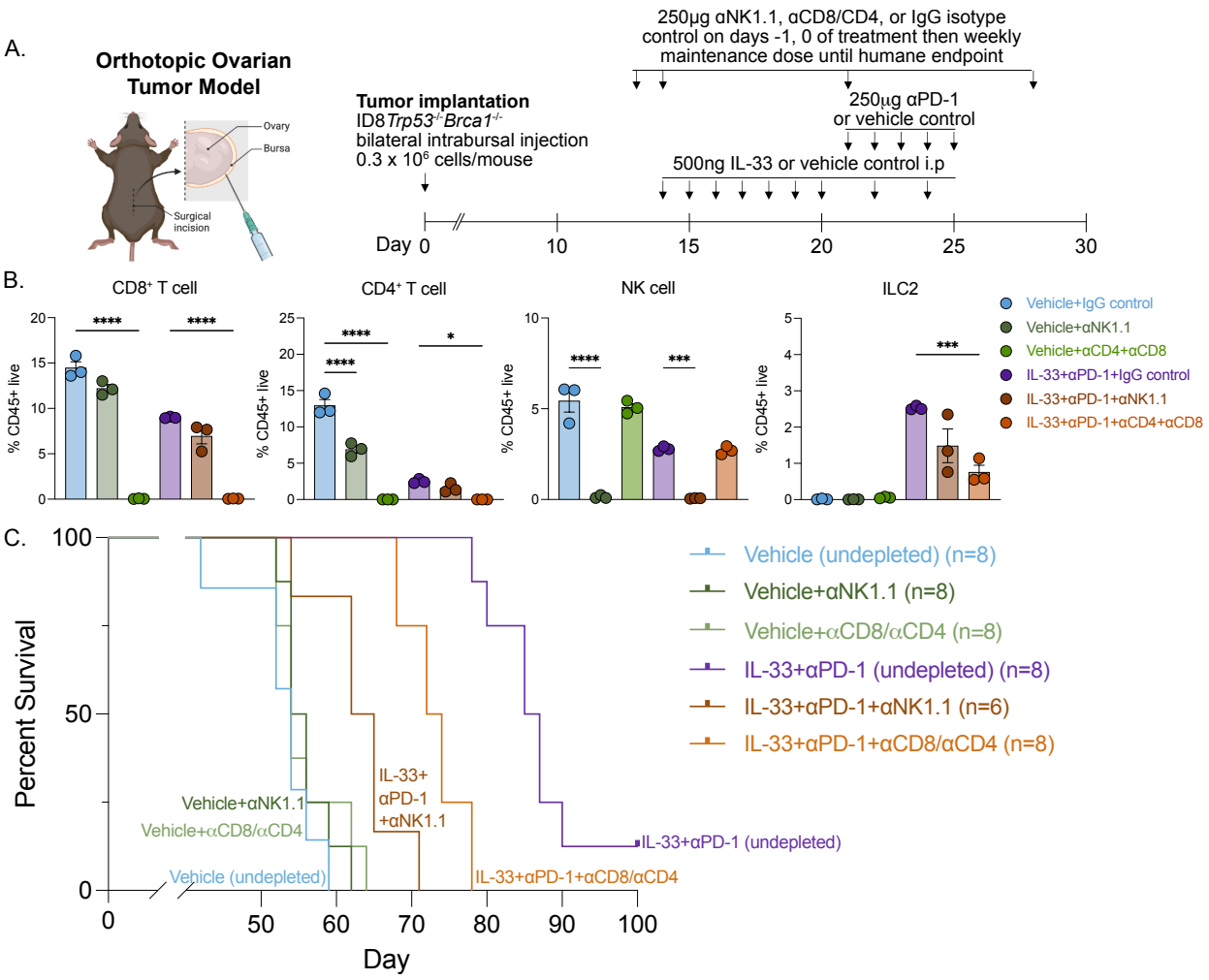

Treatment	Logrank (Mantel-Cox) test	Significance
Vehicle+IgG control vs. IL-33+αPD-1+IgG control	P<0.0001	****
Vehicle+αNK1.1 vs. IL-33+PD-1+αNK1.1	P=0.0086	**
Vehicle+αCD8/αCD4 vs. IL-33+PD-1+αCD8/αCD4	P<0.0001	****
IL-33+αPD-1+IgG control vs. IL-33+PD-1+αNK1.1	P<0.0001	****
IL-33+αPD-1+IgG control vs. IL-33+PD-1+αCD8/αCD4	P=0.0002	***

Figure 5.2: NK cell, but not T cell, depletion abrogates the therapeutic effect of IL-33+αPD-1 (A) ID8*Trp53*$^{-/-}$*Brca1*$^{-/-}$ ovarian cancer cells were orthotopically implanted in female C57Bl/6 mice. Following tumor inoculation mice were treated with 500ng of rmIL-33, or PBS vehicle control, then 250 µg of αPD-1 daily for five days. Depletion injections were initiated on day -1 and 0 of treatment and maintained weekly until humane endpoint. (B) Kaplan-Meier curve depicting survival of treated or untreated mice. *N*=6-8/group. Log-rank (Mantel-Cox) test. *p<0.05, **p<0.01, ***p<0.001, ****p<0.0001.

5.4. IL-5 and IL-13 acts on B cells and macrophages respectively

To identify potential ILC2 crosstalk in tumors treated with IL-33+αPD-1, we next investigated the downstream targets of ILC2-derived IL-5 and IL-13. Analysis of scRNA-seq data using the CellPhoneDB toolkit revealed that ILC2s engage in the highest number of significant interactions with macrophages, NK cells, and B cells in tumors treated with IL-33+αPD-1 (Figure 5.3A). Moreover, ILC2 and macrophages form one of the highest numbers of bi-directional interactions compared to ILC2 interactions with other immune cells (Figure 5.3A). Notably, B cells and eosinophils express high levels of *Il5r,* while macrophages and some DC subsets express the *Il13r*, implicating these populations as potential targets of ILC2-derived IL-5 and IL-13 (Figure 5.3B). These analyses provide insight on cellular targets through which ILC2-derived IL-5 and IL-13 may mediate their effects within the tumor microenvironment.

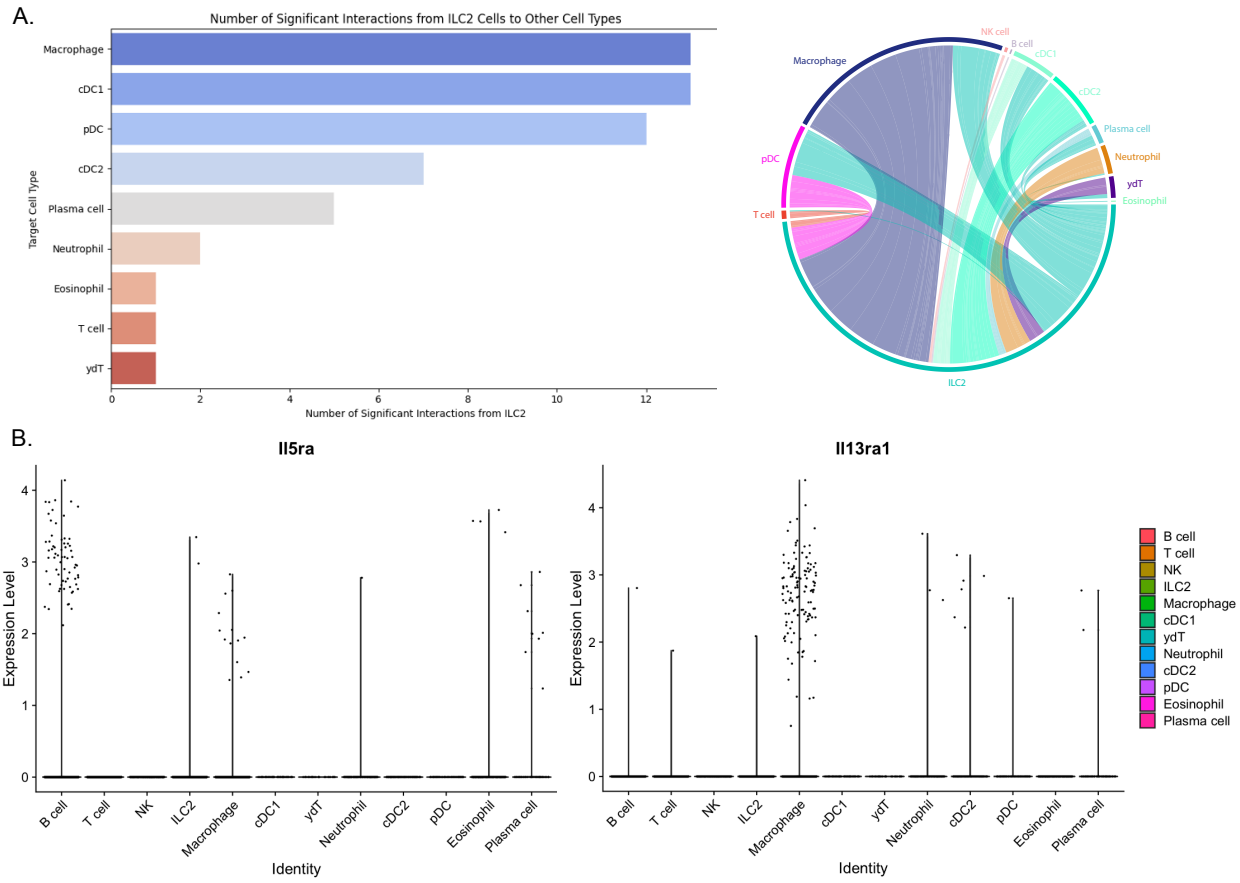

Figure 5.3: *Il5ra* and *Il13ra* is expressed on B cells and macrophages respectively. CD45^{+} live cells were sorted from ID8*Trp53*$^{-/-}$*Brca1*$^{-/-}$ tumors treated with IL-33+αPD-1 for scRNA-seq analysis. (A) Bar plot depicting number of significant interactions from ILC2s (source) to other cell types (target), and chord diagram depicting bi-directional cell communication. (B) *Il5ra* and *Il13ra1* expression on immune cell subsets in the ID8*Trp53*$^{-/-}$*Brca1*$^{-/-}$ tumors treated with IL-33+αPD-1.

5.5. IL-13 but not IL-5 contributes partial therapeutic effects of IL-33+αPD-1

Thus far our findings indicate that ILC2-derived IL-5 and IL-13 act on B cells and macrophages respectively (Graphical Abstract 2.3). ILC2-derived IL-5 has been recently reported to be a non-redundant source for B1 cell development and function (*127, 128*). B1 cells are a subset of innate-like B lymphocytes that are main sources of natural IgM production, uniquely poised to respond to pathogens in a T cell-independent manner (*128*). Given our previous data that *Il5ra* is primarily expressed on B cells, we were interested to see if exogenous IL-5 or IL-33 would alter the B cell compartment, and specifically enrich for these B1 cells.

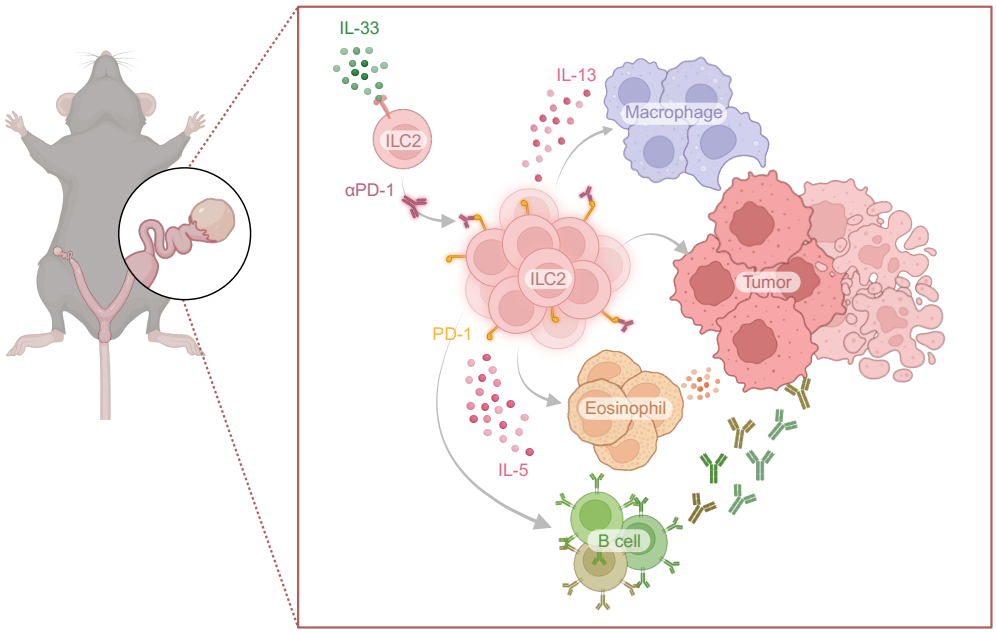

Graphical Abstract 2.3: ILC2-derived IL-5 and IL-13 may mediate anti-tumor immunity with IL-33+αPD-1 treatment. In this proposed mechanism, IL-5 promotes eosinophil recruitment and B cell responses, while IL-13 activates macrophage-mediated tumor cell phagocytosis.

Based on these observations, we examined the individual and combined contributions of IL-5 and IL-13 to the therapeutic efficacy of IL-33+αPD-1. To this end, we treated tumor-bearing mice with IL-33, IL-5, IL-13, IL-5+IL-13 or vehicle control (Figure 5.4A). Interestingly, IL-13 but not IL-5, improved survival (median survival 56d. and 75d. respectively) compared to vehicle control (median survival 56d.) (Figure 5.4B). However, IL-13 alone or IL-5+IL-13 (median survival 65d.) did not recapitulate the survival outcome of IL-33 treated mice, indicating that additional mechanisms contribute to the anti-tumor effects of IL-33.

Immunophenotyping of these tumors revealed that IL-33 and IL-5 expanded B1 cells in the tumor, specifically increasing the abundance of $CD11b^{+}$, B1a, and B1b subsets (Figure 5.4B). These data suggests a possible IL-33-ILC2-B1 cell axis in the tumor, which may contribute to the anti-tumor effects observed in IL-33+αPD-1 treatment.

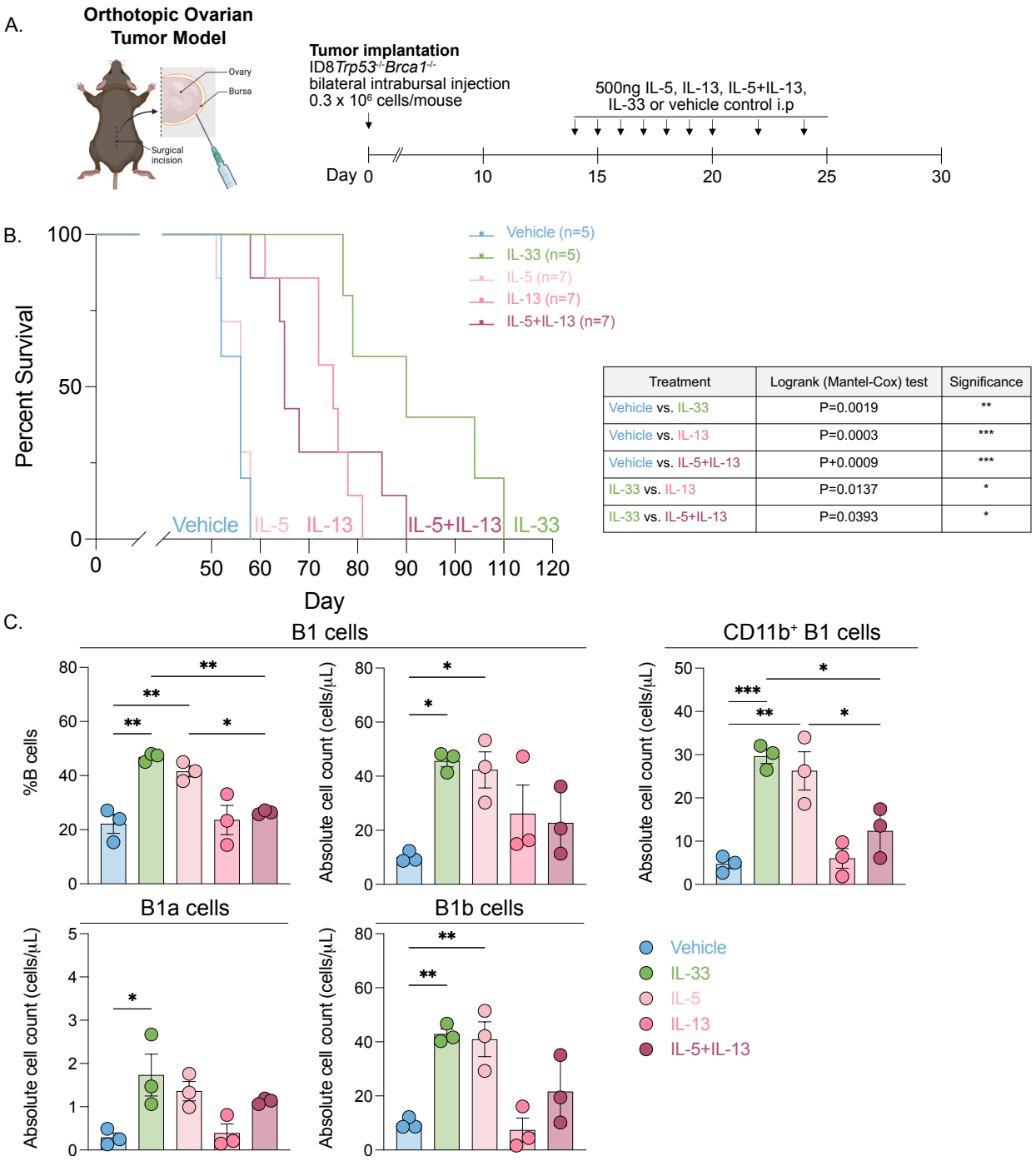

Treatment	Logrank (Mantel-Cox) test	Significance
Vehicle vs. IL-33	P=0.0019	**
Vehicle vs. IL-13	P=0.0003	***
Vehicle vs. IL-5+IL-13	P+0.0009	***
IL-33 vs. IL-13	P=0.0137	*
IL-33 vs. IL-5+IL-13	P=0.0393	*

Figure 5.4: IL-13, but not IL-5 contributes some therapeutic potential. (A) ID8*Trp53*$^{-/-}$*Brca1*$^{-/-}$ ovarian cancer cells were orthotopically implanted in female C57Bl/6 mice. Following tumor inoculation mice were treated i.p. with 500ng of IL-5, IL-13, IL-5+IL-13, IL-33, or PBS vehicle control and assessed for survival. (B) Kaplan-Meir curve depicting survival of cytokine treated or untreated mice. *N*=5-7 for each group. Log-rank (Mantel-Cox) test. **p<0.01, ***p<0.001, ****p<0.0001. (C) Tumors from cytokine-treated mice were stained for flow cytometry analysis and immune-profiling of B cell subsets. *N*=3/group. One-way ANOVA. *p<0.05, **p<0.01, and ***p<0.001.

5.6. B cell depletion abrogates the therapeutic effect of IL-33+αPD-1

B1 cells are long-lived cells that constitutively produce natural IgM, and ILC2s are a non-redundant source of IL-5 essential for their development and maintenance. ILC2-derived IL-5 also promotes recruitment, expansion, and survival of eosinophils. Thus we hypothesized that ILC2-derived IL-5 contributes to therapeutic effect of IL-33+αPD-1 by promoting eosinophil recruitment and B1-mediated production of IgM. To test this, we administered αIL-5, αCD-19, or αIgG1 on days -1 and 0 of treatment followed by weekly maintenance doses to untreated or IL-33+αPD-1-treated mice (Figure 5.5A). IL-5 blockade was employed to deplete eosinophils, while also functionally addressing the contribution of IL-5 in promoting B1 responses through ILC2 activation.

IL-5 blockade effectively depleted eosinophils, however, did not affect overall B cell abundance as confirmed by saphenous bleed on day 25 (Figure 5.5B). A small cohort of mice were sampled from this survival experiment on day 45 (~75% median survival), and tumors were weighed and immunophenotyped. As expected, untreated mice had generally larger tumor weights than treated mice. Strikingly, untreated mice receiving IL-5 blockade had significantly smaller tumors compared to isotype control, comparable to the size of tumors in IL-33+αPD-1-treated mice (Figure 5.5C). IL-5 blockade (median survival 71d.) or CD19 depletion (median survival 65d.) did not yield significant changes in overall survival of untreated mice compared to isotype control (median survival 71d.). However, depletion of B cells using the CD19 antibody significantly impaired survival in IL-33+αPD-1-treated mice (median survival 74d.) compared to isotype control (median survival 92d.), suggesting an important role for B cells in this therapeutic response (Figure 5.5D). Just as IL-5 supplementation did not affect overall survival, IL-5 blockade in IL-

33+αPD-1 mice failed to compromise survival (median survival 107d.) compared to isotype control (median survival 92d.) (Figure 5.5D).

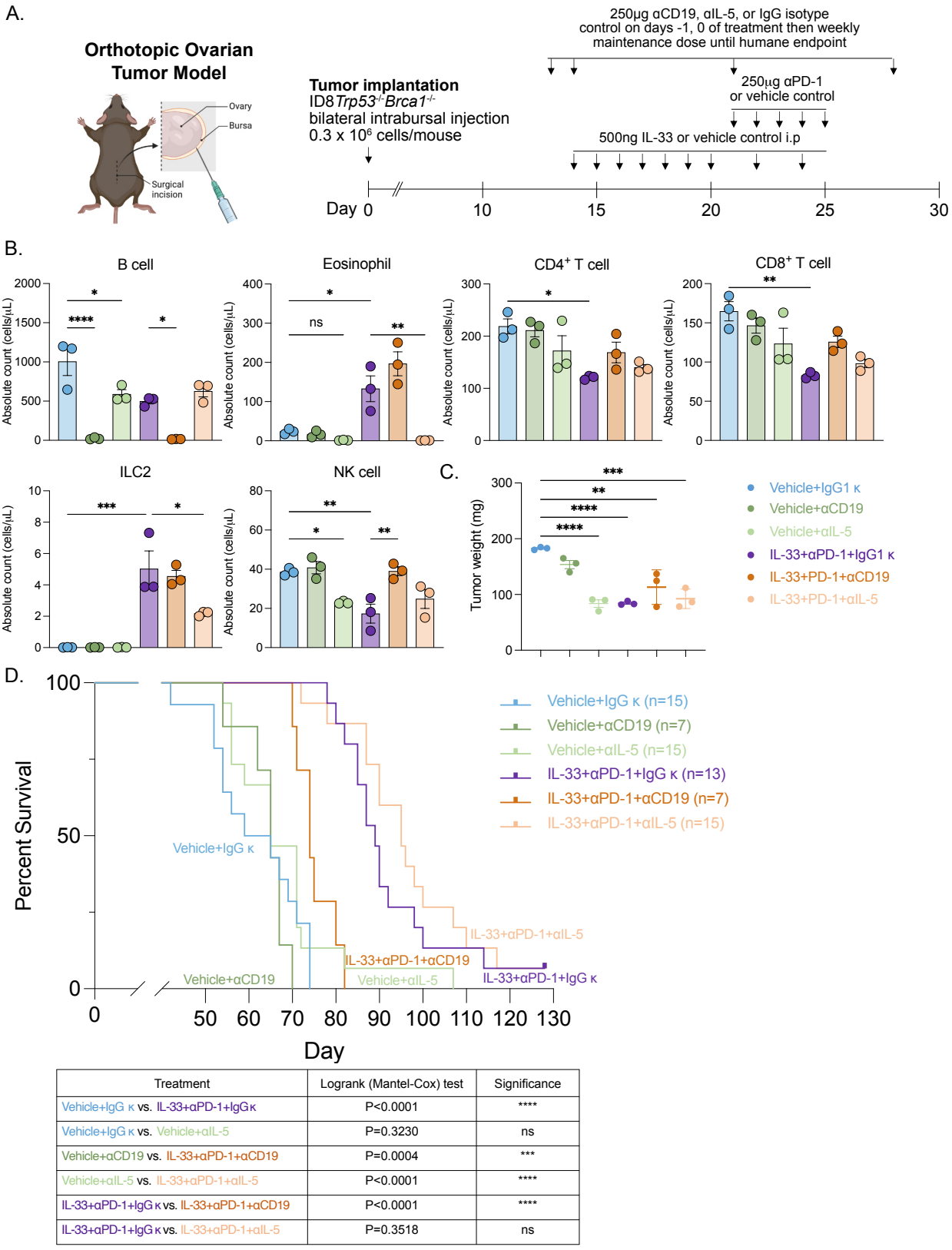

Treatment	Logrank (Mantel-Cox) test	Significance
Vehicle+IgG κ vs. IL-33+αPD-1+IgGκ	P<0.0001	****
Vehicle+IgG κ vs. Vehicle+αIL-5	P=0.3230	ns
Vehicle+αCD19 vs. IL-33+αPD-1+αCD19	P=0.0004	***
Vehicle+αIL-5 vs. IL-33+αPD-1+αIL-5	P<0.0001	****
IL-33+αPD-1+IgG κ vs. IL-33+αPD-1+αCD19	P<0.0001	****
IL-33+αPD-1+IgG κ vs. IL-33+αPD-1+αIL-5	P=0.3518	ns

Figure 5.5: B cell depletion abrogates the effects of IL-33+αPD-1 treatment. (A) ID8*Trp53*$^{-/-}$ *Brca1*$^{-/-}$ ovarian cancer cells were orthotopically implanted in female C57Bl/6 mice. Following tumor inoculation, on day 14, mice were treated with 500ng of rmIL-33, or PBS vehicle control, then 250 μg of αPD-1 daily for five days. Depletion injections were initiated on day -1 and 0 of treatment and maintained weekly until humane endpoint. (B) Validation of depletion using saphenous blood sampling on day 25. (C) Tumors weights from mice collected on day 45. (D) Kaplan-Meir curves depicting survival of mice untreated or treated mice under various depleting regimens. *N*=7-15/group. Log-rank (Mantel-Cox) test. **p<0.01, ***p<0.001, ****p<0.0001.

Collectively, these data indicate that ILC2-derived IL-5, though abundant in IL-33+αPD-1-treated mice, does not confer anti-tumor immunity in this model. IL-5 leads to eosinophil recruitment and increased abundance of B1 cells; however, experimental blockade of IL-5 suggests that these cells are dispensable for the outcome of IL-33+αPD-1 treatment (Graphical Abstract 2.3).

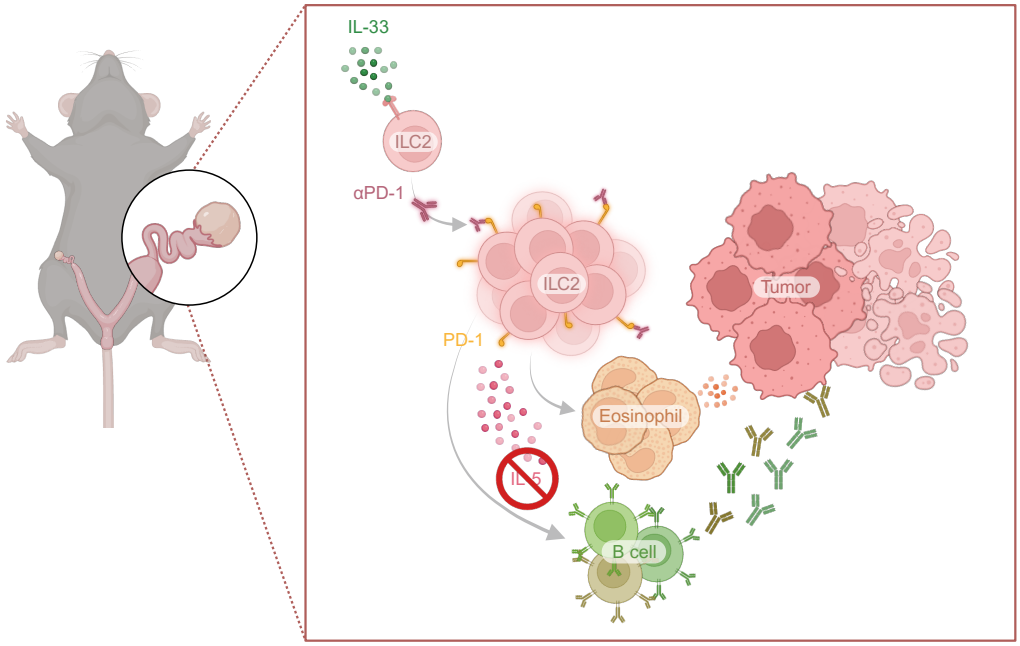

Graphical Abstract 2.3: IL-5 is dispensable for the therapeutic outcome of IL-33+αPD-1 treatment. IL-5 blockade, while effectively depleting eosinophils, did not reduce the effectiveness of IL-33+αPD-1 treatment.

5.7. IL-5 blockade reduces B1 cells but concomitantly increases follicular B cells

Immunophenotyping of the tumors, dLN, and peritoneal lavage confirmed depletion of eosinophils but revealed no major alterations in myeloid and lymphoid populations (data not shown), with the exception of marked phenotypic changes in the B cell compartment (Figure 5.6A). As expected, IL-5 blockade reduced B1 cell abundance in tumors, dLN, and peritoneal lavage. However, unexpectedly, IL-5 blockade led to a marked increase in follicular B2 cells (Figure 5.6B). In the dLN, this was associated with a significant expansion of germinal B cells (Figure 5.6B). In contrast to B1 cells that produce natural IgM, follicular B cells proliferate, undergo immunoglobulin class switch recombination, and T-cell dependent activation. Together, these results indicate that IL-33+αPD-1 treatment promotes B1 cell responses through ILC2 activation and IL-5 secretion. In this context, IL-5 blockade induces a compensatory shift within the B cell compartment from B1 cells towards B2 cells undergoing germinal center responses. Nevertheless, IL-5 –and by extension B1 cells and eosinophils– remain dispensable for the therapeutic efficacy of IL-33+αPD-1, indicating the involvement of additional non-humoral mechanisms.

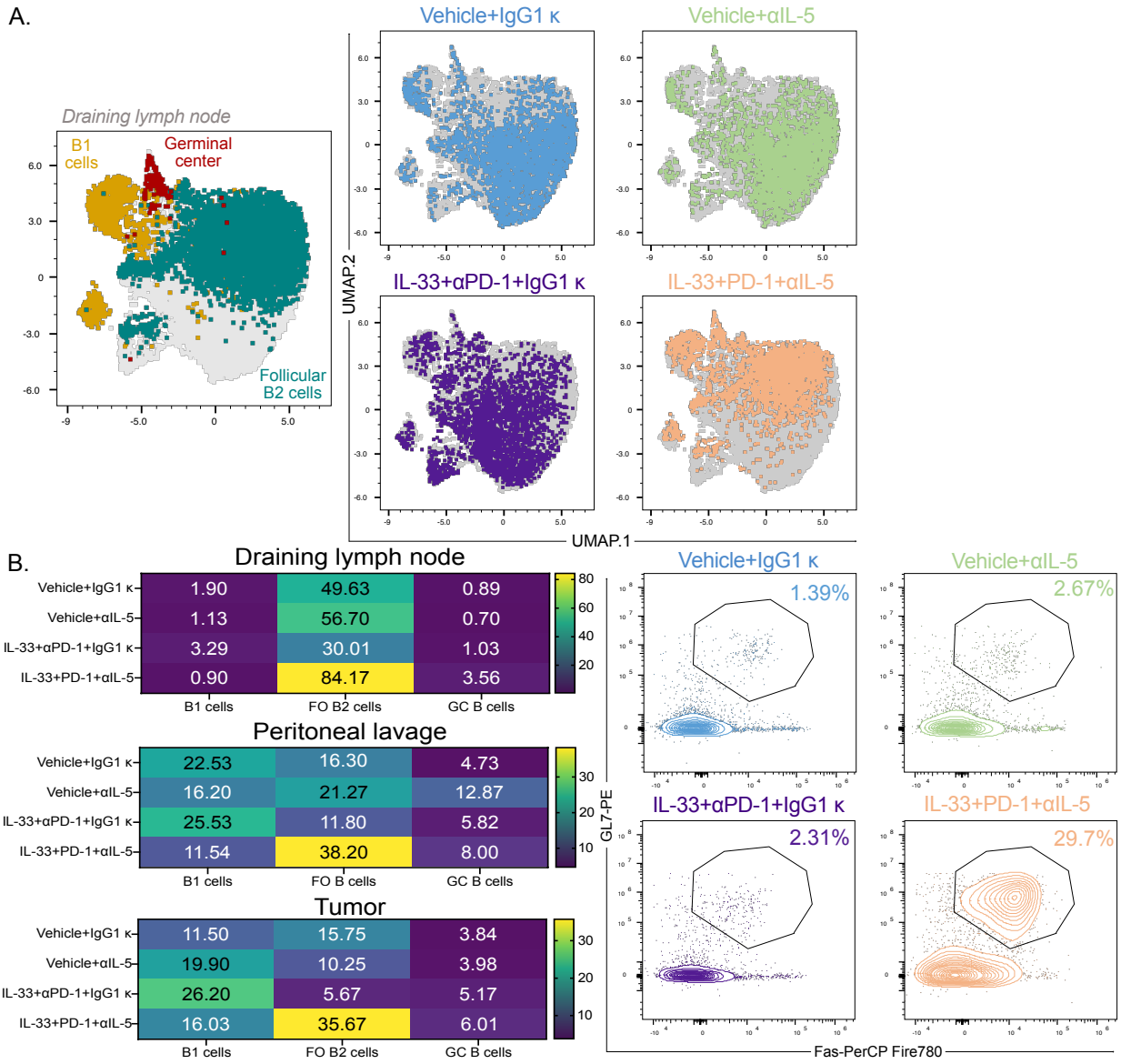

Figure 5.6: IL-5 blockade enriches B2 germinal center cells. (A) Mice were inoculated with ID8*Trp53*$^{-/-}$*Brca1*$^{-/-}$ orthotopic tumors and were treated with IL-33+αPD-1, and additional weekly doses of αIL-5 or isotype control. Tumors were collected on day 45 and stained for flow cytometry analysis and B cell phenotyping. (A) UMAP plot depicting B cell subsets in the draining lymph node. (B) Heatmaps depicting frequencies of B cell subsets in the draining lymph node, peritoneal lavage, and tumor. Flow cytometry contour plots depicting germinal center B2 cells and frequencies in the lymph node. One-way ANOVA. **p<0.01, ***p<0.001, ****p<0.0001.

Chapter 6: Discussion

6. Discussion

6.1. Summary of findings

ILC2s are emerging players of tissue inflammation and tumor immunity. In this thesis, we broadly aimed to delineate their role and regulation in ovarian health and disease. Through detailed phenotypic and functional profiling, we showed that mouse ovarian ILC2s are highly responsive to epithelial-derived cytokines and steroid hormone signalling – both of which fluctuate dynamically through the progression of the estrus cycle. Notably, ILC2s are enriched during the pre-ovulatory stage of the estrus cycle and rapidly decline in abundance post-ovulation, suggesting cyclical regulation of these cells. Although estrogen levels peak in parallel to ILC2 abundance in the ovary, functional analyses revealed that ILC2s were responsive to androgen, rather than estrogen, signalling. This androgen sensitivity prompted us to investigate the role of ILC2s in a mouse model of PCOS, a pilot study that is still under investigation. Collectively, our findings provide a detailed characterization of ILC2s in the mouse ovary – a population previously identified only at the transcriptional level (*129*).

Next, we extended our investigation of ILC2s to the ID8*Trp53*$^{-/-}$*Brca1*$^{-/-}$ mouse model of ovarian cancer where the tumoricidal capacity of ILC2s had also not yet been investigated. ILC2s were detected in orthotopic ovarian tumors where they expressed PD-1, which was further upregulated upon IL-33 treatment. This finding built the rationale to evaluate the therapeutic efficacy of IL-33 and αPD-1 combination therapy in the highly aggressive ID8*Trp53*$^{-/-}$*Brca1*$^{-/-}$ orthotopic model, which has shown limited response to αPD-1 alone (*130, 131*). IL-33+αPD-1 provided a superior and durable response compared to either monotherapy. Moreover, IL-33+αPD-1 treatment markedly remodeled the tumor microenvironment towards type 2 immunity, which was dominated

by ILC2s, eosinophils, Th2, and B1 cells. Depletion analyses revealed that NK cells, T cells, and B cells all contribute to the therapeutic benefit of IL-33+αPD-1 treatment at varying levels. Functional analyses also revealed that tumor ILC2s exhibit anti-tumor cytotoxicity revealing another potential mechanistic arm in this model. Current and future investigations aim to further delineate the role of ILC2s in this therapeutic effect.

6.2. ILC2s are important regulators of tissue inflammation in the ovary

The immune system has traditionally been studied in the context of host defense; however, its role in maintaining organ homeostasis under physiological conditions has been comparatively underappreciated. Acting as a homeostatic rheostat, the immune system orchestrates cycles of inflammation and resolution to preserve tissue integrity. The ovary represents a unique interface between the reproductive and immune systems, where this tightly regulated inflammation is essential for ovulation (*7*).

ILC2s are central drivers of tissue inflammation, with a possible role in ovulation. In mice induced to superovulate, we found that ILC2s predominate in proestrus, that is, the pre-ovulatory stage of the estrus cycle. Parallel to this, we found that *Il33* was highly expressed at the transcriptional level. These data led us to hypothesize that IL-33, an epithelial-derived alarmin, is expressed during the inflammatory response of ovulation leading to an acute expansion of ILC2s. IL-33-ST2 signalling in the ovary may therefore facilitate the process of ovulation. Indeed, blockade of IL-33 signalling led to a significant reduction of ovulated oocytes, implicating the significance of IL-33-ST2 axis in ovulation. Whether this observation was ILC2-mediated is a limitation of this study and will be addressed with appropriate models of ILC2-deficiency (as described in section 6.4)

As the newest member of the IL-1 family of cytokines, IL-33 emerges as a consequential cytokine during ovulation. While other pro-inflammatory cytokines, such as IL-6 and IL-1β have established roles in ovulation (*132, 133*), the role for IL-33 has not yet been established. We and others have shown that *Il33* is highly expressed in the mouse ovary during proestrus (*39, 40*). In our transcriptomic analysis, we also found *Areg* to be highly expressed in proestrus concurrently with *Il33*. Amphiregulin, the protein that is encoded by *Areg*, has important implications in the LH-induced cumulus expansion and follicle rupture (*134*). Amphiregulin is also highly expressed by IL-33 activated ILC2s in several inflammatory contexts to promote tissue protection under inflammatory conditions (*88, 135, 136*). Collectively, these findings indicate a possible IL-33-ILC2-amphiregulin axis in the mouse ovary, however, the precise dialogue of these interactions requires further investigation.

ILC2s are also uniquely regulated by steroid hormone signalling (*92, 93, 137*). However, unlike lung ILC2s, we found that androgen signalling positively regulated ILC2 numbers in the ovary. With selectively high expression of the androgen receptor, *Ar*, but not estrogen receptors, *Esr1* and *Esr2*, ILC2s are uniquely poised to respond to the local and temporal expression of androgen in the ovaries. Physiologically, androgen production in the ovary fulfills two important roles: providing the substrate for aromatization into estrogens, and to support the growth and maturation of the ovarian follicle. However, excess androgen production is a cardinal feature of PCOS, a condition characterized by an abundance of abnormal fluid-filled cysts in the ovaries leading to anovulation and infertility along with a constellation of symptoms including insulin resistance, cardiovascular disease, and obesity (*138-140*). Despite the multifactorial nature of the disease,

hyperandrogenism and systemic inflammation remain central facets and key diagnostic features of PCOS.

Given that inflammation and hyperandrogenism are primary features of PCOS, we hypothesized that androgen-responsive ILC2s contribute to its pathogenesis by sustaining a chronic low-grade inflammatory response. We leveraged the use of a PCOS mouse model established by slow release letrozole, an aromatase inhibitor that elevates androgen levels. Although the model requires further optimization, we have established the PCOS phenotype and show that ILC2 numbers are modestly elevated, indicating a possible role of ILC2s in the immunopathology of PCOS. Future investigations in the lab will aim to establish a role of ILC2s in the PCOS model and investigate their functional role in the development or progression of disease.

Collectively, our analyses reveal a novel presence of ILC2s in the mouse ovary during normal estrus cycling, ovulation, and potentially in hyperandrogenic conditions such as PCOS. We hope future studies from this thesis will clarify the role of ILC2s in the etiology of ovarian disorders like PCOS and explore a prognostic role for ILC2s in these conditions.

6.3. Harnessing ILC2s for immunotherapy in ovarian cancer

In this thesis we show IL-33+αPD-1 treatment improves survival in the ID8*Trp53*$^{-/-}$*Brca1*$^{-/-}$ orthotopic ovarian cancer model, providing durable anti-tumor protection and curative potential. Here we propose a model in which the therapeutic effect of IL-33+αPD-1 is mediated through an ILC2-centric framework involving multiple immune pathways (Graphical Abstract 2.4).

IL-33-responsive ILC2s accumulate in ID8*Trp53*$^{-/-}$*Brca1*$^{-/-}$ tumors and, upon IL-33 stimulation, undergo robust expansion with enhanced activation and effector function. ILC2s also express *CD266*, *Tnfsf10*, and *Tnfrsf10b* – genes associated with immune cell recognition and activation of cell death pathways, suggesting a potential role in direct tumor killing. Consistent with this, our cytotoxicity assays show that ex-vivo tumor ILC2 can direct tumor-specific killing, revealing a cell-intrinsic mechanism of ILC2-mediated tumor immunity (Graphical Abstract 2.4A). Although the mechanisms underlying ILC2-mediated cytotoxicity remain incompletely understood, these findings highlight a novel unexplored anti-tumor role for ILC2s.

In ID8*Trp53*$^{-/-}$*Brca1*$^{-/-}$ tumors treated with IL-33+αPD-1, ILC2s express canonical type 2 effector cytokines including IL-4, IL-5, IL-9, and IL-13. Furthermore, ascites collected from IL-33+αPD-1-treated mice had significantly elevated levels of IL-5 and IL-13, suggesting their role in treatment response. Our scRNA-seq data identified eosinophils and B cells as potential targets for IL-5 and macrophages as IL-13 targets. However, survival studies using IL-5 supplementation or blockade strongly indicated that IL-5 is not required for anti-tumor immunity in this model. In contrast, IL-13 offered a modest improvement in survival, suggesting it may contribute to the therapeutic effects of IL-33+αPD-1 treatment. Current and future work is aimed at investigating whether IL-13-activated macrophages mediate antibody dependent cellular phagocytosis as a potential mechanism for this model (Graphical Abstract 2.4B).

Finally, we explored the role of the adaptive immune system in this model. Although IL-33+αPD-1 treatment remained efficacious in Rag1$^{-/-}$ mice, median survival was reduced compared to C57Bl/6 mice and no long-term survivors were observed, indicating that adaptive immunity is

essential for full therapeutic efficacy. Consistent with this, depletion studies showed that B cells, NK cells, and T cells all contribute to the therapeutic effect of IL-33+αPD-1 treatment. Notably, loss of B cells or NK cells markedly impaired survival, suggesting an additional mechanistic arm in this model. We propose that IL-33+αPD-1 treatment may promote B cell antibody production that enables NK cell-mediated antibody-dependent cellular cytotoxicity (Graphical Abstract 2.4C). Future studies will investigate this mechanism alongside tumor antigen-specific T cell responses. Together these data support a model in which IL-33+αPD-1 treatment exerts its effects through multiple immune pathways, with or without direct involvement of ILC2s.

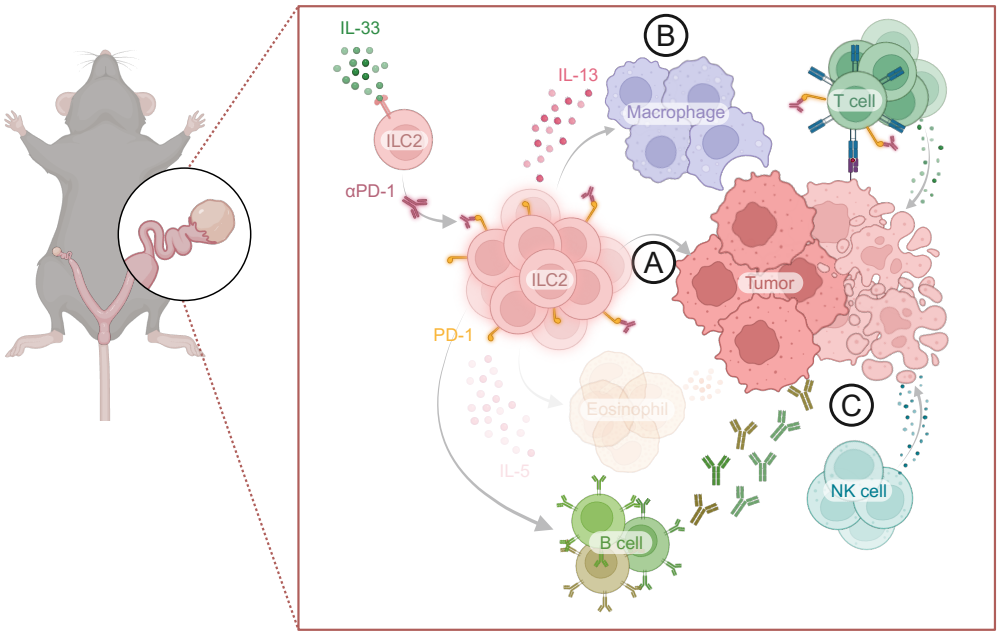

Graphical Abstract 2.4: Proposed mechanism for IL-33+αPD-1 treatment. The therapeutic mechanism for IL-33+αPD-1 treatment is centered on IL-33-responsive ILC2s acting through multiple immune pathways. (A) Tumor ILC2s can mediate direct tumor cytotoxicity. (B) ILC2-derived IL-13 contributes some therapeutic potential, possibly by activating macrophage-mediated tumor cell phagocytosis. (C) B cells, NK cells, and T cells all contribute at varying levels to the therapeutic mechanism of IL-33+αPD-1 treatment, possibly through direct cytotoxicity or antibody dependent cellular cytotoxicity.

6.4. Beyond the binary: type 1 versus type 2 immunity in tumor immunology

Within tumor immunology, type 1 and type 2 immunity have been framed as opposing arms of the immune response to cancer. Traditionally this dichotomy has shaped the prevailing model that type 2 immune cells – such as Th2 cells, ILC2s, eosinophils, and M2 macrophages – facilitate tumor progression and limit the effectiveness immunotherapy, while type 1 cytotoxic tumor-infiltrating lymphocytes (TILs) are generally associated with tumor control and better responses to immunotherapy.

IL-33+αPD-1 strongly induced a type 2 polarized tumor microenvironment in the ID8*Trp53*$^{-/-}$*Brca1*$^{-/-}$ orthotopic model. This was characterized by an accumulation of tumor-infiltrating ILC2s, Th2 cells, eosinophils, and B1 cells, along with elevated levels of IL-5 and IL-13 in the peritoneal fluid. ILC2s, the major immune cell type enriched in IL-33+αPD-1-treated tumors, formed the highest number of significant interactions with macrophages and B cells. Concurrently, we observed a reduction in tumor-infiltrating CD8^{+} lymphocytes and NK cells. Together, these data paint a picture of a type 2 dominated tumor microenvironment, normally ascribed for its pro-tumoral function. Yet, in the ID8*Trp53*$^{-/-}$*Brca1*$^{-/-}$ model, IL-33+αPD-1 treatment offered a superior therapeutic response.

Thus, we provide evidence for anti-tumoral function for type 2 immunity. In the ID8*Trp53*$^{-/-}$*Brca1*$^{-/-}$ orthotopic model treated with IL-33+αPD-1, the paucity of tumor-infiltrating CD8^{+} T cells and NK cells may seem antithetical to anti-tumor activity, but if one considers the tumoricidal capacity of type 2 immunity, it is not far-fetched to suggest that these cells are coordinating a complex multifaceted anti-tumor response. Originally type 2 immunity defend against parasitic helminth

infections, but the same mechanisms that type 2 immune cells use to expel helminth can also be repurposed to protect against cancer (*141*). After all, helminths can evade host immunity through similar evasion strategies as cancer cells (*142*).

Thus, emerging evidence in the literature, and those presented in this thesis, challenge this paradigm (*141*). The central dogma of type 1 versus type 2 immunity has confined our understanding of tumor immunology as a duality, instead of considering it as a more nuanced, multifaceted microenvironment where multiple cell types coordinate to mount anti-tumor responses.

6.5. Limitations of study

Lastly, our data supports a model where IL-33+αPD-1 treatment functions through ILC2s to mediate anti-tumor immunity. IL-33+αPD-1 strongly and preferentially expands and activates ILC2s in the tumor bed, leading to elevated levels of IL-5 and IL-13. However, in this thesis, we have not addressed the direct contribution of ILC2s to these anti-tumor effects using genetic and pharmaceutical models of ILC2-deficiency. Pharmaceutically targeting ILC2s for depletion was attempted multiple times using the CD90.2 antibody in naïve mice, and but was unable to achieve ILC2 depletion in the lungs or ovaries. Nonetheless, the CD90.2 antibody is a non-specific and outdated method to deplete ILC2s. There are now more robust genetic mouse models of ILC2 deficiency that use the Nmur1-iCre mice, which express iCre and eGFP driven by the neuromedin I receptor 1 (Nmur1). Nmur-1 is specifically expressed on ILC2s with minimal to no expression found on other immune cells. We have crossed the Nmur1-iCre mice with *Il1rl1*$^{fl/fl}$ mice to generate mice that lack the ST2 receptor on ILC2s, and with Gata3$^{fl/fl}$ mice to generate mice that are ILC2-

deficient. Both models will address the contribution of ILC2s to the therapeutic effect of IL-33+αPD-1, with the *Nmur1*$^{iCre\text{-}eGFP}$*Il1rl1*$^{fl/fl}$ mice mechanistically addressing whether IL-33 is primarily signalling through ILC2s. We anticipate that by leveraging the use of these genetic models, we will show a contribution of ILC2s to the therapeutic effect of IL-33+αPD-1 treatment.

Throughout most of this thesis we have used the ID8*Trp53*$^{-/-}$*Brca1*$^{-/-}$ orthotopic tumor model. Although this model reflects the clinical and mutational features of HGSC, it does not reflect the primary tissue of origin. We have better models to reflect this, such as the MOE and KPCA models (*144, 145*), which originate from the fallopian tube epithelium, the tissue now widely accepted to be the site from which most HGSC cases arise. Current and future investigations in the lab are testing the use of IL-33+αPD-1 treatment in these models. Lastly, the use of human ovarian cancer cell lines or primary organoid cultures have not yet been tested with this treatment. Recently, the presence of ILC2s in human ovarian carcinomas have been described (*146*), which provides a rationale to continue our studies in human ovarian tissue specimens in future investigations for the discovery of novel therapeutic strategies for ovarian cancer.

6.6. Future of immune checkpoint inhibitors in ovarian cancer

Though ovarian cancer care has rapidly evolved over the past half-century –from surgical debulking and traditional chemotherapy, to PARPi, and now to immune checkpoint inhibitors– the clinical success of precision use immunotherapy remains a challenge. Patient outcomes have greatly improved with the incorporation of these therapies in a first- or second-line setting (*81*); however, many patients will inevitably develop treatment resistance and disease recurrence. Particularly checkpoint blockade, which has been tremendously successful in other solid tumors,

show poor responses as a monotherapy in HGSC patients (*78, 143*). Although the recent FDA approval of pembrolizumab provides hope for a future of immunotherapy in ovarian cancer, improved therapeutic strategies are needed to broaden the eligibility to all ovarian cancer patients. Improved treatment strategies for ovarian cancer lies in our deeper understanding of the cellular and molecular mechanism of disease.

The ovarian tumor microenvironment is a complex one; shaped by competing tumor-immune interactions, cancer associated fibroblasts, and immunomodulatory cytokines and chemokines. Despite advances in our understanding of ovarian tumor immune biology, how this complexity translates to clinical outcomes in immunotherapy remains poorly understood. Immunophenotype of the ovarian tumor microenvironment has been correlated with sensitivity to checkpoint blockade (*81*). Cold tumors, whether they are immune desert or immune excluded, poorly respond to ICI due to the exclusion or absence of tumor-infiltrating lymphocytes. Conversely, hot tumors have an abundance of TILs that can be sensitized to ICI. The field of ovarian cancer therapy is shifting its focus on efforts to convert these so called "cold tumors" into "hot tumors". For example, while ICIs as a single agent strategy provide limited success, clinical trials of combination ICI therapy, either with chemotherapeutics or PARPi or other ICIs are showing promising early signs (*81*). Thus, adjuvant therapies that synergize with checkpoint blockade is an urgent clinical need for ovarian cancer care.

Here we propose the use of IL-33 as an adjuvant for PD-1 blockade for ovarian cancer. As a potent cytokine, IL-33 induces a robust type 2 inflammatory response – effectively converting "cold" tumors into "inflamed" or "hot" tumors in the ID8*Trp53*$^{-/-}$*Brca1*$^{-/-}$ mouse model. Treatment of

αPD-1 alone yielded a modest increase in survival in the ID8*Trp53*$^{-/-}$*Brca1*$^{-/-}$ model, in line with clinical data. However, the combination of IL-33+αPD-1 produced a robust anti-tumor response with long-lasting survival. Our preclinical data thus provides a rationale for the use of IL-33 as an adjuvant for combination therapy with checkpoint blockade.

However, for its clinical use, an appropriate platform for IL-33 must be investigated, as systemic administration of IL-33, a potent inflammatory cytokine, may trigger adverse immune reactions such as cytokine release syndrome. Here we explored the use of oncolytic therapy for delivering IL-33. Oncolytic therapy is a precision immunotherapeutic strategy that allows for gene therapy payload. The oncolytic platform we used was VSVΔ51, which is a highly lytic strain of virus. Although VSVΔ51-Il33 conferred some therapeutic potential, our immune profiling analysis showed that this was independent of ILC2 activation, and likely IL-33 expression was transient. Future projects in the lab, in collaboration with Bell and Ilkow labs, are aimed and testing other oncolytic platforms for use in preclinical mouse models.

A promising future for immunotherapy in ovarian cancer is emerging; however, substantial work remains to translate these advances to clinical reality. Combination immunotherapeutic strategies such as IL-33+αPD-1 overcome the limitations of single-agent therapies currently facing the clinic. IL-33+αPD-1 treatment provides enhanced tumor control potentially by converting immunologically "cold" tumors into "hot" tumors and thereby enhancing responsiveness to PD-1 blockade. Thus, our findings support continued therapeutic and mechanistic investigation of combination immunotherapies to improve patient outcomes, and more importantly, provide hope for patients living with ovarian cancer.

References

1. D. A. Landry, H. T. Vaishnav, B. C. Vanderhyden, The significance of ovarian fibrosis. *Oncotarget* **11**, 4366-4370 (2020).

2. C. W. McCloskey *et al.*, Metformin Abrogates Age-Associated Ovarian Fibrosis. *Clin Cancer Res* **26**, 632-642 (2020).

3. T. R. Hoage, I. L. Cameron, Folliculogenesis in the ovary of the mature mouse: a radioautographic study. *Anat Rec* **184**, 699-709 (1976).

4. M. Matousek, C. Carati, B. Gannon, M. Brännström, Novel method for intrafollicular pressure measurements in the rat ovary: increased intrafollicular pressure after hCG stimulation. *Reproduction* **121**, 307-314 (2001).

5. A. Amleh, J. Dean, Mouse genetics provides insight into folliculogenesis, fertilization and early embryonic development. *Hum Reprod Update* **8**, 395-403 (2002).

6. L. L. Espey, Ovulation as an inflammatory reaction--a hypothesis. *Biol Reprod* **22**, 73-106 (1980).

7. D. M. Duffy, C. Ko, M. Jo, M. Brannstrom, T. E. Curry, Ovulation: Parallels With Inflammatory Processes. *Endocr Rev* **40**, 369-416 (2019).

8. J. S. Richards, Z. Liu, M. Shimada, Immune-like mechanisms in ovulation. *Trends Endocrinol Metab* **19**, 191-196 (2008).

9. H. Ye *et al.*, The effect of the immune system on ovarian function and features of ovarian germline stem cells. *Springerplus* **5**, 990 (2016).

10. K. Moro *et al.*, Innate production of T(H)2 cytokines by adipose tissue-associated c-Kit(+)Sca-1(+) lymphoid cells. *Nature* **463**, 540-544 (2010).

11. D. R. Neill *et al.*, Nuocytes represent a new innate effector leukocyte that mediates type-2 immunity. *Nature* **464**, 1367-1370 (2010).

12. A. E. Price *et al.*, Systemically dispersed innate IL-13-expressing cells in type 2 immunity. *Proc Natl Acad Sci U S A* **107**, 11489-11494 (2010).

13. H. Spits *et al.*, Innate lymphoid cells--a proposal for uniform nomenclature. *Nat Rev Immunol* **13**, 145-149 (2013).

14. E. Vivier *et al.*, Innate Lymphoid Cells: 10 Years On. *Cell* **174**, 1054-1066 (2018).

15. J. A. Walker, A. N. McKenzie, Development and function of group 2 innate lymphoid cells. *Curr Opin Immunol* **25**, 148-155 (2013).

16. C. A. Steer *et al.*, Group 2 innate lymphoid cell activation in the neonatal lung drives type 2 immunity and allergen sensitization. *J Allergy Clin Immunol* **140**, 593-595.e593 (2017).

17. C. Schneider *et al.*, Tissue-Resident Group 2 Innate Lymphoid Cells Differentiate by Layered Ontogeny and In Situ Perinatal Priming. *Immunity* **50**, 1425-1438.e1425 (2019).

18. G. Gasteiger, X. Fan, S. Dikiy, S. Y. Lee, A. Y. Rudensky, Tissue residency of innate lymphoid cells in lymphoid and nonlymphoid organs. *Science* **350**, 981-985 (2015).

19. K. Moro *et al.*, Interferon and IL-27 antagonize the function of group 2 innate lymphoid cells and type 2 innate immune responses. *Nat Immunol* **17**, 76-86 (2016).

20. M. R. Karta *et al.*, β. *J Allergy Clin Immunol* **141**, 329-338.e312 (2018).

21. M. T. Stier *et al.*, IL-33 promotes the egress of group 2 innate lymphoid cells from the bone marrow. *J Exp Med* **215**, 263-281 (2018).

22. Y. Huang *et al.*, S1P-dependent interorgan trafficking of group 2 innate lymphoid cells supports host defense. *Science* **359**, 114-119 (2018).

23. D. G. Helou *et al.*, PD-1 pathway regulates ILC2 metabolism and PD-1 agonist treatment ameliorates airway hyperreactivity. *Nat Commun* **11**, 3998 (2020).

24. Y. Sakano *et al.*, ICOS regulates IL-10 production in group 2 innate lymphoid cells via cholesterol and cortisol biosynthesis. *J Clin Invest* **135**, (2025).

25. H. Maazi *et al.*, ICOS:ICOS-ligand interaction is required for type 2 innate lymphoid cell function, homeostasis, and induction of airway hyperreactivity. *Immunity* **42**, 538-551 (2015).

26. T. Y. Halim *et al.*, Group 2 innate lymphoid cells are critical for the initiation of adaptive T helper 2 cell-mediated allergic lung inflammation. *Immunity* **40**, 425-435 (2014).

27. R. R. Ricardo-Gonzalez *et al.*, Tissue signals imprint ILC2 identity with anticipatory function. *Nat Immunol* **19**, 1093-1099 (2018).

28. J. von Moltke, M. Ji, H. E. Liang, R. M. Locksley, Tuft-cell-derived IL-25 regulates an intestinal ILC2-epithelial response circuit. *Nature* **529**, 221-225 (2016).

29. H. Kabata, K. Moro, S. Koyasu, The group 2 innate lymphoid cell (ILC2) regulatory network and its underlying mechanisms. *Immunol Rev* **286**, 37-52 (2018).

30. H. Onda *et al.*, Identification of genes differentially expressed in canine vasospastic cerebral arteries after subarachnoid hemorrhage. *J Cereb Blood Flow Metab* **19**, 1279-1288 (1999).

31. E. S. Baekkevold *et al.*, Molecular characterization of NF-HEV, a nuclear factor preferentially expressed in human high endothelial venules. *Am J Pathol* **163**, 69-79 (2003).

32. J. Schmitz *et al.*, IL-33, an interleukin-1-like cytokine that signals via the IL-1 receptor-related protein ST2 and induces T helper type 2-associated cytokines. *Immunity* **23**, 479-490 (2005).

33. F. Y. Liew, J. P. Girard, H. R. Turnquist, Interleukin-33 in health and disease. *Nat Rev Immunol* **16**, 676-689 (2016).

34. E. Lefrançais *et al.*, Central domain of IL-33 is cleaved by mast cell proteases for potent activation of group-2 innate lymphoid cells. *Proc Natl Acad Sci U S A* **111**, 15502-15507 (2014).

35. S. Tominaga, A putative protein of a growth specific cDNA from BALB/c-3T3 cells is highly similar to the extracellular portion of mouse interleukin 1 receptor. *FEBS Lett* **258**, 301-304 (1989).

36. K. Yanagisawa, T. Takagi, T. Tsukamoto, T. Tetsuka, S. Tominaga, Presence of a novel primary response gene ST2L, encoding a product highly similar to the interleukin 1 receptor type 1. *FEBS Lett* **318**, 83-87 (1993).

37. A. Lingel *et al.*, Structure of IL-33 and its interaction with the ST2 and IL-1RAcP receptors--insight into heterotrimeric IL-1 signaling complexes. *Structure* **17**, 1398-1410 (2009).

38. J. Furusawa *et al.*, Critical role of p38 and GATA3 in natural helper cell function. *J Immunol* **191**, 1818-1826 (2013).

39. C. I. Carlock *et al.*, Unique temporal and spatial expression patterns of IL-33 in ovaries during ovulation and estrous cycle are associated with ovarian tissue homeostasis. *J Immunol* **193**, 161-169 (2014).

40. S. Begum *et al.*, Dynamic Expression of Interleukin-33 and ST2 in the Mouse Reproductive Tract Is Influenced by Superovulation. *J Histochem Cytochem* **68**, 253-267 (2020).

41. J. Wu *et al.*, IL-33 is required for disposal of unnecessary cells during ovarian atresia through regulation of autophagy and macrophage migration. *J Immunol* **194**, 2140-2147 (2015).

42. J. Wu *et al.*, Activation of interleukin 33-NFκB axis in granulosa cells during atresia and its role in disposal of atretic follicles†. *Biol Reprod* **110**, 924-935 (2024).

43. J. M. Doisne *et al.*, Composition, Development, and Function of Uterine Innate Lymphoid Cells. *J Immunol* **195**, 3937-3945 (2015).

44. J. Siewiera *et al.*, Circumvention of luteolysis reveals parturition pathways in mice dependent upon innate type 2 immunity. *Immunity* **56**, 606-619.e607 (2023).

45. T. Ben Yaakov, T. Wasserman, E. Aknin, Y. Savir, Single-cell analysis of the aged ovarian immune system reveals a shift towards adaptive immunity and attenuated cell function. *Elife* **12**, (2023).

46. D. A. Landry *et al.*, Metformin prevents age-associated ovarian fibrosis by modulating the immune landscape in female mice. *Sci Adv* **8**, eabq1475 (2022).

47. M. J. Schuijs *et al.*, ILC2-driven innate immune checkpoint mechanism antagonizes NK cell antimetastatic function in the lung. *Nat Immunol* **21**, 998-1009 (2020).

48. V. Lucarini *et al.*, IL-33 restricts tumor growth and inhibits pulmonary metastasis in melanoma-bearing mice through eosinophils. *Oncoimmunology* **6**, e1317420 (2017).

49. N. Jacquelot *et al.*, Blockade of the co-inhibitory molecule PD-1 unleashes ILC2-dependent antitumor immunity in melanoma. *Nat Immunol* **22**, 851-864 (2021).

50. I. Saranchova *et al.*, Type 2 Innate Lymphocytes Actuate Immunity Against Tumours and Limit Cancer Metastasis. *Sci Rep* **8**, 2924 (2018).

51. E. Jou *et al.*, An innate IL-25-ILC2-MDSC axis creates a cancer-permissive microenvironment for Apc mutation-driven intestinal tumorigenesis. *Sci Immunol* **7**, eabn0175 (2022).

52. M. F. Chevalier *et al.*, ILC2-modulated T cell-to-MDSC balance is associated with bladder cancer recurrence. *J Clin Invest* **127**, 2916-2929 (2017).

53. C. W. Xia *et al.*, A diversity of novel type-2 innate lymphoid cell subpopulations revealed during tumour expansion. *Commun Biol* **7**, 12 (2024).

54. Z. Li *et al.*, Therapeutic application of human type 2 innate lymphoid cells via induction of granzyme B-mediated tumor cell death. *Cell* **187**, 624-641 e623 (2024).

55. N. Liu *et al.*, Role of the IL-33/ST2 receptor axis in ovarian cancer progression. *Oncol Lett* **22**, 504 (2021).

56. C. Feng, L. Kou, P. Yin, Y. Jing, Excessive activation of IL-33/ST2 in cancer-associated fibroblasts promotes invasion and metastasis in ovarian cancer. *Oncol Lett* **23**, 158 (2022).

57. A. Perales-Puchalt *et al.*, IL-33 delays metastatic peritoneal cancer progression inducing an allergic microenvironment. *Oncoimmunology* **8**, e1515058 (2019).

58. A. Sekiya *et al.*, Interleukin-33 expression in ovarian cancer and its possible suppression of peritoneal carcinomatosis. *Int J Oncol* **55**, 755-765 (2019).

59. C. Robert *et al.*, Anti-programmed-death-receptor-1 treatment with pembrolizumab in ipilimumab-refractory advanced melanoma: a randomised dose-comparison cohort of a phase 1 trial. *Lancet* **384**, 1109-1117 (2014).

60. B. T. Fife *et al.*, Interactions between PD-1 and PD-L1 promote tolerance by blocking the TCR-induced stop signal. *Nat Immunol* **10**, 1185-1192 (2009).

61. A. H. Sharpe, E. J. Wherry, R. Ahmed, G. J. Freeman, The function of programmed cell death 1 and its ligands in regulating autoimmunity and infection. *Nat Immunol* **8**, 239-245 (2007).

62. Y. Yu *et al.*, Single-cell RNA-seq identifies a PD-1. *Nature* **539**, 102-106 (2016).

63. S. Taylor *et al.*, PD-1 regulates KLRG1. *J Exp Med* **214**, 1663-1678 (2017).

64. D. G. Helou *et al.*, LAIR-1 acts as an immune checkpoint on activated ILC2s and regulates the induction of airway hyperreactivity. *J Allergy Clin Immunol* **149**, 223-236.e226 (2022).

65. J. A. Moral *et al.*, ILC2s amplify PD-1 blockade by activating tissue-specific cancer immunity. *Nature* **579**, 130-135 (2020).

66. Z. Momenimovahed, A. Tiznobaik, S. Taheri, H. Salehiniya, Ovarian cancer in the world: epidemiology and risk factors. *Int J Womens Health* **11**, 287-299 (2019).

67. J. Prat, F. C. o. G. Oncology, Staging classification for cancer of the ovary, fallopian tube, and peritoneum. *Int J Gynaecol Obstet* **124**, 1-5 (2014).

68. A. De Leo *et al.*, What Is New on Ovarian Carcinoma: Integrated Morphologic and Molecular Analysis Following the New 2020 World Health Organization Classification of Female Genital Tumors. *Diagnostics (Basel)* **11**, (2021).

69. J. M. Piek *et al.*, Dysplastic changes in prophylactically removed Fallopian tubes of women predisposed to developing ovarian cancer. *J Pathol* **195**, 451-456 (2001).

70. F. Medeiros *et al.*, The tubal fimbria is a preferred site for early adenocarcinoma in women with familial ovarian cancer syndrome. *Am J Surg Pathol* **30**, 230-236 (2006).

71. A. K. Folkins *et al.*, A candidate precursor to pelvic serous cancer (p53 signature) and its prevalence in ovaries and fallopian tubes from women with BRCA mutations. *Gynecol Oncol* **109**, 168-173 (2008).

72. K. Levanon, C. Crum, R. Drapkin, New insights into the pathogenesis of serous ovarian cancer and its clinical impact. *J Clin Oncol* **26**, 5284-5293 (2008).

73. S. Lheureux, C. Gourley, I. Vergote, A. M. Oza, Epithelial ovarian cancer. *Lancet* **393**, 1240-1253 (2019).

74. I. Colombo, S. Lheureux, A. M. Oza, Rucaparib: a novel PARP inhibitor for. *Drug Des Devel Ther* **12**, 605-617 (2018).

75. J. Garcia *et al.*, Bevacizumab (Avastin®) in cancer treatment: A review of 15 years of clinical experience and future outlook. *Cancer Treat Rev* **86**, 102017 (2020).

76. E. J. Tomas, J. Davis, Y. Ramos Valdes, T. G. Shepherd, Evaluating carboplatin and PARP inhibitor combination efficacy using high-grade serous carcinoma spheroids and organoids. *Cancer Biol Ther* **27**, 2611602 (2026).

77. P. Jessmon, T. Boulanger, W. Zhou, P. Patwardhan, Epidemiology and treatment patterns of epithelial ovarian cancer. *Expert Rev Anticancer Ther* **17**, 427-437 (2017).

78. U. A. Matulonis *et al.*, Antitumor activity and safety of pembrolizumab in patients with advanced recurrent ovarian cancer: results from the phase II KEYNOTE-100 study. *Ann Oncol* **30**, 1080-1087 (2019).

79. G. Wang, H. Yang, Y. Wang, J. Qin, Ovarian cancer targeted therapy: current landscape and future challenges. *Front Oncol* **15**, 1535235 (2025).

80. N. E. James, M. Woodman, P. A. DiSilvestro, J. R. Ribeiro, The Perfect Combination: Enhancing Patient Response to PD-1-Based Therapies in Epithelial Ovarian Cancer. *Cancers (Basel)* **12**, (2020).

81. I. Colombo, K. Karakasis, S. Suku, A. M. Oza, Chasing Immune Checkpoint Inhibitors in Ovarian Cancer: Novel Combinations and Biomarker Discovery. *Cancers (Basel)* **15**, (2023).

82. L. Zhang *et al.*, Intratumoral T cells, recurrence, and survival in epithelial ovarian cancer. *N Engl J Med* **348**, 203-213 (2003).

83. E. Sato *et al.*, Intraepithelial CD8+ tumor-infiltrating lymphocytes and a high CD8+/regulatory T cell ratio are associated with favorable prognosis in ovarian cancer. *Proc Natl Acad Sci U S A* **102**, 18538-18543 (2005).

84. T. J. Curiel *et al.*, Specific recruitment of regulatory T cells in ovarian carcinoma fosters immune privilege and predicts reduced survival. *Nat Med* **10**, 942-949 (2004).

85. D. S. Chen, I. Mellman, Elements of cancer immunity and the cancer-immune set point. *Nature* **541**, 321-330 (2017).

86. Y. Huang *et al.*, IL-25-responsive, lineage-negative KLRG1(hi) cells are multipotential 'inflammatory' type 2 innate lymphoid cells. *Nat Immunol* **16**, 161-169 (2015).

87. T. Sudo *et al.*, Group 2 innate lymphoid cells support hematopoietic recovery under stress conditions. *J Exp Med* **218**, (2021).

88. S. Ryu *et al.*, The protective roles of integrin α4β7 and Amphiregulin-expressing innate lymphoid cells in lupus nephritis. *Cell Mol Immunol* **21**, 723-737 (2024).

89. K. Bartemes, C. C. Chen, K. Iijima, L. Drake, H. Kita, IL-33-Responsive Group 2 Innate Lymphoid Cells Are Regulated by Female Sex Hormones in the Uterus. *J Immunol* **200**, 229-236 (2018).

90. E. Blanquart, S. Laffont, J. C. Guéry, Sex hormone regulation of innate lymphoid cells. *Biomed J* **44**, 144-156 (2021).

91. J. Y. Cephus *et al.*, Testosterone Attenuates Group 2 Innate Lymphoid Cell-Mediated Airway Inflammation. *Cell Rep* **21**, 2487-2499 (2017).

92. S. Laffont *et al.*, Androgen signaling negatively controls group 2 innate lymphoid cells. *J Exp Med* **214**, 1581-1592 (2017).

93. E. Blanquart *et al.*, Targeting androgen signaling in ILC2s protects from IL-33-driven lung inflammation, independently of KLRG1. *J Allergy Clin Immunol* **149**, 237-251.e212 (2022).

94. P. Laurent *et al.*, TGFβ promotes low IL10-producing ILC2 with profibrotic ability involved in skin fibrosis in systemic sclerosis. *Ann Rheum Dis* **80**, 1594-1603 (2021).

95. A. M. Tsou *et al.*, Neuropeptide regulation of non-redundant ILC2 responses at barrier surfaces. *Nature* **611**, 787-793 (2022).

96. W. Y. Chen *et al.*, Group 2 innate lymphoid cells contribute to IL-33-mediated alleviation of cardiac fibrosis. *Theranostics* **11**, 2594-2611 (2021).

97. A. E. Joham *et al.*, Polycystic ovary syndrome. *Lancet Diabetes Endocrinol* **10**, 668-680 (2022).

98. S. Banerjee, L. G. Cooney, A. K. Stanic, Immune Dysfunction in Polycystic Ovary Syndrome. *Immunohorizons* **7**, 323-332 (2023).

99. A. S. Kauffman *et al.*, A Novel Letrozole Model Recapitulates Both the Reproductive and Metabolic Phenotypes of Polycystic Ovary Syndrome in Female Mice. *Biol Reprod* **93**, 69 (2015).

100. G. E. Ryan, S. Malik, P. L. Mellon, Antiandrogen Treatment Ameliorates Reproductive and Metabolic Phenotypes in the Letrozole-Induced Mouse Model of PCOS. *Endocrinology* **159**, 1734-1747 (2018).

101. S. T. Kelley, D. V. Skarra, A. J. Rivera, V. G. Thackray, The Gut Microbiome Is Altered in a Letrozole-Induced Mouse Model of Polycystic Ovary Syndrome. *PLoS One* **11**, e0146509 (2016).

102. G. M. Rodriguez *et al.*, The Tumor Immune Profile of Murine Ovarian Cancer Models: An Essential Tool For Ovarian Cancer Immunotherapy Research. *Cancer Res Commun* **2**, 417-433 (2022).

103. C. Ciancaglini *et al.*, Macrophages regulate PD-1 and CTLA-4 expression on ILC2s and their responsiveness in the tumor microenvironment. *Cell Mol Immunol* **22**, 1491-1505 (2025).

104. X. Zheng *et al.*, Single-cell analyses implicate ascites in remodeling the ecosystems of primary and metastatic tumors in ovarian cancer. *Nat Cancer* **4**, 1138-1156 (2023).

105. Y. Huang, W. E. Paul, Inflammatory group 2 innate lymphoid cells. *Int Immunol* **28**, 23-28 (2016).

106. J. Duraiswamy, G. J. Freeman, G. Coukos, Therapeutic PD-1 pathway blockade augments with other modalities of immunotherapy T-cell function to prevent immune decline in ovarian cancer. *Cancer Res* **73**, 6900-6912 (2013).

107. S. Farokhi Boroujeni *et al.*, BRCA1 and BRCA2 deficient tumour models generate distinct ovarian tumour microenvironments and differential responses to therapy. *J Ovarian Res* **16**, 231 (2023).

108. B. Pirš, E. Škof, V. Smrkolj, Š. Smrkolj, Overview of Immune Checkpoint Inhibitors in Gynecological Cancer Treatment. *Cancers (Basel)* **14**, (2022).

109. L. R. Shiow *et al.*, CD69 acts downstream of interferon-alpha/beta to inhibit S1P1 and lymphocyte egress from lymphoid organs. *Nature* **440**, 540-544 (2006).

110. M. Salimi *et al.*, Activated innate lymphoid cell populations accumulate in human tumour tissues. *BMC Cancer* **18**, 341 (2018).

111. R. N. Germain, Y. Huang, ILC2s - resident lymphocytes pre-adapted to a specific tissue or migratory effectors that adapt to where they move? *Curr Opin Immunol* **56**, 76-81 (2019).

112. K. J. Jarick *et al.*, Non-redundant functions of group 2 innate lymphoid cells. *Nature* **611**, 794-800 (2022).

113. C. Sasse *et al.*, Eosinophils, but Not Type 2 Innate Lymphoid Cells, Are the Predominant Source of Interleukin 4 during the Innate Phase of. *Pathogens* **11**, (2022).

114. R. K. Gurram, J. Zhu, Orchestration between ILC2s and Th2 cells in shaping type 2 immune responses. *Cell Mol Immunol* **16**, 225-235 (2019).

115. S. Rauber *et al.*, Resolution of inflammation by interleukin-9-producing type 2 innate lymphoid cells. *Nat Med* **23**, 938-944 (2017).

116. S. Castelli *et al.*, IL-9 signaling redirects CAR T cell fate toward CD8. *Immunity* **59**, 195-212.e111 (2026).

117. M. L. Robinette *et al.*, Transcriptional programs define molecular characteristics of innate lymphoid cell classes and subsets. *Nat Immunol* **16**, 306-317 (2015).

118. L. Knipfer *et al.*, A CCL1/CCR8-dependent feed-forward mechanism drives ILC2 functions in type 2-mediated inflammation. *J Exp Med* **216**, 2763-2777 (2019).

119. Z. Li *et al.*, Therapeutic application of human type 2 innate lymphoid cells via induction of granzyme B-mediated tumor cell death. *Cell* **187**, 624-641.e623 (2024).

120. H. L. Kaufman, F. J. Kohlhapp, A. Zloza, Oncolytic viruses: a new class of immunotherapy drugs. *Nat Rev Drug Discov* **14**, 642-662 (2015).

121. J. C. Bell, K. A. Garson, B. D. Lichty, D. F. Stojdl, Oncolytic viruses: programmable tumour hunters. *Curr Gene Ther* **2**, 243-254 (2002).

122. J. Publicover, E. Ramsburg, M. Robek, J. K. Rose, Rapid pathogenesis induced by a vesicular stomatitis virus matrix protein mutant: viral pathogenesis is linked to induction of tumor necrosis factor alpha. *J Virol* **80**, 7028-7036 (2006).

123. M. Ahmed *et al.*, Ability of the matrix protein of vesicular stomatitis virus to suppress beta interferon gene expression is genetically correlated with the inhibition of host RNA and protein synthesis. *J Virol* **77**, 4646-4657 (2003).

124. A. O. Cudmore *et al.*, Specific Genetic Mutations Impact Chemotherapy Resistance and Therapeutic Efficacy of Oncolytic Viruses in Ovarian Cancer. *Mol Cancer Ther* **24**, 1626-1639 (2025).

125. J. J. Rojas *et al.*, A new MVA ancestor-derived oncolytic vaccinia virus induces immunogenic tumor cell death and robust antitumor immune responses. *Mol Ther* **32**, 2406-2422 (2024).

126. X. Tong *et al.*, Interleukin-33 predicts poor prognosis and promotes ovarian cancer cell growth and metastasis through regulating ERK and JNK signaling pathways. *Mol Oncol* **10**, 113-125 (2016).

127. K. F. Troch *et al.*, Group 2 innate lymphoid cells are a non-redundant source of interleukin-5 required for development and function of murine B1 cells. *Nat Commun* **15**, 10566 (2024).

128. C. H. D. Barbosa, L. Lantier, J. Reynolds, J. Wang, F. Re, Critical role of IL-25-ILC2-IL-5 axis in the production of anti-Francisella LPS IgM by B1 B cells. *PLoS Pathog* **17**, e1009905 (2021).

129. J. V. V. Isola *et al.*, A single-cell atlas of the aging mouse ovary. *Nat Aging* **4**, 145-162 (2024).

130. J. Li *et al.*, Dual blockades of TIM-3 and PD-1 effectively prevent hyper-progression and enhance the efficacy of anti-PD-1 therapy in high-grade serous ovarian cancer. *Cell Death Dis* **16**, 867 (2025).

131. J. Duraiswamy, K. M. Kaluza, G. J. Freeman, G. Coukos, Dual blockade of PD-1 and CTLA-4 combined with tumor vaccine effectively restores T-cell rejection function in tumors. *Cancer Res* **73**, 3591-3603 (2013).

132. K. H. Van der Hoek, C. M. Woodhouse, M. Brännström, R. J. Norman, Effects of interleukin (IL)-6 on luteinizing hormone- and IL-1beta-induced ovulation and steroidogenesis in the rat ovary. *Biol Reprod* **58**, 1266-1271 (1998).

133. S. Kol, I. Kehat, E. Y. Adashi, Ovarian interleukin-1-induced gene expression: privileged genes threshold theory. *Med Hypotheses* **58**, 6-8 (2002).

134. L. Fang, Y. P. Sun, J. C. Cheng, The role of amphiregulin in ovarian function and disease. *Cell Mol Life Sci* **80**, 60 (2023).

135. L. A. Monticelli *et al.*, IL-33 promotes an innate immune pathway of intestinal tissue protection dependent on amphiregulin-EGFR interactions. *Proc Natl Acad Sci U S A* **112**, 10762-10767 (2015).

136. A. M. Tsou *et al.*, Neuropeptide regulation of non-redundant ILC2 responses at barrier surfaces. *Nature* **611**, 787-793 (2022).

137. B. C. Duncan *et al.*, Androgen Signaling in ILC2s Drives Sex Differences in Helicobacter-induced Gastric Inflammation and Atrophy. *Cell Mol Gastroenterol Hepatol* **20**, 101690 (2026).

138. A. Dunaif, Insulin resistance and the polycystic ovary syndrome: mechanism and implications for pathogenesis. *Endocr Rev* **18**, 774-800 (1997).

139. S. Abraham Gnanadass, Y. Divakar Prabhu, A. Valsala Gopalakrishnan, Association of metabolic and inflammatory markers with polycystic ovarian syndrome (PCOS): an update. *Arch Gynecol Obstet* **303**, 631-643 (2021).

140. M. A. Sanchez-Garrido, M. Tena-Sempere, Metabolic dysfunction in polycystic ovary syndrome: Pathogenic role of androgen excess and potential therapeutic strategies. *Mol Metab* **35**, 100937 (2020).

141. M. Wagner, H. Nishikawa, S. Koyasu, Reinventing type 2 immunity in cancer. *Nature* **637**, 296-303 (2025).

142. M. Wagner, S. Koyasu, Cancer in disguise: a parasite within. *EMBO J* **45**, 1051-1059 (2026).

143. A. Varga *et al.*, Pembrolizumab in patients with programmed death ligand 1-positive advanced ovarian cancer: Analysis of KEYNOTE-028. *Gynecol Oncol* **152**, 243-250 (2019).

144. S. Iyer *et al.*, Genetically Defined Syngeneic Mouse Models of Ovarian Cancer as Tools for the Discovery of Combination Immunotherapy. *Cancer Discov* **11**, 384-407 (2021).

145. K. Alwosaibai *et al.*, PAX2 maintains the differentiation of mouse oviductal epithelium and inhibits the transition to a stem cell-like state. *Oncotarget* **8**, 76881-76897 (2017).

146. D. C. Chung *et al.*, Characterization of innate lymphoid cell subsets infiltrating melanoma and epithelial ovarian tumors. *Oncoimmunology* **13**, 2349347 (2024).